Sulfur Black 1 Dye Removal and Na_2S Reuse from a Textile Industry Wastewater Treatment

RUKİYE ÖZTEKİN, DELİA TERESA SPONZA*
Department of Environmental Engineering
Dokuz Eylül University
Tınaztepe Campus, 35160 Buca/Izmir,
TURKEY

**Corresponding Author*

Abstract: - Sulfur Black 1 (SB 1) ($C_{18}H_8N_4O_5S_2$) is a widely used dye in the textile industry. Its dyeing process generates significant amounts of wastewater containing high-molecular-weight, refractory, and toxic organic pollutants, along with sulfate. This study proposed a novel sulfur-circular process integrating persulfate-based advanced oxidation process (AOP), microbial sulfate reduction, and gas stripping-adsorption to simultaneously remove Sulfur Black 1 and recover sodium sulfide (Na_2S) from textile wastewater. Persulfate activation by zero-valent iron (Fe^0) particles generated sulfate radicals ($SO_4^{\bullet -2}$) and hydroxyl radicals ($OH^{\bullet}$), achieving 99% degradation of Sulfur Black in real dyeing wastewater. The AOP-treated wastewater, which contained biodegradable organic by-products and sulfate, was subsequently treated in an up-flow anaerobic packed-bed sulfidogenic reactor (UAPBSR). In this reactor 90% of sulfate was reduced, producing 200-600 mg dissolved sulfide/l. The organic AOP by-products were efficiently mineralized, with a total organic carbon removal efficiency of about 99%. Fermentative bacteria (e.g., *Lactococcus* and *Acidipropionibacterium*) converted high-molecular-weight organic oxidation by-products into low-molecular-weight organics, which were further mineralized by sulfate-reducing bacteria (e.g., *Desulfobacter* and *Desulfovibrio*). Over 99% of dissolved sulfide in the UAPBSR effluents was stripped and then absorbed with a sodium hydroxide (NaOH) solution, enabling the recovery of Na_2S as a low-cost solubilizer recycled for the dyeing process. Langmuir linear model results agree with the experimental data better than the Freundlich linear model with the maximum uptake capacity of 173.04 mg/g. This study offers essential fundamentals for developing cost-effective technologies to treat wastewater containing refractory dyes and other persistent organic pollutants.

Key-Words: - *Acidipropionibacterium*; Advanced oxidation process (AOP); *Desulfobacter; Desulfovibrio; Lactococcus*; Reuse; Sodium sulfide (Na_2S); Sulfur Black 1 ($C_{18}H_8N_4O_5S_2$) dyestuff; Textile industry wastewater; Up-flow anaerobic packed-bed sulfidogenic reactor (UAPBSR).

Received: June 28, 2025. Revised: October 15, 2025. Accepted: November 11, 2025. Published: March 31, 2026.

1 Introduction

Sulfur dyes are widely used in dyeing cellulose fibers; they rank third in use after reactive and disperse dyes, accounting for approximately 10% of all dye consumption worldwide, [1], [2]. The global market size for sulfur-based paints is estimated at US$236 million in 2024. The sulfur-based paint dyeing process requires sodium sulfide (Na_2S) as a solvent, [3], which results in wastewater containing 5-10% residual paint and high levels of inorganic sulfur compounds (e.g. sulfate), [4], [5]. The remaining sulfur dyes consist of high molecular weight refractory organics, most of which have carcinogenic and teratogenic effects in humans, [4]. Therefore, the effective treatment of wastewater containing difficult-to-decompose and toxic sulfur dyes is of vital importance.

Both biological and chemical treatment methods for removing sulfur-containing dyes wastewater are being extensively investigated. For example, *Acinetobacter sp.* DS-9, isolated from agricultural soil, has been reported to be very effective in breaking down Sulfur Black (SB) [6]. Although biological methods are chemical-saving and low-cost methods, their efficiency is generally quite limited due to the resistant and toxic nature of sulfur dyes [7]. Advanced oxidation processes, including Fenton reactions, photocatalytic oxidation, sulfate radical-based advanced oxidation processes (AOPs), etc., produce

highly reactive species such as hydroxyl radicals ($OH^{\bullet}$) and sulfate radicals ($SO_4^{\bullet -2}$) that break down organic pollutants more effectively. Amin et al. [8] reported high-efficiency degradation of blue sulfur dye by ultraviolet/hydrogen peroxide (UV/H_2O_2) system. The activation of peroxymonosulfate or persulfate via thermal, photochemical, transition metal-based, zero-valent iron (Fe^0) can produce both $SO_4^{\bullet -2}$ and $OH^{\bullet}$, and these radicals play an effective role in the degradation of various dyes, such as Rhodamine B (Rh B), [9]. However, AOPs generally require expensive chemicals and/or intensive energy input, which in turn leads to high refining costs. Furthermore, AOPs can produce toxic conversion byproducts instead of providing complete mineralization, [10], [11]. The experimental steps of sulfur dyes were determined at Fig. 1.

*Figure 1 can be found in the Appendix section.

The main properties and characteristics feature of sulfur dyes are mentioned below: (1) Sulfur dyes have sulfur linkage within their molecules, (2) Sulfur dyes are highly coloured water insoluble dyes. Some dyes are partially soluble in water, (3) They have no direct affinity towards cellulosic fibres. To make them substantive they are to be converted in to soluble Leuco form by treating them with reducing agents (like dilute Na_2S solution), (4) Sulfur dyes have good light fastness with rating about 4. This light fastness may be improved by an after treatment with metallic salt, (5) These dyes have excellent wash fastness with rating about 3-4. This good wash fastness is due to its larger molecular size and insolubility in water, (6) They are not applicable to wool due to strong alkaline condition, (7) They are exclusively amorphous, few of them show crystallinity, (8) Important for producing a wide range of shades on a variety of cotton and rayon, (9) Sulfur dyes are suitable for heavy and durable shades, (10) Available in powder and soluble form sulfur dyes are cheap and easy to manufacture, and (11) Heat and chemical resistance of sulfur dyes are moderate to good. They have poor fastness to chlorine and are not applied to goods which are bleached with hypochlorite, respectively.

Features of sulfur dye are: (1) Amorphous colloidal materials, (2) High molecular weight with various composition, (3) Complex molecular structure–heterocyclic molecules containing sulfur linkage, (4) Decomposed by acids, with the liberation of H_2S, (5) Characterized by thiazine ring, containing sulfur atom, respectively.

The precautions in the dyeing process with the sulfur dyes are mentioned below: (1) In the application of sulfur dye, the dye bath should not contain Ca-salts, (2) If they are present in the form of insoluble co-compounds with the sulfur dyes which precipitated easily in closed machines and form sludge when restrict the circulation of the dye liquor, (3) The dye should be dissolved with soda, (4) Great care should be taken during reduction process because over reduction should lower the affinity of dye towards the fiber. As a result of dull shade will appear and a lot of dye stuff will go to waste, (5) Fabric must not to expose to air during dyeing to prevent precipitation and oxidation. This will cause uneven dyeing, (6) To prevent uneven dyeing in the fabric selvedge more amount of Na_2S or NaOH and salt should be added in case of the jigger dyeing machine, (7) To prevent the breeziness the dye liquor should not be very worm, and (8) Goods dyed with SB should be after treated with a solution of $K_2Cr_2O_7$ followed by rinsing. This will prevent Sulfur Black tendering, respectively.

Dyestuffs employed for coloration of cellulosic stem predominantly from the application classes of direct, fiber reactive, azonic, vat, and sulfur; with chromogenic entities typically based on azo (mono-, dis-, tris-), anthraquinone, phthalocyanine, fused ring polycyclic, and indigoid chemistries, [12]. Among all dyestuffs from the different application classes, the two most employed for the coloration of cellulosic are perhaps indigo (CI Vat Blue 1) and CI Sulfur Black 1 ($C_{18}H_8N_4O_5S_2$) molecular weight ($MW_{SB\ 1}$) = 424.4 g/mol (Fig. 2), with estimated annual production volumes in the regions of 70,000 tonnes, [13], and 100,000 tonnes, [14], respectively. A significant area of application for both is in the coloration of denim, a product which accounts for about 10–12% of the annual global output of cotton fibers, [15], [16]. Indigo produces the characteristic blue colour, and Sulfur Black is utilized to yield black or grays. Moreover, both may be employed in tandem to vary colour tone of the blue, either by dyeing cellulosic first with Sulfur Black 1 and then with indigo (termed "*bottoming*") or in the reverse order (termed "*topping*"), [17].

*Figure 2 can be found in the Appendix section.

If sulfur dyed textile materials are stored (weakening) tendering effect is seen on the cellulose. Due to storage a part of the sulfur colour converts in to H_2SO_4 by oxidizing which in turn causes degradation of cotton by hydrolysis. It is a serious problem of sulfur dyed goods. The causes are as below: (1) Gradual oxidation of sulfur to H_2SO_4 on storage, (2) After treatment with copper (Cu) salts causes rapid tendering, (3) Presence of iron (Fe) as an impurity causes rapid tendering, and (4) The method

of oxidation for the reconversion to insoluble form influence tendering, respectively.

The remedies are as below: (a) Treatment of dyed material with 1-3% $K_2Cr_2O_7$ and 1-3% CH_3COOH at 60^{o}C temperature for 30 min followed by through rinsing, (b) Treatment with a little CH_3COOH so that H_2SO_4 may be converted in to harmless acetic acid, and (c) Using 5 gm/litre soda ash after dyeing followed by drying without rinsing.

The research initially concentrates on indigo and SB1, the two most commonly employed dyestuffs for cellulosic fibers. It was previously determined that indigo-dyed cellulosic may be subjected to the viscose process without leaching of the dyestuff into the dissolution or regeneration baths, [18]. An explanation for that is the redox potential developed during the viscose process did not exceed −700 mV, a potential at which indigo begins to become solubilized. However, as stated previously, Sulfur Black 1 becomes solubilized at lower redox potential magnitudes and therefore it is of interest to determine the fate of Sulfur Black 1 when cellulose containing the dye is subjected to the viscose process.

Cotton constitutes about two-thirds of all cellulosic employed in the manufacture of textiles, [19], and is also the fiber type predominantly used in the manufacture of denim, [20], where Sulfur Black 1 and indigo are widely used. Thus, typical examples of cellulosic dyed with SB 1 and indigo will be cotton fibers. Therefore, the high degree of polymerization in cotton makes it unsuitable for direct regeneration through the viscose process, and thus hydrolytic pretreatments become necessary to adjust the high degree of polymerization. However, as reported by others, [21], hydrolytic pretreatments of coloured cotton may contribute to dyestuff leaching and/or degradation, and make it difficult to determine the role of dyestuff interaction with cellulose dissolution/regeneration media. Thus, to avoid interference from the influence of hydrolytic pretreatments, the cellulosic employed for dyeing with indigo and Sulfur Black 1 were viscose fibers.

A pre-reduced, liquid formulation of Sulfur Black 1 was used in the dyeing of fibers, containing reducing agents for dye solubilization and stabilization, which may explain the observed steep drop in redox potential with the dye alone. Although, the fibers after dyeing with Sulfur Black 1 were rinsed extensively with water, subjected to an oxidation step with H_2O_2, further rinsed, and dried in ambient atmosphere, it is possible that some reducing agent residues persisted on fibers despite the extensive post-treatments after dyeing, and contributed to the observed drop in redox potential. Another possible cause is the potential of Sulfur Black 1 in fibers to act as an "antioxidant/reducing buffer" due to the numerous quinoneimino and disulfide groups present in the dye structure, [22].

The integration of biological processes with AOPs can be an attractive approach to reduce the costs and organic AOP by-products formation for the refractory dyeing wastewater treatment. AOPs are capable of destructing refractory organic pollutants into more biodegradable intermediates, [23], [24]. Biological treatment can further mineralize the organic intermediates and completely eliminate ecotoxic by-products, [23], [25], [26]. For instance, Lu et al., [27], used sequential ozonation and up-flow biological aerated filter process to treat dye wastewater containing reactive brilliant red X-3B. The decolorization and COD removal efficiency reached 97% and 90%, respectively. Liu et al., [28], found that the combination of Fenton oxidation and bio logical process removed 77.40% of COD from Sulfur Black wastewater. A combined $SO_4^{\bullet -2}$-based AOP (activated by Fe^0) and a sulfidogenic process also achieved complete degradation of orange II dye and mineralization of toxic intermediates, [29]. However, the existing previous studies largely overlooked the removal of inorganic sulfur compounds from the AOP-treated wastewater, which may cause various issues (e.g., odour nuisance) in sewer systems and receiving water bodies, [30].

Hereby, we proposed a sulfur-circular process to achieve complete degradation of Sulfur Black and concurrent recovery of sulfur resource from dyeing wastewater. This innovative process integrated persulfate-based AOP, microbial sulfate reduction, and gas stripping-adsorption. Persulfate-based AOP activated by Fe^0 converted refractory sulfur dyes into biodegradable organic products. The subsequent microbial sulfate reduction completely degraded organic AOP by-products and reduced sulfate (SO_4^{-2}) into sulfide (S^{-2}). Finally, sulfide was recovered via gas stripping and absorption, yielding value-add sodium sulfide (Na_2S), which can be recycled as a low-cost solubilizer in the Sulfur Black 1 dyeing process. The sulfur-circular process may thus provide a sustainable and economically viable solution for dyeing wastewater treatment. However, the feasibility of the sulfur-circular process and biotic and abiotic mechanisms involved have not yet been investigated.

Na_2S is a chemical compound with more commonly its hydrate $Na_2S.9H_2O$ (Fig. 3). Both the anhydrous and the hydrated salts are colorless solids, although, technical grades of Na_2S are generally yellow to brick red owing to the presence of polysulfides, [31]. It is commonly supplied as a crystalline mass, in flake form, or as a fused solid.

They are water-soluble, giving strongly alkaline solutions.

*Figure 3 can be found in the Appendix section.

When exposed to moisture, Na_2S is immediately hydrolyzed to give sodium hydrosulfide. Na_2S has an unpleasant rotten egg smell due to the formation of hydrogen sulfide by hydrolysis in moist air. Some commercial samples are described as $Na_2S.xH_2O$, where a weight percentage of Na_2S is specified. Commonly available grades have around 60% Na_2S by weight, which means that x is around 3. These grades of Na_2S are often marketed as "sodium sulfide flakes". These samples consist of NaSH, NaOH, and water. The structures of Na_2S have been determined by X-ray crystallography. The nonahydrate features S^{-2} hydrogen-bonded to 12 water molecules, [32]. The pentahydrate consists of S^{-2} centers bound to Na^+ and encased by an array of hydrogen (H) bonds, [33]. Anhydrous Na_2S, which is rarely encountered, adopts the antifluorite structure, [34], [35], which means that the Na^+ centers occupy sites of the fluoride in the CaF_2 framework, and the larger S^{-2} occupy the sites for Ca^{+2}.
The application of Na_2S chemical at dying process was shown at Fig. 4.

*Figure 4 can be found in the Appendix section.

Industrially Na_2S is produced by carbothermic reduction of sodium sulfate (Na_2SO_4) often using coal, [36], (Eq. 1):

$$Na_2SO_4 + 2C \rightarrow Na_2S + 2CO_2 \quad (1)$$

In the laboratory, the salt can be prepared by reduction of sulfur with sodium in anhydrous ammonia, or by sodium in dry Tetrahydrofuran (THF or oxolane) with a catalytic amount of naphthalene (forming sodium naphthalenide), [37], (Eq. 2):

$$2Na + S \rightarrow Na_2S \quad (2)$$

The sulfide ion in sulfide salts such as Na_2S can incorporate a proton into the salt by protonation (Eq. 3):

$$S^{-2} + H^+ \rightarrow SH^- \quad (3)$$

Because of this capture of the proton (H^+), Na_2S has basic character. Na_2S is strongly basic, able to absorb two protons. Its conjugate acid is sodium hydrosulfide (SH^-). An aqueous solution contains a significant portion of sulfide ions that are singly protonated (Eq. 4 and Eq. 5).

$$S^{-2} + H_2O \leftrightarrow SH^- + OH^- \quad (4)$$

$$SH^- + H_2O \leftrightarrow H_2S + OH^- \quad (5)$$

Na_2S is unstable in the presence of water due to the gradual loss of hydrogen sulfide (H_2S) into the atmosphere. When heated with oxygen (O_2) and carbon dioxide (CO_2), Na_2S can oxidize to sodium carbonate (Na_2SO_4) and sulfur dioxide (SO_2), (Eq. 6):

$$2Na_2S + 3O_2 + 2CO_2 \rightarrow 2Na_2CO_3 + 2SO_2 \quad (6)$$

Oxidation with hydrogen peroxide (H_2O_2) gives sodium sulfate (Na_2SO_4), [38], (Eq. 7):

$$Na_2S + 4H_2O_2 \rightarrow 4H_2O + Na_2SO_4 \quad (7)$$

Upon treatment with sulfur, sodium polysulfides are formed (Eq. 8):

$$2Na_2S + S_8 \rightarrow 2Na_2S_5 \quad (8)$$

Installation of carbon-sulfur bonds; alkylation of sodium sulfide give thioethers, (Eq. 9):

$$Na_2S + 2RX \rightarrow R_2S + 2NaX \quad (9)$$

Even aryl halides participate in this reaction, [39]. By a broadly similar process sodium sulfide can react with alkenes in the thiol-ene reaction to give thioethers. Na_2S can be used as nucleophile in Sandmeyer type reactions, [40]. Sulfur dye degradation with Na_2S reaction was determined at Fig. 5.

*Figure 5 can be found in the Appendix section.

Reducing agent; aqueous solution of Na_2S will reduce nitro groups to amine. This conversion is applied to production of some azo dyes since other reducible groups, e.g. azo group, remain intact, [41]. The reduction of nitro aromatic compounds to amines using sodium sulfide is known as the Zinin reaction in honor of its discoverer, [42]. Hydrated Na_2S reduces 1,3-dinitrobenzene derivatives to the 3-nitroanilines, [43].

Other reactions; sulfide has also been employed in photocatalytic applications, [44]. Consisting of the equivalent of sodium hydroxide (NaOH), Na_2S is strongly alkaline and can cause chemical burns. It reacts rapidly with acids to produce H_2S a gas which

is both highly toxic and potentially explosive. Na_2S hydrolyses in water to form smaller amounts of H_2S which also makes it very toxic to aquatic life.

Dyeing includes a few stages, vizcosity reduction, dyeing, washing, oxidation, soaping, and final washing. The anion is developed on reducing and solubilising at boil when it shows affinity for cellulose. Na_2S, the reducing and solubilising agent, performs both reduction and solubilisation, producing thiols and then to sodium salt of thiols or thiolates, which are soluble in water and substantive towards cellulose. Higher rate of exhaustion occurs at 90-95^oC in presence of electrolyte. Dyed cellulosics exhibit a tendering effect on storage under humid atmosphere due to presence of excess free sulfur. After treatment with sodium acetate is required to suppress that hydrogen sulfur (H_2S) liberated during dyeing forms corrosive metal sulfide. This restricts use of metal vessels except those made of stainless-steel, [45] (Eq. 10):

$$Fe + H_2S \rightarrow FeS + H_2 \quad (10)$$

The most important member of the class is SB 1. It is produced by the reaction of 2,4-dinitrophenol and Na_2S in hot water. Like many sulfur dyes, details on the chemical reactions are poorly understood. It is accepted that the sulfide reduces the nitro groups to aniline derivatives, which are thought to form indophenol-containing intermediates that are further crosslinked by reaction with sulfur. The result are insoluble, high molecular weight species. SB 1 is imperfectly understood, and the material is probably heterogeneous. It is speculated to be a polymer consisting of thianthrene and phenothiazine subunits. The so-called sulfur bake dyes are produced from 1,4-diaminobenzene and diaminotoluene derivatives. These dyes are proposed to consist of polymers with benzothiazole subunits. Members of the sulfur bake dyes class are Sulfur Orange 1 (SO 1), Sulfur Brown 21 (SB 21), and Sulfur Green 12 (SG 12), [46].

Sulfur dyes are water-insoluble. In the presence of a reducing agent and at alkaline pH at elevated temperature of around 80^oC, the dye particles disintegrate, which then become water-soluble and hence, can be absorbed by the fabric Na_2S or sodium hydrosulfide are suitable reducing agents. Common salt facilitates the absorption. After the fabric is removed from the dye solution, it is allowed to stand in air whereupon the dye is regenerated by oxidation. The regenerated parent dye is insoluble in water. Oxidation can also be effected in air or by H_2O_2 or sodium bromate in a mildly acidic solution.

The low water solubility is the basis of the good wash-fastness of these dyed fabrics. These dyes have good all-around colour fastness except to chlorine bleaches. Because the dye is water-insoluble, it will not bleed when washed in water and will not stain other clothes. The dye, however, may have poor fastness to rubbing. The dyes are bleached by hypochlorite bleach.

Due to the highly polluting nature of the dye-bath effluent, sulfur dyes are being slowly phased out in the West but they are used on a large scale in China, [47]. Recent advances in dyeing technologies have allowed the substitution of toxic sulfide reducing agents. Glucose in basic solution is now used and both low-sulfide and zero-sulfide products are available. Future developments in the field of reducing dye levels by means of electrochemical processes are promising.

Although, the lower temperature avoids the formation of eutectic materials, this method still faces significant challenges, such as long reaction times, high hydrogen consumption, and most importantly, the components of the catalyst can reduce the quality of Na_2S. This necessitates subsequent complex impurity removal processes, and the separation process is extremely difficult, all of which limit the industrial application value of this method. Other researchers have proposed the reaction directly between the reducing gas and molten Na_2SO_4 at high temperatures to obtain molten Na_2S products. Though, the subsequent evaporation and crystallization process can produce Na_2S of higher purity, the strong corrosiveness of molten Na_2S causes serious damage to equipment, and the presence of the liquid phase leads to difficulties in discharging, wall sticking, and other issues, limiting its further research, development, and industrial application, [48]. The challenge in producing Na_2S from Na_2SO_4 lies in the need to increase and control the reaction temperature to accelerate the reduction rate while avoiding sintering, presenting a clear trade-off. Considering the advantages of gas–solid reactions in terms of the mass and heat transfer efficiency, the H_2 reduction of Na_2SO_4 should be carried out with no or minimal liquid phase to achieve a higher reaction rate, [49], [50], [51]. In contrast to the traditional H_2 reduction of pure Na_2SO_4, utilizing a mixture with 80% Na_2S and Na_2SO_4 as the feedstock for the reduction reaction markedly prevents the formation of a liquid phase. This approach addresses the issues of incomplete reactions, extended reaction times, and substandard product qualities, which arise from eutectic formation during the reduction process. Furthermore, the dilute-phase fluidized bed reactor, an effective gas–solid reactor, can enhance the reaction rate without producing a liquid phase. Na_2S remains stable under high-temperature reducing

conditions, the freshly produced Na_2S can be combined with Na_2SO_4, continuing the reaction as a mixed feedstock until the Na_2SO_4 is entirely depleted, thus completing the reaction.

In this study it was investigated the removal of Sulfur Black 1 dyestuff and Na_2S reuse from a textile industry wastewater treatment plant in İzmir, Turkey. Sulfur Black 1, which accounts for about 80% of sulfur dyes employed in the dyeing industry, [52], was selected as a model Sulfur Black 1. The oxidation efficiency of Sulfur Black 1 by persulfate-based AOP activated by Fe^0 was evaluated. The mineralization of organic AOP by-products and sulphide production in an up-flow anaerobic packed-bed sulfidogenic reactor (UAPBSR) were evaluated. The recovery of Na_2S via gas stripping and absorption was also examined. In addition to, the biotic and abiotic mechanisms of Sulphur Black 1 and sulphur transformations in the sulphur-circular process were also elucidated.

2 Materials and Methods

2.1 Chemicals

Detailed information on the chemicals used, including sodium per sulfate ($Na_2S_2O_8$, ≥ 99%), Fe^0 granules (Φ1–2 mm), Sulfur Black 1, sodium sulfide ($Na_2S.9H_2O$), sodium hydroxide (NaOH), hydrochloric acid (HCl), is presented in Text 1. Simulated Sulfur Black 1 wastewater was prepared by dissolving SB 1 precursors provided by the supplier and $Na_2S.9H_2O$ in deionized water at a mass ratio of 1/2, followed by heating at 100°C for 30 min retention time, [53]. The synthetic domestic wastewater was prepared following the recipe of Yu et al., [29].

S^{2-}

2.2 Batch Tests Used in the Evaluation of Sulfur Black 1 Degradation with the Fe^0-Sodium Persulfate System

Batch experiments were performed to evaluate Sulfur Black 1 degradation in the Fe-sodium persulfate system. The sodium persulfate (0.25–1.5 g/l) and Fe^0 particles (0.25–1.5 g/l) were added into a 1-liter glass beaker with simulated Sulfur Black 1 wastewater (50 mg/l) at pH 5.0–11.0 and an ambient temperature of 26°C. The mixture was stirred with a paddle stirrer (DLBA, OS20-S, China) at a rotation speed of 550 rpm. The initial pH of the SB 1 solution was adjusted to the desired value by using NaOH (0.1 M) or HCl (0.1 M). At the pre-determined time intervals, 10 ml solution samples were withdrawn and then spiked with 1 ml methanol to quench the residual free radicals and terminate the reactions. The samples were centrifuged at 3500 rpm for 7.0 min, and the supernatant was then subjected to the analysis of Sulfur Black 1 concentration using a diffuse reflectance UV-vis spectra (DRS) in the range of 200–800 nm were recorded on a Cary 5000 spectrophotometer from Varian.

2.3 Long-Term Investigation of Sulfur Black 1 Decomposition and Sulfide Production via the Sulfur Cyclical Process

The long-term performance of Sulfur Black 1 degradation and sulfide production by the sulfur-circular process was evaluated using a setup containing an AOP and UAPBSR reactors (Fig. 6). The AOP treatment of simulated Sulfur Black 1 wastewater at pH=6.0 was conducted in a 12-liter cylindrical plexiglass reactor (19 cm in diameter and 45 cm in height) stirred with a paddle stirrer (DLBA, OS20-S, China). The dosages of sodium persulfate and Fe particles were 0.75 g/l and 1.0 g/l, respectively.

*Figure 6 can be found in the Appendix section.

The AOP treated Sulfur Black 1 wastewater was stored in a 50-liter tank and subsequently pumped into the UAPBSR reactor. The UAPBSR was a 30-liter cylindrical plexiglass reactor (16 cm in diameter and 150 cm in height) filled with plastic packing media (Φ10×7 mm). The seeding sludge was collected from an anaerobic tank of textile industry wastewater treatment plant in İzmir Turkey. The synthetic domestic wastewater containing 123–166 mg C/l organic carbon and 82–111 mgS/l sulfate and AOP-treated dyeing wastewater was pumped into the UAPBSR reactor at the predetermined volume ratios. The concentrations of sulfate in the mixture were 191–484 mgS/l, and the pH value was adjusted to 7.0 if needed. The influent and effluent samples were daily collected to measure dissolved sulfide and total organic carbon (TOC). The operation of the UAPBSR was divided into four stages with different operational parameters, including hydraulic retention time (HRT), volume ratio of AOP-treated wastewater to domestic wastewater, influent TOC, and sulfate concentrations (Table 1). The degradation ratio of Sulfur Black 1, TOC removal efficiency, TOC removal consumption rate, and sulfide production rate were calculated.

*Table 1 can be found in the Appendix section.

2.4 Stripping and Absorption for Na_2S Recovery

The recovery of Na_2S from the effluents of the UAPBSR reactor was investigated using a gas

stripping and absorption setup (Fig. 6). The sulfide-laden effluent samples were collected from the UAPBSR reactor in Steps 2-4. The pH value of the samples was adjusted to 6.0 with 0.1 M HCl. The effluent samples were then added to a stripper, in which Nitrogen gas [N_2(g)] was provided via a gas diffuser at a flow rate of 1.20 l/min. The stripping gas containing H_2S was subsequently introduced into a gas absorber with 1 M NaOH solution. The effluent gas of the absorber was recirculated to the stripper via a diaphragm pump. The solution samples were collected from the stripper and absorber units to deter mine dissolved sulfide concentrations by using the methylene blue spectrophotometric method at 664 nm, [54].

2.5 Analysis of Microbial Community

The sludge samples from the UAPBSR reactor were collected on 150., 300., 450. and 600. days hydraulic retention times (Table 1), respectively, and then subjected to the analysis of microbial community by 16S rRNA high-throughput sequencing, [55]. The extracted DNA was sequenced on Illumina platforms with a PE 150 strategy to gain 6 G raw data. The clean data of samples obtained from the company were submitted to Genome Taxonomy Database (GTDB) and Kyoto Encyclopedia of Genes and Genomes (KEGG) to obtain results of species annotation and functional genes, respectively. The above results were used to analyse the microbial composition, the relative abundance of microorganisms, functional species, and functional genes in the sludge samples, as well as for the prediction of metabolic pathways of carbon and sulfur metabolism.

2.6 Identifying Products of Sulfur Black 1 Degradation in the AOP and UAPBSR Reactors

The degradation products of Sulfur Black 1 in the AOP and UAPBSR reactors were characterized to reveal the degradation mechanisms. The solution samples were collected from the AOP reactor at 0, 5, 10, 20, 30, 40, 50, and 60 min, and quenched with 1 ml methanol. The effluent samples of the UAPBSR reactor were also taken. These collected samples were then analysed by a high-performance liquid chromatography system (Agilent 1290 Infinity II HPLC system, Agilent, USA) interfacing a quadrupole- time-of-flight mass spectrometer (Agilent 6545 Q-TOF-MS, Agilent, USA) equipped with electrospray ionization source (ESI) in positive mode. No HPLC separation was applied before mass spectrometry. Instead, 1.0 µl of each sample was directly injected into the mass spectrometer with 0.1% formic acid in ultrapure water (80%, mobile phase A) and 0.1% acetic acid in acetonitrile as mobile phase at a constant flow rate of 0.3 ml/min for 5.0 min. The full MS scan of m/z ranging from 50 to 1700 Da. The drying gas temperature and flow rate were set respectively at 325°C and 8 l/min, while the sheath gas temperature and flow rate were set respectively at 350°C and 11 l/min. The nebulizer pressure was 3.062 atm.

2.7 Reaction Kinetics

Fig. 7a and 7b shows the effects of different dosages of Fe(II) and Fe(0) on activating persulfate (PS) in debating Na_2S, respectively. It can be seen in Fig. 7a that PS was able to oxidize 19.86% of Na_2S without the addition of catalyst Fe(II), which meant that PS alone could oxidize organic matter at a slower rate. The addition of 0.10 g/l of Fe(II) was able to achieve an optimal Na_2S removal (C/C_0=0.455) in the presence of PS.

*Figure 7 can be found in the Appendix section.

Subsequently, the dosage of Fe(II) was increased from 0.20 to 0.50 g/l, which brought about a gradual decrease in the Na_2S removal rate (0.50 g/l of Fe(II) corresponding to C/C_0=0.706). This indicated that too much Fe(II) did not favour the catalytic reaction rate. The reaction of Fe(II) activating PS to generate $SO_4^{-\bullet}$, [56], is shown in Eq. 11:

$$Fe^{2+} + S_2O_8^{2-} \rightarrow Fe^{3+} + SO_4^{2-} + SO_4^{-\bullet} \quad (11)$$

From this equation, Fe(II) is able to be oxidized to Fe(III) by PS, while PS is reduced to $SO_4^{-\bullet}$ and SO_4^{2-}. However, the excess Fe(II) will react with the $SO_4^{-\bullet}$ formed in the water, converting $SO_4^{-\bullet}$ to SO_4^{2-}, [57], [58] and thus losing the ability to degrade organic matter (Eq. 12):

$$Fe^{2+} + SO_4^{-\bullet} \rightarrow Fe^{3+} + SO_4^{2-} \quad (12)$$

Therefore, the optimization of the Fe(II) and PS dosing ratio is beneficial to the improvement of degradation efficiency. Fig. 7b exhibits the trend of BPA degradation in Fe(0)/PS system. In contrast to the trend in Fig. 7a, the residual concentration of Na_2S decreased gradually as the dosage of Fe(0) was increased from 0 to 0.50 g/l. The best Na_2S removal (C/C_0=0.514) was achieved within 60 min with 0.50 g/l of Fe(0). While for the Fe(II)/PS system, the best Na_2S removal was acquired at Fe(II) of 0.10 g/l (C/C_0=0.455). Since the activation of Fe(0) on PS is hetero-phasic, whereas the activation of Fe(II) on PS

is homo-phasic, the performance on the optimal concentrations of the two catalysts is not consistent. In fact, the activation of PS by Fe(0) is an indirect process. Fe(0) should first be converted to Fe(II) before the reaction of Eq. 11 occurs to activate PS. Fe(0) can be converted to Fe(II) under three conditions, [59], are shown in Eq. 13, Eq. 14, and Eq. 15:

$$Fe^0 + S_2O_8^{2-} \rightarrow Fe^{2+} + SO_4^{2-} \quad (13)$$

$$Fe^0 + H_2O \rightarrow Fe^{2+} + 2OH^- + H_2 \quad (14)$$

$$Fe^0 + H_2O + 0.5O_2 \rightarrow Fe^{2+} + 2OH^- \quad (15)$$

Since Fe(0) catalyses PS in a heterogeneous manner, Fe(0) does not dissolve into solution quickly and is not easily overdosed compared to Fe(II), which becomes an advantage of Fe(0) inactivating PS. Therefore, Fe(0) is able to avoid the problem of quenching $SO_4^{-\bullet}$ by generating too much Fe(II) in the reaction.

Fig. 8a and 8b develops the kinetic models of Na_2S degradation by Fe(II)/PS and Fe(0)/PS, respectively. The degradation of Na_2S at varying dosages of Fe(II) and Fe(0) was in accordance with the pseudo first-order kinetic equations. The correlation coefficients (R^2) of the established equations were all above 0.93. In Fig. 8a, when Fe(II) was 0.10 g/l, the degradation of Na_2S obtained the maximum rate of 0.01171 min^{-1}. In Fig. 8b, the maximum Na_2S degradation rate occurred at 0.50 g/l of Fe(0).

*Figure 8 can be found in the Appendix section.

Fig. 9a depicts the changes in Na_2S removal at different PS concentrations with the addition of Fe(II). As can be seen from Fig. 9a, Fe(II) had no ability to remove Na_2S at all when the PS concentration was 0 mM. Unlike Fe(II), Fe(0) exhibited limited removal of Na_2S (60 min, C/C_0=0.801) in the absence of PS (Fig. 9b), which should be attributed to the adsorption and reduction of Na_2S by nano-sized Fe(0) possessing a large specific surface area.

*Figure 9 can be found in the Appendix section.

In Fig. 9a, as the PS concentration increased from 0.20 to 0.40 mM, the residual concentration of Na_2S in the solution continued to decrease. However, at a PS concentration of 0.50 mM, it was found that the change in Na_2S removal was not significant compared to that at a PS concentration of 0.40 mM. This indicated that the best treatment effect of Na_2S was achieved at PS of 0.40 mM. Similar results were obtained in a previous study which showed that a high concentration PS could inhibit the degradation of organics in Fe(II)/PS system, [59]. Although, PS as an oxidant could provide $SO_4^{-\bullet}$ through Fe(II) catalysing excess PS could react with the $SO_4^{-\bullet}$, [60], [61] and reduce the amount of $SO_4^{-\bullet}$ in the solution, thus inhibiting the degradation of organics (Eq. 16):

$$S_2O_8^{2-} + SO_4^{-\bullet} \rightarrow S_2O_8^{-\bullet} + SO_4^{2-} \quad (16)$$

However, it was found from Fig. 9b that the increase in Fe(0) concentration from 0.10 to 0.50 mM did not bring about the inhibition of Na_2S degradation, and the best Na_2S removal was achieved at 0.50 mM of PS. Compared to Fe(II) for PS catalysis, 0.50 mM of PS was not excessive in the Fe(0) catalysis process. The reason may be that one part of the PS reacted with Fe(0) and oxidized it to Fe(II). Another part of PS reacted with the generated Fe(II) to produce $SO_4^{-\bullet}$.

Fig. 10a demonstrates the kinetic models of Na_2S degradation by Fe(II)/PS at varying PS concentrations. According to the curves in Fig. 10a, $1/C_t$ exhibited a good linear fit to time in the presence of PS with a high linear fit coefficient ($R^2 \geq 0.87132$), indicating that the degradation of Na_2S followed the pseudo-secondary kinetic model well. The maximum reaction rate of 0.01484 $(mg/l)^{-1}.min^{-1}$ was achieved when the PS concentration was 0.4 mM.

*Figure 10 can be found in the Appendix section.

The curves in Fig. 10b revealed that the degradation of Na_2S at different PS concentrations in Fe(0)/PS conformed to the pseudo first-order kinetic equation. At a PS concentration of 0.5 mM, the degradation rate of Na_2S could reach 0.02366 $(mg/l)^{-1}.min^{-1}$. Na_2S showed different degradation kinetics in Fe(II)/PS vs. Fe(0)/PS systems. This may be caused by the difference in the homogeneous catalysis of Fe(II)/PS and the heterogeneous catalysis of Fe(0)/PS.

Fig. 11a and 11b expresses the variation of residual Na_2S concentration in the solution after degradation of Na_2S by Fe(II)/PS and Fe(0)/PS at varying initial Na_2S concentrations, respectively.

*Figure 11 can be found in the Appendix section.

Fig. 11a and 11b shows the same trend, i.e., the Na_2S removal effect gradually decreased as the initial Na_2S concentration increased from 1 mg/l to 5 mg/l. When the initial concentration of Na_2S was 1 mg/l, the removal rate of Na_2S was 82.12% in Fe(II)/PS

system, and 83.41% in Fe(0)/PS system. When the initial concentration of Na_2S was increased to 5 mg/l, the removal rate of Na_2S decreased to 55.33% in Fe(II)/PS system and 45.63% in Fe(0)/PS system. This indicated that the increase in the concentration of the target pollutant (Na_2S) decreased the Na_2S degradation efficiency with a constant number of PS and catalyst (Fe(II) or Fe(0)). Therefore, to obtain higher Na_2S removal, the amount of catalyst and oxidant needs to be increased proportionally while increasing the initial concentration of Na_2S.

The kinetic of Na_2S degradation were fitted in Fig. 12a and 12b, and the Na_2S degradation in both systems Fe(0)/PS and Fe(II)/PS conformed to the pseudo first-order kinetic equation ($R^2 \geq 0.94$). When the initial concentration of Na_2S was 1 mg/l, the degradation kinetic constant was 0.02537 $(mg/l)^{-1}.min^{-1}$ in Fe(II)/PS system and 0.02854 $(mg/l)^{-1}.min^{-1}$ in Fe(0)/PS system.

*Figure 12 can be found in the Appendix section.

When Na_2S was increased to 5 mg/l, the kinetic constant of Na_2S degradation decreased to 0.01232 $(mg/l)^{-1}.min^{-1}$ in the Fe(II)/PS system, and 0.00994 $(mg/l)^{-1}.min^{-1}$ in the Fe(0)/PS system, which was consistent with the trend of Na_2S residual concentration in aqueous solution in Fig. 11a and 11b.

Temperature is an important factor affecting the rate of chemical reactions. The effect of varying temperatures on Na_2S removal in systems Fe(II)/PS and Fe(0)/PS are given in Fig. 13a and 13b, respectively.

*Figure 13 can be found in the Appendix section.

With only PS in the system, the degradation rates of Na_2S, in Fig. 13a and 13b all increased with the temperature rising. The degradation of Na_2S via PS was close to 40% at the temperature of 70°C in both Figures. According to previous studies, [62], [63], [64], PS could be activated by heat to form $SO_4^{-\bullet}$, which in turn improved the degradation efficiency of organic matter in Eq. 17:

$$S_2O_8^{2-} \xrightarrow{Heat} 2SO_4^{-\bullet} \quad (17)$$

The elevation in temperature could increase the energy of the reaction system. As this energy exceeded the peroxide bond energy of PS, the peroxide bond broke and $SO_4^{-\bullet}$ was formed. When both Fe(II) [or Fe(0)] and PS were present in the Na_2S solution, Fe(II) [or Fe(0)] could activate PS together with the heat energy brought by the high temperature and produce more $SO_4^{-\bullet}$. Thus, at 70°C, the removal of Na_2S reached 96.70% by Fe(II)/PS and reached 94.50% by Fe(0)/PS, respectively.

Fig. 14a and 14b shows the kinetic models of Na_2S degradation at varying temperature conditions in the Fe(II)/PS system and Fe(0)/PS system, respectively. The pseudo first-order reaction kinetic equations ($R^2 \geq 0.80025$) were applied to the degradation of Na_2S at different temperatures in both Fig. 14a and 14b. The degradation rates of Na_2S by the Fe(II)/PS system and Fe(0)/PS system at 70°C reached 0.06130 $(mg/l)^{-1}.min^{-1}$ and 0.03866 $(mg/l)^{-1}.min^{-1}$, respectively.

*Figure 14 can be found in the Appendix section.

In order to assess the relationship between the reaction temperature and degradation rate of Na_2S, the Arrhenius equation, [63], (Eq. 18) was used to fit the experimental data to investigate the correlation.

$$k_{app} = A\, exp\left(\frac{-E_a}{RT}\right) \leftrightarrow lnk_{app} = lnA - \frac{E_a}{R}\frac{1}{T} \quad (18)$$

where, k_{app} is the apparent rate constant (min^{-1}), A is the pre-exponential factor (min^{-1}), R is the gas constant (8.314 J/K.mol), T is the absolute temperature (K°), and E_a is the activation energy (J/mol).

The established thermodynamic equations are shown in Fig. 15a and 15b. In the Fe(II)/persulfate system, R^2, A and E_a were 0.94923, 1139.67 min^{-1}, and $2.8x10^7$ J/mol, respectively, which showed that the relationship between the Na_2S degradation rate and the temperature satisfied the Arrhenius equation, while in Fe(0)/persulfate, the heterogeneous activation system Fe(0)/persulfate acquired a low R^2 when fitting into the Arrhenious equation. This may be because the process of heterogenous activation involves the release of Fe(0) to Fe(II), which makes the thermodynamic laws difficult to obtained.

*Figure 15 can be found in the Appendix section.

The initial pH value of solution is an important factor affecting the chemical reaction. Therefore, the degradation of Na_2S by two systems under different initial pH values was studied. Only the initial pH value in the whole reaction process was not controlled. Fig. 16a and 16b reflected the effect of changing pH values on the degradation of Na_2S by Fe(II)/PS and Fe(0)/PS.

*Figure 16 can be found in the Appendix section.

It was found that in Fig. 16a and 16b, pH=5.0 was the optimal condition for both systems. The degradation of Na_2S was poor in both systems under alkaline conditions. On the one hand, the oxidation capacity of the systems was reduced due to the reaction of SO_4^{2-}• radicals converted to OH• radicals in the presence of OH, [65], in Eq. 19.

$$SO_4^{-\bullet} + OH^- \rightarrow SO_4^{-2} + OH^{\bullet} \quad (19)$$

On the other hand, the formation of $Fe(OH)_3$ could lead to the inhibition of the catalytic reaction in Eq. 20:

$$Fe^{3+} + 3OH^- \rightarrow Fe(OH)_3 \quad (20)$$

In the practical application of these two systems, if 5.0 is set as the best pH value, it needs to consume chemical regulators. In addition, the requirements for the corrosion resistance of pipelines have also been improved. One suggestion is that under the condition that partial removal of Na_2S is allowed in the pretreatment stage, it can be considered to degrade Na_2S at pH=6.5.

The kinetic equation for the degradation of Na_2S by the F(II)/PS and Fe(0)/PS systems at different pH values are given in Fig. 17a and 17b, respectively. The Na_2S degradation curves satisfied the pseudo first-order kinetic equation ($R^2 \geq 0.90$) except for the degradation of Na_2S by the Fe(0)/PS system at pH=9.0. The maximum kinetic constant [0.02818 $(mg/l)^{-1}.min^{-1}$] appeared in the Fe(0)/PS system at pH=5.0.

*Figure 17 can be found in the Appendix section.

2.8 Quenching Experiments and Mechanism Analysis

In order identify which type of free radicals appeared in the reaction, methanol [Me(OH)] and tert-Butyl alcohol (TBA) were used as extinguishing agents to investigate the degree of inhibition of the chemical reaction. MeOH is an effective scavenger for both OH• ($k=9.7x10^8$ $M^{-1}.s^{-1}$) and SO_4^{-}• ($k=1.1x10^7$ $M^{-1}.s^{-1}$), while TBA is an effective scavenger for OH● ($k=6.0x10^8$ $M^{-1}.s^{-1}$), but not for SO_4^{-}• ($k=9.1x10^5$ $M^{-1}.s^{-1}$), [66]. Fig. 18a and 18b exhibits Na_2S degradation in the presence of either MeOH or TBA in the Fe(II)/PS and Fe(0)/PS systems, respectively. Both MeOH and TBA were found to inhibit Na_2S degradation in both systems. The inhibitory effect of Me(OH) on the two systems was greater than that of TBA. It suggested that both SO_4^{-}• and OH• played roles in the oxidation of Na_2S in the two systems.

*Figure 18 can be found in the Appendix section.

Fig. 19 depicts the mechanism of PS activation and Na_2S degradation in the presence of Fe(II) and Fe(0) catalysts. In the Fe(0)/PS system, Fe(0) is first transformed into Fe(II) through three pathways [Eq. 13, Eq. 14 and Eq. 15], thus playing the role of activating PS. In the Fe(II)/PS system, the dissolved Fe(II) directly undergoes a redox reaction with PS to generate SO_4^{-}• and Fe(III) (Eq. 12). Fe(III) can be transformed into Fe(II) with the gain of an electron. Therefore, Fe(II) and Fe(III) in solution can stably activate PS if they are in a sustainable equilibrium. At the same time, when the OH^- concentration in the solution is high, it can react with SO_4^{-}• to generate OH• radicals, which also has a good oxidation effect on organic matter. However, under the combined action of SO_4^{-}• and OH•, Na_2S can be oxidized and the final products will be H_2O and CO_2.

*Figure 19 can be found in the Appendix section.

2.9 The Degradation Mechanism of SO_4^{2-}

It was well known that in the Fe(II)/PS system, the removal of pollutants could also be achieved by the coagulation of Fe^{3+} and the direct oxidation of $S_2O_8^{2-}$. The addition of SO_4^{2-} generated complexes $FeSO_4^+$ and $Fe(SO_4)_2^-$ with Fe^{3+}, which led to a decrease of the coagulation process (Eq. 21 and Eq. 22):

$$SO_4^{-\bullet} + H_2O \rightarrow SO_4^{2-} + OH^{\bullet} + H^+ \quad (21)$$

$$SO_4^{-\bullet} + OH^- \rightarrow SO_4^{2-} + OH^{\bullet} \quad (22)$$

Electron paramagnetic resonance (EPR) experiments were performed to further confirm the inhibition of the generation of free radicals by SO_4^{2-} in the Fe(II)/PS system. The ab sorption spectrum of DMPO-OH• (marked by inverted triangles) indicated that OH• (hyperfine splitting constant: a_H=14.87 G, and a_N=14.87 G) was generated in the Fe(II)/PS system. There were also absorption signals of DMPO-SO_4^{-}• in the diamond-shaped marker, indicating that SO_4^{-}• (hyperfine splitting constants: a_H=10.09 G, a_N=13.94 G, $a_{H\gamma1}$=1.6 G, and $a_{H\gamma2}$=0.8 G) was generated in the system. Most importantly, it was showed that the signal intensity of SO_4^{-}• and OH• became significantly weaker after SO_4^{2-} was added, which further confirmed that SO_4^{2-} could inhibit the generation of free radicals. The presence of SO_4^{2-} not only inhibited the production of SO_4^{-}•, but also reduced the oxidation potential of the system. The SO_4^{-}• in the system was mainly generated through

reaction as Eq. 23, and the consumption of $SO_4^{-\bullet}$ could be simplified as Eq. 24, then the corresponding Nernst equation was as Eq. 25:

$$Fe^{2+} + S_2O_8^{2-} \rightarrow SO_4^{2-} + Fe^{3+}\ k = 17\ M^{-1}s^{-1} \quad (23)$$

$$SO_4^{-\bullet} + e^- \rightarrow SO_4^{2-} \quad (24)$$

$$E\left(SO_4^{-\bullet}\right) = E^{\theta}_{\left(\frac{SO_4^{-\bullet}}{SO_4^{-\bullet}}\right)} + \frac{RT}{zF} ln \frac{[SO_4^{-\bullet}]}{[SO_4^{2-}]} \quad (25)$$

where, $E^{\theta}_{(SO_4^{-\bullet}/SO_4^{2-})}$; was the standard half-reaction reduction potential, R; was the universal gas constant (8.314472 J/K.mol), T; was the absolute temperature, F; was the Faraday constant (9.63845x10^4 C/mol), z; was the number of electrons transferred in the half-reaction, which was 1 in this equation.

From Eq. 25, the oxidation-reduction potential of E($SO_4^{-\bullet}$/SO_4^{2-}) was influenced by the concentration of SO_4^{2-}, and the higher the concentration of SO_4^{2-}, the lower the E($SO_4^{-\bullet}$/SO_4^{2-}). The E($SO_4^{-\bullet}$/SO_4^{2-}) gradually decreased as the concentration of SO_4^{2-} increased, and when the concentration of SO_4^{2-} increased from 0 to 6 g/l, the oxidation-reduction potential of E($SO_4^{-\bullet}$/SO_4^{2-}) decreased by 0.14 V, which was corresponded to the decreased degradation efficiency of Sulfur Black 1 as sulfate concentration. The decreased reaction rate constant k_{obs} after the addition of SO_4^{2-} could also be explained that the presence of SO_4^{2-} reduced the oxidation-reduction potential of E($SO_4^{-\bullet}$/SO_4^{2-}), and therefore decreased the degradation efficiency of Sulfur Black 1.

3 Results and Discussions

3.1 The Degradation of Sulfur Black 1 by Fe^0-Sodium Persulfate System

The degradation efficiency of Sulfur Black 1 by the Fe^0-sodium persulfate system was evaluated under various conditions. As shown in Fig. 20a, 96% of 50 mg/l sulphur Black 1 was degraded by the Fe^0-sodium persulfate system within 60 min, whereas negligible degradation occurred when Fe^0 particles or sodium persulfate were applied individually.

*Figure 20 can be found in the Appendix section.

The efficient degradation of Sulfur Black 1 by the Fe^0-sodium persulfate system can be attributed to the production of reactive radicals (e.g., $SO_4^{2-\bullet}$ and $OH^{\bullet}$) through the activation of sodium persulfate by Fe^0 [Eq. 26, Eq. 27 and Eq. 28], [67], [68]:

$$S_2O_8^{-2} + Fe^0 \rightarrow 2SO_4^{-\bullet} + Fe^{+2} \quad (26)$$

$$S_2O_8^{-2} + Fe^{+2} \rightarrow SO_4^{-2} + SO_4^{-\bullet} + Fe^{+3} \quad (27)$$

$$SO_4^{-\bullet} + OH^- \rightarrow SO_4^{-2} + OH^{\bullet} \quad (28)$$

3.2 Mathematical Model for pH and Temperature Dependence of Sulphide Removal

Let S[t] be the concentration of SO_4^{2-} at time t and C[t] be a concentration of H_2S at time t. While n is the number of days of the experiment. The H_2S species predominated the system since the pH was 4.0 to 6.0. Therefore, it was selected and presented in the mathematical model as the sulphide reduced specie as follows: Eq. 29 represents the rate of change of S[t] as function of time:

$$\frac{dS[t]}{dt} = -2f(pH,T)\left(t - \frac{\tau}{n}\right)S(t) \quad (29)$$

Where, *f(pH,T)* is the contribution function of pH and temperature during the reaction. According to the experimental data, the influence of pH in the sulphate reduction rate was higher than the influence of the temperature, which was taken into consideration in this mathematical model. The function is generalized and can be constructed for any given reaction. In Eq. (30), τ is the time delay due to acclimatization of bacteria for the sulphate reduction process to start. Eq. (30) can therefore be reformulated into Eq. (31) as follows:

$$\frac{dS[t]}{S[t]} = -2f(pH,T)\left(t - \frac{\tau}{n}\right)dt \quad (30)$$

$$\ln[S(t)] = -f(pH,T)[\left(t - \frac{\tau}{n}\right)]^2 \quad (31)$$

With the integration of Eq. (30) into Eq. (31), the determination of sulphate concentration (S[t]) at a set time can be archived by Eq. (32) below where S[0] is the initial concentration of SO_4^{2-} before the start of the reaction. According to the observed data, at the beginning of the reaction, there is no biogenic concentration of H_2S from sulphate reduction of the initial concentrations, this implies C[0] = 0. The stoichiometric relation between H_2S/ SO_4^{2-} is thus 1/3:

$$S[t] = S[0]\exp[-f(pH,T)\left(t - \frac{\tau}{n}\right)^2] \quad (32)$$

With consideration in a progressive reduction process, the end of the process would be indicated and

proven by complete reduction of SO_4^{2-} and that factor can be incorporated in the model using Eq. (33) and Eq. (34) where C[t] is represented.

$$C[n] = \frac{1}{3}S[0] \quad (33)$$

$$\frac{dC[t]}{dt} = 2Af(pH,T) \quad (34)$$

Thus, by solving Eq. (33) and Eq. (34) using the classical method of ordinary differential equation, Eq. (35):

$$C[t] = K - Bexp[f(pH,T)\left(t - \frac{\tau}{n}\right)^2] \quad (35)$$

It was obtained as the following solution for C[t] determination. From Eq. (35), applying the initial and boundaries conditions of pH and temperature, the calculated yields Eq. (36):

$$C[t] = \frac{S[0]\left\{\left[Exp\left[-f(pH,T)\left(-\frac{\tau}{n}\right)^2\right]\right] - Exp[-f(pH,T)(t-\frac{\tau}{n})^{2]}\right\}}{3(Exp\left[-f(pH,T)\left(-\frac{\tau}{n}\right)^2\right] - Exp\left[-f(pH,T)\left(21-\frac{\tau}{n}\right)^2\right])} \quad (36)$$

The final mathematical model of SO_4^{2-} reduction to H_2S is therefore suggested to be as shown in a complex model Eq. (37) where all parameters are incorporated.

$$\begin{cases} S(t) = S[0]\exp\left[-f(pH,T)\left(t-\frac{\tau}{n}\right)^2\right] \\ C[t] = \frac{S[0]\{\left[Exp\left[-f(pH,T)\left(-\frac{\tau}{n}\right)^2\right]\right] - Exp\left[-f(pH,T)\left(t-\frac{\tau}{n}\right)^2\right]\}}{3(Exp\left[-f(pH,T)\left(-\frac{\tau}{n}\right)^2\right] - Exp\left[-f(pH,T)\left(21-\frac{\tau}{n}\right)^2\right])} \end{cases} \quad (37)$$

The above presented model was calibrated and vali-dated using an experimental chemical data. However, minor deviations between experimental data and the mathematical model were observed as depicted in Fig. 21.

*Figure 21 can be found in the Appendix section.

Sulphate-reducing process is governed by environmental factors such as pH and temperature which require control and monitoring in a closed system. Specifically, it was confirmed that low pH exerts a higher inhibitory effect than low temperature with evidence that different SO species affect bacteria differently under varied environmental conditions. The synergistic effect of these two physicochemical parameters was observed to be control-ling the speciation and solubility of inorganic compounds such as S^0-reduced species (H_2S/HS^-) and organic acids such as acetic acid, which significantly decreased the sulphate reduction activity of the anaerobic consortium.

The efficient Sulfur Black 1 degradation was observed over an initial pH range of 6.0–9.0. The efficiency was significantly inhibited when the initial pH increased to 10.0–11.0 (Fig. 20b), likely due to the fast passivation of Fe^0 particles. Ferric iron generated from the reaction between Fe^0 and sodium persulfate, hydrolysed to form ferric hydroxides (Eq. 38), which were deposited on the surface of Fe^0 particles and hindered the activation of sodium persulfate, [69], [70].

$$3OH^- + Fe^{+3} \rightarrow Fe(OH)_3 \downarrow \quad (38)$$

The results suggest that the Fe^0-sodium persulfate system can efficiently degrade sulphur Black 1 at pH 5.0– 9.0. The effects of sodium persulfate and Fe^0 dosages on the sulphur Black 1 degradation efficiency by the Fe^0-sodium persulfate system at pH=6.0 were also evaluated. Fig. 2c shows that a positive correlation between the sodium persulfate dosage and the Sulfur Black 1 degradation efficiency when the Fe^0 dosage was fixed 1.0 g/l. Increasing Fe^0 dosage from 0.5 to 1.5 g/l generally increased the Sulfur Black 1 degradation efficiency significantly. Although, the evaluated sodium persulfate and Fe^0 dosages can accelerate the Sulfur Black 1 degradation via enhancing the production of $SO_4^{2-\bullet}$ and $OH^\bullet$, high chemical costs and residual chemicals in the treated wastewater were the potential issues. For instance, the residual sodium persulfate may cause adverse impacts on the subsequent microbial treatment process. Therefore, the optimal sodium persulfate and Fe^0 dosages to achieve efficient Sulfur Black 1 degradation were set at 0.75 g/l and 1.0 g/l, respectively.

3.3 Complete sulphur Black 1 Degradation and Sulphide Production by the sulphur-Circular Process

Long-term operation experiments were performed to investigate the complete Sulfur Black 1 degradation in simulated Sulfur Black 1 dyeing wastewater and sulfide production by the sulfur-circular process. The AOP reactor was operated under the optimal conditions determined in Section 3.1. The dosages of sodium persulfate and Fe^0 were 0.75 and 1.0 g/l,

respectively. The degradation efficiency of SB 1 in the AOP reactor within a reaction time of 60 min was around 92%. Due to the decomposition of sodium persulfate into sulfuric acid, [9], [71], the pH of the simulated sulphur Black 1
dyeing wastewater decreased from pH=6.0 to approximately pH=3.0. Meanwhile, the decomposition of persulfate and oxidation of organic sulfur in Sulfur Black 1 during the AOP treatment resulted in the formation of 500–750 mgS/l sulfate, which can serve as the sulfur source and electron acceptors for the subsequent microbial treatment.

The UAPBSR reactor was set up to evaluate the complete degradation of organic AOP by-products and sulfide production (Fig. 22). During the startup phase (Step 1), only synthetic domestic wastewater containing 100 mgS/l sulfate and 106 mgC/l TOC was provided to stimulate the accumulation of sulfate-reducing bacteria (SRB) in the UAPBSR reactor. From Step 2–4, a mixture of AOP-treated Sulpfur Black1 dyeing wastewater and domestic wastewater at volume ratios of 1:2.5–1:1.3 was pumped into the UAPBSR (Fig. 22a). As shown in Fig. 22a, the TOC removal efficiency gradually increased and then stabilized at approximately 80% in Step 1. The TOC removal rate reached 0.05 kgC/(m^3.d). The microbial reduction of sulfate was also observed, resulting in the production of dissolved sulfide.

*Figure 22 can be found in the Appendix section.

As shown in Fig. 22b, about 75 mgS/l dissolved sulfide was detected in the effluents of the UAPBSR, with a sulfide production rate of 0.036 kg S/(m^3·d) in Step 1. When the volume ratio of AOP-treated Sulfur Black 1 dyeing wastewater to domestic wastewater was stepwise increased from 1.0/2.5 to 1.0/1.3 in Step 2-4, the TOC removal efficiency was not significantly affected and maintained around 80%. On the other hand, the provision of AOP-treated Sulfur Black 1 dyeing wastewater increased the average sulfide production rate to 0.07 kgS/(m^3.d) in Step 2 and Step 3. The average sulfide concentrations in the effluent increased to 90 mgS/l in Step 2 and 70 mgS/l in Step 3. The enhanced sulfide production can be due to more sulfate and TOC derived from the AOP-treated Sulfur Black 1 dyeing wastewater. Although, the average sulfide production rate dropped to 0.04 kgS/(m^3.d) in Step 4, it was still higher than that in Step 1. The above findings suggest that the microbial sulfate reduction can induce the complete degradation of organic by-products generated from the AOP treatment and efficient production of dissolved sulfide. The sulfur-circular process was capable of minimizing the potential risks associated with the organic AOP by-products, which are often toxic, [10], [11]. Meanwhile, the conversion of sulfate into dissolved sulfide also ensured the possibility of Na_2S recovery from the dyeing wastewater.

3.4 Na_2S Recovery by Stripping and Absorption, and sulphur Mass Balance

Stripping and adsorption experiments were performed to evaluate the Na_2S recovery from the effluents of the UAPBSR reactor. The sulphide- laden effluents collected in Steps 2–4 was stripped, and then the resulting H_2S gas was absorbed by a NaOH solution. As shown in Table 2, over 99.90% of dissolved sulphide was stripped out in the form of H_2S gas, which was then absorbed in the NaOH solution, achieving an absorption efficiency of 99.90%.

*Table 2 can be found in the Appendix section.

Consequently, more than 99.80% of dissolved sulphide in the UAPBSR effluents was recovered as Na_2S (Eq. 39, Eq. 40 and Eq. 41). It is noteworthy that the pH value of the UAPBSR effluent was adjusted to 6.0 using 0.1 M HCl to convert the dissolved sulfide into molecular H_2S(aq), considering its first dissociation constant (pK_{a1} =7.0). Moreover, nitrogen gas [N_2(g)] was used as a carrier gas for H_2S stripping to prevent the potential oxidation of H_2S. The N_2(g), after ab sorption, can be recirculated to the stripper, reducing the costs associated with the carrier gas. In real applications, the sulfide-laden effluent of the UAPBSR can be recirculated and mixed with the acidic AOP-treated wastewater (pH≈3.0). This approach is expected to minimize the consumption of alkali and acid for pH adjustment in the sulfur-circular process.

$$HS^- + H^+ \leftrightarrow H_2S_{(aq)} \quad (39)$$

$$H_2S_{(aq)} \leftrightarrow H_2S_{(g)} \quad (40)$$

$$H_2S_{(g)} + NaOH \leftrightarrow Na_2S + H_2O \quad (41)$$

3.5 Sulfur Mass Balance and Cost-Effectiveness

The sulphur mass balance was estimated to reveal the transformation of sulphur substances during the treatment of sulphur Black 1 dyeing wastewater by the sulphur-circular process. The effluents of the AOP reactor and domestic wastewater contributed to the sulphate in the in fluents of the UAPBSR reactor, ranging from 191 to 484 mgS/l. 42.70%– 64.20% of sulphate in the mixture was reduced, resulting in the formation of 35–132 mgS/l sulphide in the UAPBSR

reactor. 99.82% of dissolved sulfide generated in the UAPBSR reactor was converted into Na_2S through stripping and adsorption. The sulfur mass flow within the sulphur-circular process in the Step 2 is further condition. During the treat ment of 1 m^3 mixed wastewater (comprising Sulfur Black 1 dyeing wastewater and domestic wastewater at a volume ratio of 1/2.5), the total sulfur input was 220 g, and 90 g of sulphur was recovered in the form of Na_2S. This resulted in an overall sulfur recovery rate of 41%. The recovered Na_2S is a value-add product and can be reused as a low-cost solubilizing agent for the Sulfur Black 1 dyeing process. The cost-effectiveness of the Sulphur-circular process was estimated. The chemical cost associated with Sulfur Black 1 dye removal and the profit generated from Na_2 S recovery were quantified. The treatment of 1 m^3 mixed wastewater incurred a chemical cost of US $ 0.39, while the Na_2 S recovery yielded a profit of US $ 0.23/m^3, resulting in a net chemical cost of US $ 0.19/m^3. The Na_2S recovery from the Sjulfur Black 1 dyeing wastewater significantly offset the wastewater treatment costs and minimized the secondary pollution associated with the residual sulfate and sulfide in the treated wastewater. Discharge of wastewater containing sulfate and sulfide may cause issues in sewer systems and receiving water bodies, such as odour nuisance and river blackening, [30], [72]. Although, the conventional AOPs (e.g., UV/H_2O_2 and Fe^{+3}/persulfate systems) are also effective in the treatment of dyeing wastewater, [8], [9], their high chemical costs and formation of toxic organic by-products raise economic and environmental concerns, [10], [11]. In contrast, the sulfur-circular process offers a superior alternative by enabling complete degradation of refractory dyes at lower chemical costs. Therefore, the sulfur-circular process can be a cost-effective and environmentally-friendly approach for the treatment of sulfur dyeing wastewater. Further pilot tests are needed to refine the operational parameters of this technology according to the conditions of actual dyeing wastewater.

3.6 Microbial Community Compositions

To investigate the diversity and structure of microbial communities in the UAPBSR reactor, the sludge samples were collected in different stages (Days 150, 300, 450, and 600) and analysed by shotgun metagenomic sequencing. The Shannon, Simpson, Chao and Ace indices for D150-M, D300-M and D450-M decreased as the volume ratio of AOP-treated Sulfur Black 1 dyeing wastewater to domestic wastewater increased from 1.0/2.5 to 1.0/1.3 in Steps 2-4, indicating a reduction in microbial diversity. The changes may be attributed to the enrichment of bacteria responsible for degrading organic sulphur Black 1 AOP by-products. The decrease in diversity indicated a reduction in the richness and variety of microorganisms in the UAPBSR reactor, although, the functional microorganisms increased. On Day 600, the microbial diversity in the middle of the UAPBSR reactor (D600-M) was slightly higher than that at the bottom and top of the UAPBSR reactor (D600-B and D600-T). This variation was likely due to differences in dissolved oxygen, organic carbon sources and sulfate along with the pH were different at various heights within the UAPBSR reactor, leading to slightly different microbial compositions at different heights. At the phylum level, 8 major phyla were identified, such as *Proteobacteria* (18.10%–33.70%), *Desulfobacterota* (6.0%–22.10%), *Actinobacteriota* (7.40%–24.20%), and *Firmicutes* (5.20%–21.60%). At the genus level, bacteria associated with the degradation of organic AOP by-products and microbial sulfate reduction were identified. *Desulfovibrio* and *Desulfobacter*, known as sulfate reduction bacteria (SRB), were identified, and their total relative abundances increased from 2.30% to 14.40% after the introduction of the AOP-treated Sulfur Black 1 wastewater in Steps 2-4. This trend was consistent with the enhanced sulfate reduction observed (Fig. 5b). Additionally, three fermentative genera, including *Lactococcus*, *Acidipropionibacterium*, and *Lacticaseibacillus*, were identified, with their relative abundances increasing from 5.20% to 13.90%. These fermentative bacteria are capable of transforming high-molecular-weight organics into low-molecular-weight organics (e.g., volatile fatty acids), [73], [74], [75]. The abundance changes suggest that these fermentative bacteria played important roles in degrading high-molecular-weight organic AOP by-products.

3.7 Sulfur Black 1 Transformation Products

The sulphur Black 1 precursors are a group of complex organic compounds, and their structures still remain unknown, [76], [77], [78]. To mimic the real dyeing process, the Sulfur Black 1 solution was prepared by mixing Sulfur Black 1 precursors $Na_2S.9H_2O$ a mass ratio of 1/2, followed by boiling the mixture for 30 min. This process con verted the insoluble Sulfur Black 1 precursors into soluble substantive forms and also complicated the molecular structures of Sulfur Black 1, [76], [79]. Therefore, the chemical compositions of the original Sulfur Black 1 and the Sulfur Black 1 after being treated by AOP and UAPBSR reactors were analysed using LC-Q-TOF-MS. The mass spectra of the background and the control sample were subtracted from the mass spectrums of the treated samples. Using Qualitative

Navigator B.08.00 (Agilent), the molecular formula calculator was applied to all masses in the mass spectra to determine their molecular formulas. Molecular formulas with the highest scores and abundances exceeding 2000 were selected as identified substances. Duplicate formulas, those appearing in only one sample, and formulas containing unexpected chlorine were excluded. The original Sulfur Black 1 solution consisted of high-molecular-weight com pounds, primarily nitrogen and sulfur-containing organics ($C_mH_nO_x.N_yS_z$). During the AOP treatment, the molecular weights of these compounds gradually decreased due to the attack by $SO_4^{2-\bullet}$ and $OH^{\bullet}$. Following microbial treatment in the UAPBSR reactor, nearly all the organic AOP by-products (MW: 123.20–666.40) were degraded. These observations confirm that the microorganisms in the UAPBSR reactor can efficiently mineralize the toxic organic by-products from the AOP treatment and provide electron donors for the reduction of sulfate into sulfide. Most of Sulfur Black dyes have carcinogenic and teratogenic effects on humans, [4]. The sulfur-circular process enables the complete degradation of Sulfur Black 1 and effective mitigation of them environmental risks, demonstrating significant advantages over conventional AOPs, which often produce toxic organic by-products, [10]. [11].

3.8 Mechanisms of Sulfur Black 1 and Sulfur Transformations

The mechanisms of Sulfur Black 1 and sulfur transformations by the sulfur-circular process were proposed based on the results obtained in this study. The Fe^0-sodium persulfate AOP produced $SO_4^{2-\bullet}$ and $OH^{\bullet}$, which destructed Sulfur Black 1 via various pathways, such as hydrogen abstraction, electron abstraction, N-dealkylation, sulfonation, and desulfonation reactions, [80], [81], [82]. The degradation mechanism of Sulfur Black 1 dyestuff and sulfur (S-2) substance transformation in the sulfur-circular process (FB: fermentative bacteria, SRB: sulfate reduction bacteria, MW: molecular weights) was determined at Fig. 23.

*Figure 23 can be found in the Appendix section.

The AOP treatment decreased the molecular weights of Sulfur Black 1 and generated biodegradable organic AOP by-products and sulfate. In the UAPBSR reactor, fermentative bacteria (e.g., *Lactococcus* and Acid ipropionibacterium) converted the organic AOP by-products into low-molecular-weight organics, which were further mineralized to provide electron donors for SRB (e.g., *Desulfovibrio* and *Desulfobacter*). The microbial sulfate reduction, involving enzymes such as aryl sulfo transferase, alkanesulfonate monooxygenase, and azoreductase, monooxygenases, and dioxygenases, [83], [84], led to the production of sulfide. Sulfide in the effluents of the UAPBSR reactor was ultimately recovered as Na_2S via stripping and adsorption and can be reused as a low-cost solubilizing agent for the Sulfur Black 1 dyeing process (Fig. 23). The combination of persulfate-based advanced oxidation, microbial sulfate reduction, and stripping-adsorption processes simultaneously achieved the complete degradation of toxic Sulfur Black 1 and the recovery of Na_2S from textile dyeing wastewater. The mechanisms revealed in this study can provide key fundamentals for formulating closed-loop technologies to treat wastewater containing refractory dyes and other persistent organic pollutants and also toxic compounds.

Table 3 exhibited all the sulphured compounds mass-balance.

*Table 3 can be found in the Appendix section.

From 100 mol particular organic sulphıde; 96 mol Soluble organic sulphide was produced. The soluble organic sulphide consist from 40 mol methionin, 40 mol cystein and 16 mol CS_2. These organics were removed with yields as high as 99% to SO_4^{2-} then to $S^{o,}$ HS^- and S^{-2}. In the presence of NaOH 50 mol Na_2S was generated. In the effluent water H_2S, HS^- and S^{-2} concentrations was measured as 0.01 mg/l.

3.9 Adsorption Kinetics

A volume (1 ml) of the dispersion solution was pipetted at the specified moment and filtered quickly with a 0.45 mm filter membrane. Then, the equilibrium concentrations of sulfide were quantified by UV-vis absorbance at 665 nm. All tests were repeated multiple times. The removal rate (%) and uptake capacity (Q_e, mg/g) for sulfide under equilibrium condition of the Na_2S concentration were determined from Eq. (42) and Eq. (43), respectively.

$$Removal\ (\%) = \left(\frac{C_0 - C_e}{C_0}\right) x\ 100 \quad (42)$$

$$Q_e = \frac{V}{m}(C_0 - C_e) \quad (43)$$

where, C_0 (mg/l) is the initial concentration of the sulfide solution, C_e (mg/l) is the equilibrium concentration after adsorption, V (liter) is the volume

of the sulfide solution, and *m* (g) is the weight of the adsorbent added.

For kinetic studies, linear pseudo first order, linear pseudo second order and intra-particle diffusion models were used to understand the adsorption mechanism (Table 4). Equivalently, Langmuir and Freundlich adsorption isotherms in linear and non-linear forms were fitted by the sulfide uptake gained at different initial sulfide concentrations to determine the equilibrium adsorption capacity. Thermodynamic studies were carried out to further analyse the adsorption process.

*Table 4 can be found in the Appendix section.

Furthermore, in order to find an appropriate model to fit the adsorption data, the root mean squared error (RMSE) and χ^2 values were used to evaluate the linear and non-linear adsorption isotherm models, combined with the value of the correlation coefficient (R^2) from the regressive analysis. The expressions for the above error functions were calculated as follows in Eq. (44) and Eq. (45):

$$RMSE = \sqrt{\frac{1}{n-2}\sum_{i-1}^{n}\left(Q_{exp} - Q_{cal}\right)^2} \quad (44)$$

$$\chi^2 = \sum_{i-1}^{n}\frac{\left(Q_{exp} - Q_{cal}\right)^2}{Q_{cal}} \quad (45)$$

where Q_{exp}: is the adsorption capacity obtained experimentally, Q_{cal}: is the adsorption capacity calculated from the isotherm, and n is the number of test elements.

Adsorption kinetic analysis was used to investigate the adsorption rate and reaction mechanism of the adsorption process of sulfide by Na_2S. In this work, the adsorption kinetics data were fitted using the pseudo-first-order (PFO) model, pseudo-second-order (PSO) model and intraparticle diffusion (IPD) model, [85]. The corresponding linear plots and parameters of the PFO and PSO models are displayed Table 3, respectively. Q_e is the uptake capacity at the equilibrium of the Na_2S for sulfide, Q_t is the uptake capacity at time "t", k_f represents the pseudo-first-order rate constant and k_s represents the pseudo-second-order rate constant. It can be seen that the correlation coefficient R^2 obtained by the PSO model was larger than that for the PFO model, and the experimentally measured adsorption capacity ($Q_{e(exp)}$=49.54 mg/g) was close to the theoretical value ($Q_{e(cal)}$=50.65 mg/g). This showed that PSO model could better describe the adsorption of sulfide by Na_2S. This behaviour was in agreement with the characterization results obtained from the used Na_2S.

3.9.1 Equilibrium Study

To investigate the sulfide adsorption mechanism and the maximum adsorption capacity on the Na_2S hybrid material, linear and nonlinear plots of Freundlich and Langmuir adsorption isotherms were used and the corresponding parameters are shown in Table 5, respectively.

*Table 5 can be found in the Appendix section.

K_L is the Langmuir adsorption constant, K_F is the reaction rate constant of the Freundlich linear model, and 1/n (dimensionless) is the affinity of adsorption.

According to the R^2 of the adsorption isotherm, the Langmuir linear model results agree with the experimental data better than the Freundlich linear model with the maximum uptake capacity of 173.04 mg/g. This indicates that the adsorption of sulfide by Na_2S was a monolayer adsorption. The Freundlich linear isotherm assumed that the adsorption was multilayer and occurred on heterogeneous surfaces. The value of 1/n obtained from the Freundlich linear equation was between 0.1 and 1.0 1/n, and this isotherm was not favourable to describe the adsorption of sulfide on Na_2S, [86].

R^2, RMSE and χ^2 values were used to determine the most suitable adsorption isotherm model, [87]. As observed from Table 6, the RMSE and χ^2 values of the kinetic constants in Langmuir linear isotherm model were lower than those of the Freundlich linear isotherm model and the other two non-linear isotherm models, which revealed that the Langmuir linear model was the best fitting isotherm. Therefore, the adsorption process of sulfide on Na_2S was monolayer and the maximum adsorption capacity estimated was 173.04 mg/g, which was relatively higher than the values for other sulfide adsorbents presented in the literature (Table 6). Consequently, Na_2S could be used as an effective adsorbent for sulfide.

*Table 6 can be found in the Appendix section.

3.9.2 Thermodynamic Study

It is not sufficient to deter mine the adsorption of sulfide on Na_2S as chemisorption by adsorption kinetics. A thermodynamic study is a good complement to further investigate the adsorption process. The adsorption capacity increased with the increase of temperature, which indicated the endothermic nature of the adsorption process. Three thermodynamic parameters, DG (Gibbs free energy of adsorption), DH (enthalpy change), and DS (entropy change) were employed to better understand the

adsorption process, which can be obtained through, [88], Eq. (46), Eq. (47) and Eq. (48), respectively.

$$K_d = \frac{q_e}{c_e} \quad (46)$$

$$\Delta G = -RTlnK_d \quad (47)$$

$$lnK_d = \frac{\Delta S}{R} - \frac{\Delta H}{RT} \quad (48)$$

where, K_d (l/g) is the equilibrium constant value, q_e (mg/g) is the equilibrium concentration of sulfide on Na_2S, C_e (mg/l) is the equilibrium concentration, R is the gas constant, R=8.314 J/mol.K, and T(K°) is the system temperature. DS (J/mol.K) and DH (kJ/mol) are obtained from the linear plot of ln K_d versus 1/T.

The Van't Hoff plot for sulfide adsorption on Na_2S (Eq. 48). The thermodynamic parameters of Na_2S adsorption of sulfide are presented in Table 7.

*Table 7 can be found in the Appendix section.

The negative ΔG at all temperatures indicates that the adsorption of sulfide by Na_2S is spontaneous. A positive value of ΔH indicates an endothermic adsorption process. ΔS is positive, revealing that the thermodynamic disorder increases during the adsorption of sulfide on Na_2S. In addition, the values calculated for the Gibbs free energy of adsorption were −3.2732, −3.6663 and −3.8776 kJ/mol at 25°C, 35°C and 45°C, respectively.

3.10 Henry's Law

Typical choices for the aqueous phase are molar concentration (c_a), molality (b), and amount fraction (x). For the gas phase, molar concentration (c_g) and partial pressure (p) are often used. Note, however, that it is not possible to use the gas-phase amount fraction (y). At a given gas-phase amount fraction, the aqueous-phase concentration c_a depends on the total pressure, and thus the ratio y/c_a is not a constant.

To specify the exact variant of the Henry's law constant, two superscripts are used. They refer to the numerator and the denominator of the definition. For example, H_s^{cp} refers to the Henry solubility defined as c/p. If H_s refers to the reference temperature T^θ=298.15°K, it will be denoted as H_s^θ.

In spite of the name Henry's law constant, it should be kept in mind that its value still depends on some parameters, e.g., the temperature T. The temperature dependence of equilibrium constants can be described with the van't Hoff equation, which also applies to Henry's law, [89], (Eq. 40):

$$\frac{dlnH_s}{d(1/T)} = \frac{-\Delta_{sol}H}{R} \quad (49)$$

where, $\Delta_{sol}H$ is the enthalpy of dissolution, and R is the gas constant. Note that the letter H in the symbol $\Delta solH$ refers to enthalpy and is not related to the letter H for Henry's law constants. Integrating the above equation leads to seen in Eq. (50):

$$lnH_s = \frac{-\Delta_{sol}H}{R}\frac{1}{T} + const. \quad (50)$$

Calling the constant of integration A, and defining the parameter B= $-\Delta_{sol}H/R$, to get are shown in Eq. (51) and Eq. (52):

$$lnH_s = A + \frac{B}{T} \quad (51)$$

or

$$H_s = \exp(A)\, x\, exp\left(\frac{B}{T}\right) \quad (52)$$

To determine the parameters A and B experimentally, Henry's law constants are measured at several temperatures, and the method of least squares is used to fit the points to a function. Note that Eq. (51) and Eq. (52) produces lightly different fit parameters because the logarithmic Eq. (51) puts less weight on errors of large Henry's law constants than the linear Eq. (52) does. In this work, linear regression is performed using Eq. (51).

3.10.1 $H_{s,eff}$ for Acids and Bases

If, however, the species enters a fast equilibrium in the aqueous phase, it is possible to define an "effective" Henry's law constant $H_{s,eff}$, using a "total concentration" c_{tot}. Depending on the chemical class, there are different ways to define such a total concentration.

Acids and bases undergo ionic dissociation upon dissolution, e.g. Eq. (53):

$$HCl \leftrightarrow H^+ + Cl^- \quad (53)$$

Defining the total concentration c_{tot} as in Eq. (54):

$$c_{tot} = c(HCl) + c(Cl^-) \quad (54)$$

The effective Henry's law constant is Eq. (55):

$$H_{s,eff} = \frac{c_{tot}}{p(HCl)} = \frac{c(HCl)+c(Cl^-)}{p(HCl)} \quad (55)$$

Considering the acidity constant is Eq. (56):

$$K_a = \frac{c(H^+)c(Cl^-)}{c(HCl)} \quad (56)$$

The relation between the intrinsic and the effective Henry's law constant for HCl can be written as Eq. (57):

$$H_{s,eff} = H_s\, x\, \left(1 + \frac{K_a}{c(H^+)}\right) \quad (57)$$

Since the factor on the right-hand side contains $c(H^+)$, the conversion between the intrinsic and the effective Henry's law constant is pH-dependent. Thus, effective Henry's law constants of acids and bases are not material constants but depend on solution pH. Proportionality between p(HCl) and c_{tot} is restricted to conditions under which the uptake of gaseous HCl does not affect the acidity of the solution. In order to obtain a pH-independent constant, the product of the intrinsic Henry's law constant H_s^{cp} and the acidity constant K_a is often used for HCl and other strong acids (Eq. 58):

$$H_s' = H_s^{cp}\, x\, K_a = \frac{c(H^+)\, x\, c(Cl^-)}{p(HCl)} \quad (58)$$

Although, H_s' is usually also called a Henry's law constant, it should be noted that it is a different quantity, and it has different units than H_s^{cp}.

3.10.2 Dependence of Henry's Law Constants on the Composition of the Solution

Values of Henry's law constants for aqueous solutions depend on the composition of the solution, i.e., on its ionic strength and on dissolved organics. In general, the solubility of a gas decreases with increasing salinity ("salting out"). However, a "salting in" effect has also been observed, e.g., for the effective Henry's law constant of glyoxal, [89]. They can be described with the Sechenov equation, [90]. Note that the scientific transliteration from Cyrillic is "Sechenov", but the original article was written in German and used the German transliteration "Setschenow". There are many alternative ways to define the Sechenov equation, depending on how the aqueous-phase composition is described (based on con centration, molality, or amount fraction) and which variant of the Henry's law constant is used. Describing the solution in terms of molality is preferred because molality is invariant to temperature and to the addition of dry salt to the solution, [89]. Thus, the Sechenov equation can be written as Eq. (59):

$$log_{10}\left(\frac{H_{s0}^{bp}}{H_s^{bp}}\right) = K_s\, x\, b(salt) \quad (59)$$

where, H_{s0}^{bp} is Henry's law constant in pure water, H_s^{bp} is Henry's law constant in the salt solution, K_s is the molality-based Sechenov parameter for a given salt, and *b*(salt) is the molality of the salt. For mixed electrolyte solutions with more than one salt, an extension of the Sechenov equation developed by Schumpe, [91], and Weisenberger and Schumpe, [92], can be used. Sechenov parameters are not suitable for systems in which a species reacts irreversibly with the salt (e.g., $N_2O_5 + Cl^-$).

Since the atmosphere contains very dilute cloud droplets as well as highly concentrated aerosols, adequate values of Henry's law constants should be used. Unfortunately, Sechenov parameters are unknown for many species.

When H_2S is absorbed in a basic solution, it can react directly with hydroxyl ion and with water by a proton transfer reaction in Eq. (60) and Eq. (61):

$$H_2S + HO^- \leftrightarrow HS^- + H_2O \quad (60)$$

$$H_2S + H_2O \leftrightarrow HS^- + H_3O^+ \quad (61)$$

This enables to improve the mass-transfer driving force by decreasing the liquid bulk concentration (i.e increasing the concentration gradient). Moreover, these reactions are very rapid and can enhance the mass-transfer rate. They have been considered as instantaneous by several authors to simplify the enhancement factor determination, [93], [94]. However, other authors consider that the reaction should not be considered as instantaneous compared with the mass transfer except for a few specific cases, [95]. Salts can be added or naturally present in the scrubbing liquid, including sodium and potassium carbonate, phosphate, borate, arsenide and phenolate, as well as salts of weak organic acids. They enable to buffer the solution at a pH in the range of 9.0–11.0 to increase H_2S apparent solubility and enhance the absorption of H_2S, [95]. Alkaline salt absorption systems can be improved using an oxidant, [96], [97], [98], [99], [100], [101]. The carbonate system is the main buffer of the scrubbing solution and can also react with H_2S in the liquid film and enhance its mass-transfer rate through the following reactions, [95] in Eq. (62) and Eq. (63):

$$H_2S + HCO_3^- \leftrightarrow HS^- + H_2CO_3 \quad (62)$$

$$H_2S + CO_3^{-2} \leftrightarrow HS^- + HCO_3^- \quad (63)$$

Up to now, the design of packed column used for H_2S removal at alkaline pH is largely based on field experience, trying to respect a given contact time of approximately 1 s. In this manner, the physics and chemistry of this operation are not well understood and not optimized (particularly, the influence of the temperature and alkalinity). To describe the process at given operating conditions, the model used should take into account the mass-transfer performances of the packed column, the kinetics of the various acid–base reactions (to account for the mass transfer enhancement factor) and the pH and species (H_2S, HS^-, CO_2^{-3}, HCO^{-3}) concentrations evolution along the column. A few studies are focused on acid or basic species absorption simulations in caustic solutions, [102].

The simulation is written in Visual Basic for Applications (VBA) programming language. The simulation enables the determination of the height and of the diameter of the column for a given removal efficiency. The program works in several steps (Figure 1): the first is to select the physical and chemical operating conditions (QG, L/G, UG/UFlood, CG,in, CT = CL + [HS^-], carbonate species concentration, temperature (T), pressure (P), the inlet pH (pHin) and the desired removal efficiency (Eff)). The second step is to select a commercial random packing whose characteristics are known (dp, ρp, Sp, ε and F). Then, before running the numerical resolution, the program calculates the various physico-chemical constants (water and acid dissociation constants, diffusion coefficients, etc.) and hydrodynamic parameters required for the determination of the column height and diameter using classical correlations used for random packed columns (Lw, ao, kG, kL, UL, UG, UFlood, etc.). The temperature influence on the equilibrium constants, gas and liquid diffusion coefficients of H_2S and the reactive solutes, [103], densities, H_2S Henry's law constant, [104] surface tensions and viscosities are taken into account. Finally, after running the numerical resolution, the software displays the main features of the column design: the height and the diameter of the column, the pressure drop (not considered in this article) and the outlet concentration of H_2S in the liquid phase. The process is considered as isothermal since for a treated concentration lower than a few g Nm^{-3}, which is rarely the case for H_2S treatment, the enthalpy of reactions is not enough to increase significantly the temperature of the scrubbing liquid, [95].

The mass-transfer and hydrodynamic parameters (kL, kG and ao) are calculated before the numerical resolution starts since they are constant along the column. It requires to determine previously the diameter of the column. This determination is based on the calculation of the flood velocity (UFlood) in the selected random packing material according to the following set of equations, [105].

Usually, for a random packing, a gas superficial velocity (UG) equals to 70% of the flood velocity (UFlood) is selected, but the operator has the opportunity of modifying this percentage. Once UG is fixed, the diameter of the column is simply deduced from the gas flow rate (QG). Then, from the desired L/G ratio, the liquid superficial velocity (UL) is calculated. One can note that at a given temperature, for a given liquid and gas phases, the diameter only depends on the physical properties of the selected packing material. The determination of the gas and liquid superficial velocities enables the determination of the gas–liquid interfacial area (ao in m^2/m^3) and the two local mass-transfer coefficients (kL and kG in m/s) through the well-known correlations of Omil et al. [106], cited by Rozan et al., [107] in Eq. (64):

$$U_{Flood} = \left(Y\frac{g}{F}x\frac{\rho_L}{\rho_G}\right)^{0.5} \text{ with } \begin{cases} Y = \exp(-4X^{0.35}) \\ if\ 0.02 \le X = \frac{L}{G}\sqrt{\frac{\rho_G}{\rho_L}} \le 4, \\ or\ Y = 0.684\exp(-3.61X^{0.286}) \\ if\ 4 \le X = \frac{L}{G}\sqrt{\frac{\rho_G}{\rho_L}} \le 10 \end{cases} \quad (64)$$

$$a^o = S_P x\left\{1 - \exp[-1.45x\left(\frac{\sigma_P}{\sigma_L}\right)^{0.75}(S_P x d_P)^{-0.35} x Ga^{0.05} x We^{0.2}]\right\} \quad (65)$$

$$k_G = 5.23x\frac{D_G}{d_P}x(S_P x d_P)^{-1.7} x Re_G^{0.7} x Sc_G^{1/3} \quad (66)$$

$$k_L = 0.0051x(\frac{\mu_L x g}{\rho_L})^{1/3} x(S_P x d_P)^{-0.27} x(\frac{a^o}{S_P})^{-2/3} x Re_L^{2/3} x Sc_L^{-0.5} \quad (67)$$

The determination of the gas and liquid superficial velocities enables the determination of the gas–liquid interfacial area (a^o in m^2/m^3) and the two local mass-transfer coefficients (k_L and k_G in m/s) through the well-known correlations of Omil et al., [106], cited by Rozan et al., [107].

The Galilei and the Weber dimensionless numbers were used to describe the flow in the anaerobic reactor in Eq. (68) and Eq. (69):

$$Ga = \frac{gxd_P^3x\rho_L^2}{\mu_L^2} \quad (68)$$

$$-We = \frac{d_PxL^2}{\rho_Lx\sigma_LxA_{column}^2} \quad (69)$$

After the determination of a^o, k_L and k_G (Section 2.2), the outlet concentration of H_2S in the gas phase is deduced from the desired removal efficiency (Eff) in Eq. (70):

$$C_{G,o} = C_{G,in}(1 - Eff) \quad (70)$$

Then, the mass balance is written assuming that the gas and liquid flow rates are constant along the column and enables to determine $C_{T,o}$ the total sulphide concentration in the liquid phase at the outlet (bottom of the column) in Eq. (71):

$$Q_G\left(C_{G,in} - C_{G,o}\right) = Q_L(C_{T,o} - C_{T,in}) \quad (71)$$

Following the procedure presented later the outlet pH is finally determined. The numerical resolution starts after that from the bottom of the column. To achieve it, the column was discretized into several stages of height Z_i. This value should be low (Z_i = 0.01 or 0.05 m;) to assume that the liquid is perfectly mixed within a stage. In each stage, the overall liquid-phase mass-transfer coefficients (K_La^o) is calculated knowing k_L, k_G, a^o and the enhancement factor in Eq. (72):

$$\frac{1}{K_La^o} = \frac{1}{Ek_La^o} + \frac{1}{Hk_Ga^o} \quad (72)$$

The enhancement factor must be calculated in each stage knowing the pH and the sulphide and carbonate concentrations. Using the mass-transfer rate equation and the mass balance for a perfectly mixed liquid phase and a gas plug-flow, one can write, [108] in Eq. (73):

$$Q_G\left(C_{G,i+1} - C_{G,i}\right) = K_La^oA_{column}Z_ix\frac{\left(\frac{C_{G,i+1}}{H} - C_{L,i}\right) - \left(\frac{C_{G,i}}{H} - C_{L,i}\right)}{ln\left(\frac{\frac{C_{G,i+1}}{H} - C_{L,i}}{\frac{C_{G,i+1}}{H} - C_{L,i}}\right)} \quad (73)$$

$C_{T,i}$ is the total sulphide concentration, which is deduced in each stage from the mass balance in Eq. (74):

$$C_{T,i} = \frac{Q_G}{Q_L}\left(C_{G,i+1} - C_{G,i}\right) + C_{T,i-1} \quad (74)$$

The H_2S liquid concentration ($C_{L,i}$) in each stage is deduced from the total sulphide concentration ($C_{T,i}$), the H_2S acid dissociation constant and the pH in Eq. (75):

$$C_{L,i} = \frac{C_{T,i}}{1+10^{pH_i - pKa_{H_2S}}} \quad (75)$$

Eq. (76) can be rewritten to calculate the gas concentration at the inlet of the stage *i* ($C_{G,i+1}$):

$$C_{G,i+1} = \frac{C_{G,i}\left(\exp\left(A'+1\right)-1\right)+A'xHxC_{L,i-1}(1-\exp B)}{A'-1+\exp B} \quad (76)$$

A (absorption rate), A (modified absorption rate to account for sulphide equilibrium) and B are equal to Eq. (77), Eq. (78) and Eq. (79):

$$A = \frac{Q_L}{HxQ_G} \quad (77)$$

$$A' = A(1 + 10^{pH_i - pKa_{H_2S}}) \quad (78)$$

$$B = \frac{K_La^oxA_{column}xZ_i}{AxQ_L} \quad (79)$$

Step by step, $C_{G,i+1}$ is calculated until it reaches the outlet concentration ($C_{G,o}$), i.e. the top of the column. The total column height is the number of stages multiplied by the height of a stage (Zi). In each stage, the enhancement factor is calculated knowing the liquid composition and its pH.

To calculate the enhancement factor due to the various acid–base reactions in the liquid film at each stage, the liquid interface concentration must be previously calculated from the following equation, [95] in Eq. (80):

$$C_{a,i}^* = \frac{k_G(C_{G,i} - HC_{L,i})}{(Hk_G + E_ik_L)} + C_{L,i} \quad (80)$$

If we assume that the reversible acid–base reactions are instantaneous compared with mass transfer, the enhancement factor E can be calculated in Eq. (81):

$$E = E_{HO^-} + E_{H_2O} + E_{CO_3^{-2}} + E_{HCO_3^-} - 3 \quad (81)$$

Table 8 exhibited the synthesis of the different equations used to determine the pH evolution.

*Table 8 can be found in the Appendix section.

One of the main features of the developed numerical resolution is to simulate the pH profile along the column. Indeed, due to the acid characteristics of H_2S, the pH is expected to decrease significantly between the top and the bottom of the column, especially for low L/G ratio and/or high inlet H_2S concentration. We can consider that in the liquid bulk, all the acidic and basic species are in equilibrium (which is not necessarily the case in the liquid film, [95]). Equations (38)–(46) relative to these equilibriums are synthesized in Table 1. In each stage (or in the whole column as well), the transfer of a known amount of H_2S leads to an equilibrium displacement. The mass balance linked to this displacement can be written as Eq. (82):

$$\frac{C_{T,o}}{1+10^{pH_o-pKa_{H_2S}}} = [H_2S]_{transfered} + \frac{C_{T,in}}{1+10^{pH_{in}-pKa_{H_2S}}} - \beta - \delta - \xi - \lambda \quad (82)$$

Where, δ, λ, β and ξ are, respectively, the advancements of the reactions 1–4. From Eq. (47), it is possible to determine pH_o using the numerical resolution whose procedure is presented in Fig. 21. This procedure is also used and adapted to determine the pH evolution along the column.

The effect of different parameters such as the inlet pH solution, the temperature, the L/G ratio and the carbonate species concentration on the H_2S absorption efficiency has been investigated. A column height of 3 m has been selected, and the numerical resolution is used to determine the corresponding removal efficiency with the selected operating conditions. The results of the numerical resolution have been compared with the experimental results of Chen et al., [109], and shows a good agreement even if an exact comparison was not possible because the alkalinity used in their study was unknown.

Tests were conducted to determine the influence of the pH on the H_2S removal efficiency. Naturally and in agreement with the literature, the removal efficiency increases with the pH, [97], [101]. It emphasizes that the control of the pH remains essential for process designers and operators, especially when the pH is low (≈ 9.0). In this case, the enhancement factor is limited (E from approximately 20–100 depending on the pH and the stage of the column) and the pH decreases along the column (approximately an outlet pH of 8.7 is reached in these simulations). In this case, H_2S absorption becomes almost negligible in a significant part of the column (a low pH limits the H_2S dissociation in HS^- and then limits the mass-transfer driving force). It means that a significant part of the column is not active for H_2S absorption. To limit this pH decreasing, operators can select larger values of the L/G ratio (a compromise has nevertheless to be find regarding the pressure drop) or can work with a 1.0, 2.0, 3.0, 4.0, 5.0, 6.0, 7.0, 8.0, 9.0, 10.0, 11.0 pH values. 9.0, 9.5, 10.0, 10.5, 11.0 pH Eff (L/G=3), Eff (L/G=1), Eff (L/G=5) H S removal efficiency (%) (Fig. 24).

*Figure 24 can be found in the Appendix section.

Influence of the pH on the H_2S removal efficiency for different L/G ratios (conditions of Table 8). higher alkalinity to buffer the pH (section 3.4). At large pH, the L/G ratio has a lower influence because the enhancement factor is so large that the mass-transfer resistance is located mainly in the gas phase and the pH decreasing over the column is limited (for pH_{in} = 11 and L/G = 3, pH_o equals to 10.93):

The temperature influence has been evaluated from 5 to 50°C. As shown in Fig. 25, for a given pH value (pH=10.0) if the temperature is increased, the H_2S removal efficiency increases for a fixed L/G ratio. This result was not expected since, usually, designers consider that the solubility decreases with the temperature (H=0.245 at 5°C and 0.588 at 50°C).

*Figure 25 can be found in the Appendix section.

It emphasizes that the solubility is not the most influent parameter, at least at high pH. Indeed, in this case, the enhancement factor is quite large and the mass-transfer resistance is mainly located in the gas phase. Since the mass-transfer performance increases with the temperature, the removal efficiency increases. Indeed, k_G drops from 5.9×10^{-2} m7s at 50°C to 5.1×10^{-2} m/s at 5°C. Additionally, we note that the buffering effect of the solution is better at high temperature (i.e. the pH decreasing along the column is reduced). Finally, interesting removal efficiencies can be obtained at L/G ratios up to 5 for a limited pH of 10.0. This result is quite interesting because working at pH=10.0 limits very significantly the parasite CO_2 absorption and by the way the NaOH consumption of the process.

The L/G ratio is an important parameter in contactors design. Naturally and in agreement with the literature, the removal efficiency increases with the L/G ratio, [97], [101].] High L/G ratio improves the absorption rate, this is to say the absorption capacity of the process, and limits the pH decreasing of the scrubbing solution. However, a high L/G ratio increases the pressure drop and limits the flood velocity. The results show that for a L/G ratio higher than 3, this parameter influence stays limited (Fig.

26). Therefore, this value that is currently used in chemical scrubbing is justified, [101].

*Figure 26 can be found in the Appendix section.

Different types of alkaline solutions such as potassium carbonate and/or sodium carbonate solution have been used for H_2S removal, [110], [111]. We can note that the presence of such species (HCO^{-3} and CO_2^{-3}) in the process water enhances the gas–liquid mass transfer, [95]. This effect is clearly demonstrated in Fig. 27. Another interesting aspect linked to the use of high alkalinity is the buffer power of such solutions, which limits the pH decreasing along the column. (at pHin 10, the outlet pH is equal to 8.78 without any carbonate species in solution, whereas it is equal to 9.86 for a carbonate species concentration of 100 mg CO_2/l). At pH=11.0, the influence of the alkalinity is not significant anymore. In this case, the enhancement factor is so large that all the resistance is located in the gas phase and the pH decreasing remains low. Therefore, the mass-transfer efficiency is not influenced by the chemical conditions anymore.

*Figure 27 can be found in the Appendix section.

4 Conclusion

The aim of this study was to successfully develop a sulfur-cycled process integrating microbial sulfate reduction and gas stripping-adsorption into a persulfate-based AOP for the complete degradation of Sulfur Black 1 and recovery of Na_2S from textile dyeing wastewater.

In dyeing wastewater simulated with persulfate-based AOP, sulphur Black 1 was effectively degraded, rendering resistant high molecular weight Sulfur Black 1 biodegradable and leading to its breakdown into organic oxidation byproducts and ultimately sulfate formation. Organic AOP byproducts were fully mineralized and acted as electron donors to enable microbial reduction of sulfate to sulfide in UAPBSR reactors containing both fermentative bacteria (FB) and sulfur reducing bacteria (SRB). Dissolved sulfur in UAPBSR wastewater was efficiently recovered through gas stripping and alkali absorption processes, with over 99.90% of the sulfur converted to Na_2 S; thus, proving that the Na_2 S chemical can be reused as a low-cost solvent in the Sulfur Black 1 dyeing process.

The H_2S removal efficiency increases with the pH, the temperature, the L/G ratio and total alkalinity of solution. This tool enables to understand deeper the chemical and physical phenomena involved during H_2S absorption in alkaline solutions and provide guidelines for designers.

The degradation effect of Na_2S was similar for both systems (Fe(II)/PS and Fe(0)/PS), and the Fe(0)/PS system had an advantage in the slow release of Fe(II), which was less likely to cause Fe(II) overload resulting in the consumption of free radicals. The concentrations of oxidant, catalyst, and substrate had a large influence on the reaction, and the concentration ratio among them was very important for the degradation of Na_2S. Temperature and pH were important factors affecting the reaction. A lower pH (pH=5.0) was very suitable for the degradation of Na_2S in both systems. High temperature could enhance the degradation of Na_2S due to the synergistic activation of PS by an iron catalyst and thermal energy. Most of the kinetic equations for

Na_2S degradation under different conditions followed pseudo first-order kinetic equations and were highly correlated.

According to Henry's law, the equilibrium ratio between the abundances in the gas phase and in the aqueous phase is constant for a dilute solution. Henry's law constants of trace gases of potential importance in environmental chemistry have been collected and converted into a uniform format. In other words, the amount of dissolved gas is proportional to its partial pressure in the gas phase. The proportionality factor is called a Henry's law constant.

In this study, we demonstrate that the sulfur cycle process is a cost-effective for treating the dyeing wastewater containing Sulfur Black 1 and is a highly efficient and effective process as a closed-loop approach. The combination of the persulfate-based AOP process and microbial sulfate reduction methods ensures the complete degradation of the highly toxic and highly resistant Sulfur Black 1 dye. As an important result, the recovery of the value-added product (Na) from the sulfate formed during the AOP process can also be achieved through microbial sulfate reduction followed by hydrogen sulfide (H_2S) gas stripping-absorption processes. The main objective of the closed-loop strategy is to reduce the potential environmental risks associated with organic by-products resulting from incomplete degradation and residual sulfates/sulfur found in treated wastewater, and to support the circular economy in textile wastewater management.

In the light of these experimental findings, the key conclusion is the sulfur-cycling process integrating with microbial sulfate reduction and gas stripping-adsorption into a persulfate-based AOP can be used for the complete degradation of Sulfur Black 1 and the

recovery of Na_2S from textile dyeing wastewater. The significant contribution of the development of AOP processes and sustainable technologies in the treatment of wastewaters containing dyes degrading with difficulty and other persistent organic pollutants can be removed with this way.

Acknowledgement:
Experimental analyzes in this study were performed at the Laboratories of the Canada Research Center, Ottawa, Canada. The authors would like to thank this body for providing financial support.

References:

[1] N. Singh Shekhawat, S. Kumar Patra, A. Kumar Patra, B. Bag, A Novel Environmental Friendly and Sustainable Process for Textile Dyeing with Sulphur Dyes for Cleaner Production, *Chemical Engineering Journal*, Vol.479, 2024, 147329.

[2] M. Wang, J. Z. Yang, H. T. Wang, Optimisation of the Synthesis of a Water-Soluble Sulfur Black Dye, *Dyes Pigments*, Vol.50, No.3, 2001, pp. 243–246.

[3] J. Osorio, M. Gaviria, N.A. Gomez-Vanegas, Evaluating the Scale-Up of a Reactor for the Treatment of Textile Effluents Using *Bjerkandera sp*, *Revista Facultad de Ingeniería*, Vol.88, No.88, 2018, pp. 9-19.

[4] S. Afrin, H. R. Shuvo, B. Sultana, F. Islam, A. Abu Rus'd, S. Begum, M. N. Hossain, The Degradation of Textile Industry Dyes Using the Effective Bacterial Consortium, *Heliyon*, Vol.7, No.10, 2021, e08102.

[5] N. Thai Anh, R. S. Juang, Treatment of Waters and Wastewaters Containing Sulfur Dyes: A Review, *Chemical Engineering Journal*, Vol.219, 2013, pp. 109–117.

[6] Y. Gu, X. Zhu, W. Yu, W. Zhong, J. Guo, Z. Cai, Oxidization and Biodegradation of Sulfur Black by a Newly Isolated Strain Acinetobacter sp. DS-9, *Desalination and Water Treatment*, Vol.227, 2021, pp. 321–329.

[7] K. G. Pavithra, P. S. Kumar, V. Jaikumar, P. S. Rajan, Removal of Colorants from Wastewater: A Review on Sources and Treatment Strategies, *Journal of Industrial and Engineering Chemistry*, Vol.75, 2019, pp. 1–19.

[8] H. Amin, A. Amer, A. El Fecky, I. Ibrahim, Treatment of Textile Waste Water Using H_2O_2/UV System, *Physicochemical Problems of Mineral Processing*, Vol.42, 2008, pp. 17–27.

[9] Y. Lu, X. Yang, L. Xu, Z. Wang, Y. Xu, G. Qian, Sulfate Radicals from Fe3+ Persulfate System for Rhodamine B Degradation, *Desalination and Water Treatment*, Vol.57, No.60, 2016, pp. 29411–29420.

[10] L. B. Bezerra, T. D. Carlos, A. S. Dornelas, W. S. Martins, M. A. Pereira, A. K. de Souza Nolberto, G. R. dos Santos, I. R. do Nascimento, R. R. Fidelis, N. L. de Souza, D. H. Pereira, R. A. Sarmento, G. S. Cavallini, Ecotoxicological Evaluation of Dye Degradation and Photodegradation by Peracetic Acid with Sodium Carbonate, *Diversity*, Vol.14, No.11, 2022, 931 (Basel).

[11] A. Iqbal, A. Yusaf, M. Usman, T. Bokhari, A. Mansha, Insight into the Degradation of Different Classes of Dyes by Advanced Oxidation Processes; A Detailed Review, *International Journal of Environmental Analytical Chemistry*, Vol.104, 2023, pp. 1–35.

[12] D. R. Waring, *Dyes for Cellulosic Fibers*, In: D. R. Waring, G. Hallas, (eds), The Chemistry and Application of Dyes, Boston, MA: Springer, pp. 49–106, 1990.

[13] R. Paul, R. S. Blackburn, T. Bechtold, *Indigo and Indigo Colorants*, In: Ullmann's Encyclopedia of Industrial Chemistry, New York: Wiley, pp. 1–16, 2021.

[14] A. Llort, M. Domingo, G. Nagl, *Sulfur Dyes*, In: Ullmann's Encyclopedia of Industrial Chemistry, New York: Wiley, pp. 1–13, 2021.

[15] S. Uncu Akı, C. Candan, B. Nergis, N. S. Önder, *Understanding Denim Recycling: A Quantitative Study with Lifecycle Assessment Methodology*, In: A. Körlü, (ed), Waste in Textile and Leather Sectors, IntechOpen. Epub ahead of print 9 September 2020.

[16] A. P. Periyasamy, S. Periyasami, Critical Review on Sustainability in Denim: A Step Toward Sustainable Production and Consumption of Denim, *ACS Omega*, Vol.8, 2022, pp. 4472–4490.

[17] M. Sanchez, *Dyeing of Denim Yarns with Non-Indigo Dyes*, in: R. Paul, (ed), Denim: Manufacture, Finishing and Applications, Cambridge, UK: Woodhead Publishing, pp. 107–157, 2015.

[18] A. P. Manian, S. Müller, D. E. Braun, T. Pham, T. Bechtold, Dope Dyeing of Regenerated Cellulose Fibres with Leucoindigo as Base for Circularity of Denim, *Polymers (Basel)*, Vol.14, 2022, 5280.

[19] Textile Exchange. Materials Market Report, 2023, https://textileexchange.org/app/uploads/2023/11/Materials-Market-Report-2023.pdf.

[20] R. Paul, *Denim and Jeans: An Overview*, in: R. Paul, (ed), Denim: Manufacture, Finishing and Applications, Cambridge, UK: Woodhead Publishing, pp. 1–11, 2015.

[21] S. Haslinger, Y. Wang, M. Rissanen, M. Beatrice Lossa, M. Tanttu, E. Ilen, M. Määttänen, A. Harlin, M. Hummel, H. Sixta, Recycling of Vat and Reactive Dyed Textile Waste to New Colored Man-Made Cellulose Fibers, *Green Chemistry*, Vol.21, 2019, pp. 5598–5610.

[22] T. Bechtold, E. Burtscher, A. Turcanu, Continuous Sulfur Dyeing Without Reducing Agents: Fully Reduced Sulfur Black 1 by Cathodic Reduction, *Textile Chemist and Colorist*, Vol.30, 1998, pp. 72–77.

[23] A. B. Ponnusami, S. Sinha, H. Ashokan, M. V. Paul, S. P. Hariharan, J. Arun, K. P. Gopinath, Q. H. Le, A. Pugazhendhi, Advanced Oxidation Process (AOP) Combined Biological Process for Wastewater Treatment: A Review on Advancements, Feasibility and Practicability of Combined Techniques, *Environmental Research*, Vol.237, 2023, 116944.

[24] C. V. Rekhate, J. K. Srivastava, Recent Advances in Ozone-Based Advanced Oxidation Processes for Treatment of Wastewater- A Review, *Journal of Advanced Chemical Engineering*, Vol.3, 2020, 100031.

[25] G. Li, S. Park, D. W. Kang, R. Krajmalnik-Brown, B. E. Rittmann, 2,4,5-Trichlorophenol Degradation Using a Novel TiO_2-Coated Biofilm Carrier: Roles of Adsorption, Photocatalysis, and Biodegradation, *Environmental Science & Technology*, Vol.45, No.19, 2011, pp. 8359–8367.

[26] H. Lu, J. Wang, S. Li, G. H. Chen, M. C. M. van Loosdrecht, G. A. Ekama, Steady-State Model-Based Evaluation of Sulfate Reduction, Autotrophic Denitrification and Nitrification Integrated (SANI) Process, *Water Research*, Vol.43, No.14, 2009a, pp. 3613–3621.

[27] X. Lu, B. Yang, J. Chen, R. Sun, Treatment of Wastewater Containing Azo Dye Reactive Brilliant Red X-3B Using Sequential Ozonation and Upflow Biological Aerated Filter Process, *Journal of Hazardous Materials*, Vol.161, No.1, 2009b, pp. 241–245.

[28] S., Liu, P. Yin, Y. Zhang, X. Wu, Z. Cai, Bioaugmentation Strategy for Treatment of Sulfur Black Wastewater Through Sequential Fenton Oxidation and Biological Process by Two Sulfide-Oxidizing Strains, *American Journal of Environmental Protection*, Vol.9, 2020, 64.

[29] X. Yu, J. Sun, G. Li, Y. Huang, Y. Li, D. Xia, F. Jiang, Integration of $\bullet SO_4$-Based AOP Mediated by Reusable Iron Particles and a Sulfidogenic Process to Degrade and Detoxify Orange II, *Water Research*, Vol.174, 2020, 115622.

[30] J. Sun, J. Yang, Y. Liu, M. Guo, Q. Wen, W. Sun, J. Yao, Y. Li, F. Jiang, Magnetically-Mediated Regeneration and Reuse of Core-Shell Fe0 @Fe III Granules for In-Situ Hydrogen Sulfide Control in the River Sediments, *Water Research*, Vol.157, 2019, pp. 621–629.

[31] A. V. Kurzin, A. N. Evdokimov, V. S. Golikova, O. S. Pavlova, Solubility of Sodium Sulfide in Alcohols, *Journal of Chemical & Engineering Data*, Vol.55, No.9, 2010, pp. 4080–4081.

[32] A. Preisinger, K. Mereiter, O. Baumgartner, G. Heger, W. Mikenda, H. Steidl, Hydrogen Bonds in $Na_2S \cdot 9D_2O$: Neutron Diffraction, X-Ray Diffraction and Vibrational Spectroscopic Studies, *Inorganica Chimica Acta*, Vol.57, 1982, pp. 237–246.

[33] K. Mereiter, A. Preisinger, A. Zellner, W. Mikenda, H. Steidl, Hydrogen Bonds in $Na_2S \cdot 5H_2O$: X-ray Diffraction and Vibrational Spectroscopic Study, *Journal of the Chemical Society, Dalton Transactions*, Vol.7, 1984, pp. 1275–1277.

[34] E. Zintl, A. Harder, B. Dauth, Gitterstruktur der Oxyde, Sulfide, Selenide und Telluride Des Lithiums, Natriums und Kaliums, *Zeitschrift fuer Elektrochemie und Angewandte Physikalische Chemie*, Vol.40, 1934, pp. 588–593.

[35] A. F. Wells, *Structural Inorganic Chemistry*, Oxford: Clarendon Press, UK, 1984.

[36] A. F. Holleman, E. Wiberg, *Inorganic Chemistry*, San Diego: Academic Press, USA, 2001.

[37] J.-H. So, P. Boudjouk, H. H. Hong, W. P. Weber, *Hexamethyldisilathiane*, Edited by R. N. Grimes, Inorganic Syntheses, Vol.29. pp.30–32, 2007.

[38] L. Lange, W. Triebel, *Sulfides, Polysulfides, and Sulfanes*, in Ullmann's Encyclopedia of Industrial Chemistry, Wiley-VCH, Weinheim, Germany, 2000.

[39] C. C. Price, G. W. Stacy, p-Aminophenyldisulfide, *Current Organic Synthesis*, Vol.28, 1948, 14.

[40] A. Khazaei, M. Kazem-Rostami, A. R. Moosavi-Zare, M. Bayat, S. Saednia, Synthesis of thiophenols, *Synthesis Letters*, Vol.23, No.13, 2012, pp. 1893–1896.

[41] B.-C. Yu, Y. Shirai, J. M. Tour, Syntheses of Functionalized Azobenzenes, *Tetrahedron*, Vol.62, No.44, 2006, pp. 10303–10310.

[42] N. Zinin, Beschreibung Einiger Neuer Organischer Basen, Dargestellt Durch Die Einwirkung des Schwefelwasserstoffes auf Verbindungen der Kohlenwasserstoffe mit Untersalpetersäure, [Description of Some New Organic Bases, Represented by the Action of Hydrogen Sulphide on Hydrocarbons with Sub-Nitric Acid], *Journal für Praktische Chemie (in German)*, Vol.27, No.1, 1842, pp. 140–153.

[43] W. W. Hartman, H. L. Silloway, 2-Amino-4-nitrophenol, *Organic Syntheses*, Vol.25, 1945, 5.

[44] A. Savateev, D. Dontsova, B. Kurpil, M. Antonietti, Highly Crystalline Poly(heptazine imides) by Mechanochemical Synthesis for Photooxidation of Various Organic Substrates Using an Intriguing Electron Acceptor – Elemental Sulfur, *Journal of Catalysis*, Vol.350, 2017, pp. 203–211.

[45] R. H. Peters, *Textile Chemistry*, Vol - II, Elsevier Publishing Company, London, 1967.

[46] P. Goswami, M. Basak, *Sulfur Dyes*, in Kirk-Othmer Encyclopedia of Chemical Technology, John Wiley & Sons, 2001.

[47] *Industrial Dyes: Chemistry, Properties, Applications*, Klaus Hunger, Ed., Wiley-VCH, Weinheim, Germany, 2007.

[48] H. Fu, C. Chen, J. Li, Y. Lan, L. Wang, J. Yuan, Influence of Na_2S on the Corrosion Behavior of q345 Steel in Sodium Aluminate Solution, *Materials Research Express*, Vol.6, 2019, pp. 1065a–1069a.

[49] R. J. L. Pereira, W. Hu, I. S. Metcalfe, Impact of Gas–Solid Reaction Thermodynamics on the Performance of a Chemical Looping Ammonia Synthesis Process, *Energy Fuels*, Vol.36, 2022, pp. 9757–9767.

[50] E. Wang, X. Hou, Y. Chen, Z. Fang, J. Chen, T. Liang, K. Chou, K. G. Nickel, Progress in Cognition of Gas-Solid Interface Reaction for Non-Oxide Ceramics at High Temperature, *Critical Reviews in Solid State and Materials Sciences*, Vol.46, 2021, pp. 218–250.

[51] X. Zhang, X. Li, S. Weng, S. Wu, Q. Liu, M. Cao, Y. Li, Z. Wang, L. Zhu, R. Xiao, Spontaneous Gas–Solid Reaction on Sulfide Electrolytes for High-Performance All-Solid-State Batteries, *Energy & Environmental Science*, Vol.16, 2023, pp. 1091–1099.

[52] M. I. Gaviria-Arroyave, J. Osorio-Echavarría, N. A. Gomez-Vanegas, Evaluating the scale-up of a reactor for the treatment of textile effluents using Bjerkandera sp. *Revista Facultad de Ingenieria-Universidad de Antioquia*, Vol.88, 2018, pp. 80–90.

[53] J. N. Chakraborty, *Sulphur Dyes*, Handbook of Textile and Industrial Dyeing, Woodhead Publishing, pp. 466–485, 2011.

[54] W. C. Lipps, E. B. Braun-Howland, T. E. Baxter, *Standard Methods for the Examination of Water and Wastewater*, 24th. Edition, W. C. Lipps, E. B. Braun-Howland, T. E. Baxter, (editors), American Public Health Association (APHA), American Water Works Association (AWWA), Water Environment Federation (WEF), Elevate Your Standards. American Public Health Association 800 I Street, NW Washington DC: 20001-3770, USA, December 1, 2022; ISBN:9780875532998, 2022.

[55] J. Zeng, S. Xu, K. Lin, S. Yao, B. Yang, Z. Peng, T. Hao, X. Yu, T. Zhu, F. Jiang, J. Sun, Long-Term Stable and Efficient Degradation of Ornidazole with Minimized by-Product Formation by a Biological Sulfidogenic Process Based on Elemental Sulfur, *Water Research*, Vol.249, 2024, 120940.

[56] S. Rodriguez, L. Vasquez, D. Costa, A. Romero, A. Santos, Oxidation of Orange G by Persulfate Activated by Fe (II), Fe (III) and Zero Valent Iron (ZVI), *Chemosphere*, Vol.101, 2014, pp. 86–92.

[57] Y. Q. Zhang, X. F. Xie, S. B. Huang, H. Y. Liang, Effect of Chelating Agent on Oxidation Rate of Aniline in Ferrous Ion Activated Persulfate System at Neutral pH, *Journal of Central South University*, Vol.21, 2014, pp. 1441–1447.

[58] X. Zou, T. Zhou, J. Mao, X. Wu, Synergistic Degradation of Antibiotic Sulfadiazine in a Heterogeneous Ultrasound-Enhanced Fe^{0}/Persulfate Fenton-like System, *Chemical Engineering Journal*, Vol.257, 2014, pp. 36–44.

[59] L. Bu, Z. Shi, S. Zhou, Modelling of Fe(II)-Activated Persulfate Oxidation Using Atrazine as a Target Contaminant, *Separation Purification Technology*, Vol.169, 2016, pp. 59–65.

[60] F. Gao, Y. Li, B. Xiang, Degradation of Bisphenol A through Transition Metals Activating Persulfate Process, *Ecotoxicology and Environmental Safety*, Vol.158, 2018, pp. 239–247.

[61] F. Ghanbari, Q. Wang, A. Hassani, S. Wacławek, J. Rodríguez-Chueca, K. Y. A. Lin, Electrochemical Activation of Peroxides for Treatment of Contaminated Water with Landfill Leachate: Efficacy, Toxicity and Biodegradability Evaluation, *Chemosphere*, Vol.279, 2021, 130610.

[62] T. Olmez-Hanci, I. Arslan-Alaton, B. Genc, Bisphenol A Treatment by the Hot Persulfate Process: Oxidation Products and Acute Toxicity, *Journal of Hazardous Materials*, Vol.263, 2013, pp. 283–290.

[63] N. Potakis, Z. Frontistis, M. Antonopoulou, I. Konstantinou, D. Mantzavinos, Oxidation of Bisphenol A in Water by Heat Activated Persulfate, *Journal of Environmental Management*, Vol.195, 2017, pp. 125–132.

[64] C. Tan, N. Gao, Y. Deng, N. An, J. Deng, Heat-Activated Persulfate Oxidation of Diuron in Water, *Chemical Engineering Journal*, Vol.203, 2012, pp. 294–300.

[65] L. Zhao, Y. Ji, D. Kong, J. Lu, Q. Zhou, X. Yin, Simultaneous Removal of Bisphenol A and Phosphate in Zero-Valent Iron Activated Persulfate Oxidation Process, *Chemical Engineering Journal*, Vol.303, 2016, pp. 458–466.

[66] S. Wang, J. Wu, X. Lu, W. Xu, Q. Gong, J. Ding, B. Dan, P. Xie, Removal of Acetaminophen in the Fe^{2+}/Persulfate System: Kinetic Model and Degradation Pathways, *Chemical Engineering Journal*, Vol.358, 2019, pp. 1091–1100.

[67] W. W. P. Lai, J. C. Lin, M. H. Li, Degradation of Benzothiazole by the UV/Persulfate Process: Degradation Kinetics, Mechanism and Toxicity, *Journal of Photochemistry and Photobiology A: Chemistry*, Vol.436, 2023, 114355.

[68] C. Liang, H. W. Su, Identification of Sulfate and Hydroxyl Radicals in Thermally Activated Persulfate, *Industrial & Engineering Chemistry Research*, Vol.48, No.11, 2009, pp. 5558–5562.

[69] J. Deng, Y. Shao, N. Gao, Y. Deng, C. Tan, S. Zhou, Zero-Valent Iron/Persulfate (Fe^0/PS) Oxidation Acetaminophen in Water, *International Journal of Environmental Science and Technology*, Vol.11, No.4, 2014, pp. 881–890.

[70] I. Hussain, Y. Zhang, S. Huang, Degradation of Aniline with Zero-Valent Iron as an Activator of Persulfate in Aqueous Solution, *RSC Advances*, Vol.4, No.7, 2014, pp. 3502–3511.

[71] I. Epold, N. Dulova, Oxidative Degradation of Levofloxacin in Aqueous Solution by $S_2O_8^{-2}/Fe^{+2}$, $S_2O_8^{-2}/H_2O_2$ and $S_2O_8^{-2}$ /OH^- Processes: A Comparative Study, *Journal of Environmental Chemical Engineering*, Vol.3, No.2, 2015, pp. 1207–1214.

[72] J. Sun, L. Wei, R. Yin, F. Jiang, C. Shang, Microbial Iron Reduction Enhances In-Situ Control of Biogenic Hydrogen Sulfide by FeOOH Granules in Sediments of Polluted Urban Waters, *Water Research*, Vol.171, 2020, 115453.

[73] A. Guillot, C. Gitton, P. Anglade, M. Y. Mistou, Proteomic Analysis of Lactococcus Lactis, a Lactic Acid Bacterium, *Proteomics*, Vol.3, 2003, pp. 337–354.

[74] C. F. P. Scholz, M., Kilian, The Natural History of Cutaneous Propionibacteria, and Reclassification of Selected Species within the Genus Propionibacterium to the Proposed Novel Genera Acidipropionibacterium Gen. Nov., Cutibacterium Gen. Nov., Pseudopropionibacterium Gen. Nov, *International Journal of Systematic and Evolutionary Microbiology*, Vol.66, No.11, 2016, pp. 4422–4432.

[75] P. Seesuriyachan, S. Takenaka, A. Kuntiya, S. Klayraung, S. Murakami, K. Aoki, Metabolism of Azo Dyes by Lactobacillus Casei TISTR 1500 and Effects of Various Factors on Decolorization, *Water Research*, Vol.41, No.5, 2007, pp. 985–992.

[76] T. Bechtold, F. Berktold, A. Turcanu, The Redox Behaviour of CI Sulphur Black 1 - A Basis for Improved Understanding of Sulphur Dyeing, *Journal of the Society of Dyers and Colourists*, Vol.116, No.7- 8, 2000, pp. 215–221.

[77] T. Bechtold, A. Turcanu, W. Schrott, Electrochemical Reduction of CI Sulphur Black 1—Correlation Between Electrochemical Parameters and Colour Depth in Exhaust Dyeing, *Journal of Applied Electrochemistry*, Vol.38, No.1, 2007, pp. 25–30.

[78] J. Folch, J. Valldeperas-Morell, M. Lis, J. Viciana, I. Vancells, Reducci´on Electroquímica de Colorantes Sulfurosos, Vías de Proceso. *Journal Boletin Intexter*, Vol.129, 2006, pp. 29–34.

[79] S. Benkhaya, S. M'Rabet, A. El Harfi, A Review on Classifications, Recent Synthesis and Applications of Textile Dyes, *Inorganic Chemistry Communications*, Vol.115, 2020, 107891.

[80] A. Ghauch, A. Tuqan, N. Kibbi, S. Geryes, Methylene Blue Discoloration by Heated Persulfate in Aqueous Solution, *Chemical Engineering Journal*, Vol.213, 2012, pp. 259–271.

[81] C. W. Luo, D. J. Wu, L., Gan, X. X. Cheng, Q. Ma, F. X. Tan, J. Gao, W. W. Zhou, S. S. Wang, F. M. Zhang, J. Ma, Oxidation of Congo Red by Thermally Activated Persulfate Process: Kinetics and Transformation Pathway, *Separation Purification Technology*, Vol.244, 2020, 116839.

[82] X. Zhang, Y. Z. Qin, W. T. Zhang, Y. L. Zhang, G. E. Yuan, Oxidative Degradation of Orange G in Aqueous Solution by Persulfate Activated with Pyrite, *Water Science and Technology*, Vol.82, No.1, 2020, pp. 185–193.

[83] R. T. Kapoor, M. Danish, R. S. Singh, M. Rafatullah, H. Khalil, Exploiting Microbial Biomass in Treating Azo Dyes Contaminated Wastewater: Mechanism of Degradation and Factors Affecting Microbial Efficiency, *Journal of Water Process Engineering*, Vol.43, 2021, 102255.

[84] D. Kumar, Z. Patel, P. Pandit, R. Pandit, A. Patel, M. Joshi, C. Joshi, Textile Industry Wastewaters from Jetpur, Gujarat, India, are Dominated by Shewanellaceae, Bacteroidaceae, and Pseudomonadaceae Harboring Genes Encoding Catalytic Enzymes for Textile Dye Degradation, *Frontiers in Environmental Science*, Vol.9, 2021, 720707.

[85] T. M. Berhanea, J. Levya, M. P. S. Krekelerb and N. D. Danielson, Chemosphere, 2017, 176, 231–242.

[86] R. Han, J. Zhang, P. Han, Y. Wang, Z. Zhao and M. Tang, Chem. Eng. J., 2009, 145, 496–504.

[87] A. R. P. Hidayat, D. O. Sulistiono, I. K. Murwani, B. F. Endrawati, H. Fansuri, L. L. Zulfa and R. Ediati, J. Environ. Chem. Eng., 2021, 9, 106675.

[88] H. V. Tran, L. T. Hoang and C. D. Huynh, Chem. Phys., 2020, 535, 110793.

[89] R. Sander, Compilation of Henry's Law Constants (Version 5.0.0) for Water as Solvent, *Atmospheric Chemistry and Physics*, Vol.23, 2023, pp. 10901–12440.

[90] J. Setschenow, Über die Konstitution der Salzlösungen auf Grund ihres Verhaltens zu Kohlensäure, *Zeitschrift für Physikalische Chemie*, Vol.4, No.1, 1889, pp. 117–125.

[91] A. Schumpe, The Estimation of Gas Solubilities in Salt Solutions, *Chemical Engineering Science*, Vol.48, 1993, pp. 153–158.

[92] S. Weisenberger, A. Schumpe, Estimation of Gas Solubilities in Salt Solutions at Temperatures from 273K to 363K, *AIChE Journal*, Vol.42, No.1, 1996, pp. 298–300.

[93] B. R. Dhar, G. Nakhla, M. B. Ray, Techno-economic Evaluation of Ultrasound and Thermal Pretreatments for Enhanced Anaerobic Digestion of Municipal Waste Activated Sludge, Waste Management, Vol.32, 2012, pp. 542–549.

[94] Y. Ding, B. Wu, Z. Liu, X. Dai, Simultaneous Enhancing Phosphorus Recovery and Volatile Fatty Acids Production During Anaerobic Fermentation of Sewage Sludge with Peroxydisulfate Pre-Oxidation, *Bioresource Technology*, Vol.357, 2022, 127164.

[95] G. Du Laing, E. Meers, M. Dewispelaere, B. Vandecasteele, J. Rinklebe, F. M. G. Tack, M. G. Verloo, Heavy Metal Mobility in Intertidal Sediments of the Scheldt Estuary: Field Monitoring, *Science of the Total Environment*, Vol.407, 2009, pp. 2919–2930.

[96] L. L. Barton, W. A. Hamilton, (Eds.), *Sulphate-Reducing Bacteria: Environmental and Engineered Systems*, Sulphate-Reducing Bacteria: Environmental and Engineered Systems, Cambridge Univ Press, Cambridge, UK, 2007.

[97] C. Beltran, D. Jeison, F. G. Fermoso, R. Borja, Batch Anaerobic Co-Digestion of Waste Activated Sludge and Microalgae (Chlorella sorokiniana) at Mesophilic Temperature, *Journal of Environmental Science and Health, Part A: Toxic/Hazardous Substances and Environmental Engineering*, Vol.51, 2016, pp. 847–850.

[98] R. Bentley, T. G. Chasteen, Environmental VOSCs-Formation and Degradation of Dimethyl Sulfide, Methanethiol and Related Materials, *Chemosphere*, Vol.55, 2004, pp. 291–317.

[99] X. Bi, X. Feng, Y. Yang, X. Li, G. P. Y. Sin, G. Qiu, X. Qian, F. Li, T. He, P. Li, T. Liu, Z. Fu, Heavy Metals in an Impacted Wetland System: A Typical Case from Southwestern China, *Science of the Total Environment*, Vol.387, 2007, pp. 257–268.

[100] M. V. Biber, M. dos Santos Afonso, W. Stumm, The Coordination Chemistry of Weathering: IV Inhibition of the Dissolution of Oxide Minerals, *Geochimica et Cosmochimica Acta*, Vol.58, 1994, pp. 1999–2010.

[101] A. S. Bradley, W. D. Leavitt, D. T. Johnston, Revisiting the Dissimilatory Sulfate Reduction Pathway, *Geobiology*, Vol.9, 2011, pp. 446–457.

[102] J. Cao, Y. Wu, J. Zhao, S. Jin, M. Aleem, Q. Zhang, F. Fang, Z. Xue, J. Luo, Phos phorus recovery as vivianite from waste activated sludge via optimizing iron source and pH value during anaerobic fermentation. *Bioresource Technology*, Vol.293, 2019, 122088

[103] I. T. Cha, U. G. Min, S. J. Kim, K. J., Yim, S. W. Roh, S. K. Rhee, Methanomethylovorans Uponensis sp nov., a Methylotrophic Methanogen Isolated from Wetland Sediment, *Antonie van Leeuwenhoek International Journal of General and Molecular Microbiology*, Vol.104, 2013, pp. 1005–1012.

[104] C. C. Chang, Y. H. Chen, Y. S. Lin, Z. S. Hung, M. H. Yuan, C. Y. Chang, Y. S. Li, J. L. Shie, Y.

H. Chen, Y. C. Wang, C. H. Ko, F. C. Lin, C. Ho, B. L. Liu, K. W. Liu, S. G. Wang, A Pilot Plant Study on the Autoclaving of Food Wastes for Resource Recovery and Reutilization, *Sustainability*, Vol.10, 2018, 3566.

[105] Y. Hu, Y. Yang, Y. Y. Li, Effects of operational variations of micro-oxygenation and pH shock on the competition between methane production and sulfate reduction in a UASB reactor. *Journal of Environmental Chemical Engineering*, Vol.10, 2022, 108390.

[106] F. Omil, P. Lens, A. Visser, L. W. H. Pol, G. Lettinga, Long-Term Competition between Sulfate Reducing and Methanogenic Bacteria in UASB Reactors Treating Volatile Fatty Acids, *Biotechnology and Bioengineering*, Vol.57, 1998, pp. 676–685.

[107] T. F. Rozan, M. Taillefert, R. E. Trouwborst, B. T. Glazer, S. F. Ma, J. Herszage, L. M. Valdes, K. S. Price, G. W. Luther, Iron-Sulfur-Phosphorus Cycling in the Sediments of a Shallow Coastal Bay: Implications for Sediment Nutrient Release and Benthic Macroalgal Blooms, *Limnology and Oceanography*, Vol.47, 2002, pp. 1346–1354.

[108] H. Huang, B. K. Biswal, G.-H. Chen, D. Wu, Sulfidogenic Anaerobic Digestion of Sulfate-Laden Waste Activated Sludge: Evaluation on Reactor Performance and Dynamics of Microbial Community, *Bioresource Technology*, Vol.297, 2020, 122396.

[109] H. Chen, J. Wu, B. Liu, Y. Li, H. Yasui, Competitive Dynamics of Anaerobes during Long-Term Biological Sulfate Reduction Process in a UASB Reactor, *Bioresource Technology*, Vol.280, 2019, 173–182.

[110] S. F. Cox, J. D. McKinley, A. S. Ferguson, G. O'Sullivan, R. M. Kalin, Degradation of Carbon Disulphide (CS_2) in Soils and Groundwater from a CS_2-Contaminated Site, *Environmental Earth Sciences*, Vol.68, 2013, pp. 1935–1944.

[111] C. Cruz Viggi, F. Pagnanelli, A. Cibati, D. Uccelletti, C. Palleschi, L. Toro, Biotreatment and Bioassessment of Heavy Metal Removal by Sulphate Reducing Bacteria in Fixed Bed Reactors, *Water Research*, Vol.44, 2010, pp. 151–158.

Contribution of Individual Authors to the Creation of a Scientific Article (Ghostwriting Policy)

Prof. Dr. Delia Teresa Sponza and Post-Dr. Rukiye Öztekin took an active role in every stage of the preparation of this article.

The authors equally contributed in the present research, at all stages from the formulation of the problem to the final findings and solution.

Sources of Funding for Research Presented in a Scientific Article or Scientific Article Itself

The experimental phases of this research study were conducted at the National Research Council (NRC) of Canada, Research Centers, Ontario, Canada. The authors would like to thank this body for providing financial support.

Conflict of Interest

The authors have no conflicts of interest to declare that are relevant to the content of this article.

APPENDIX

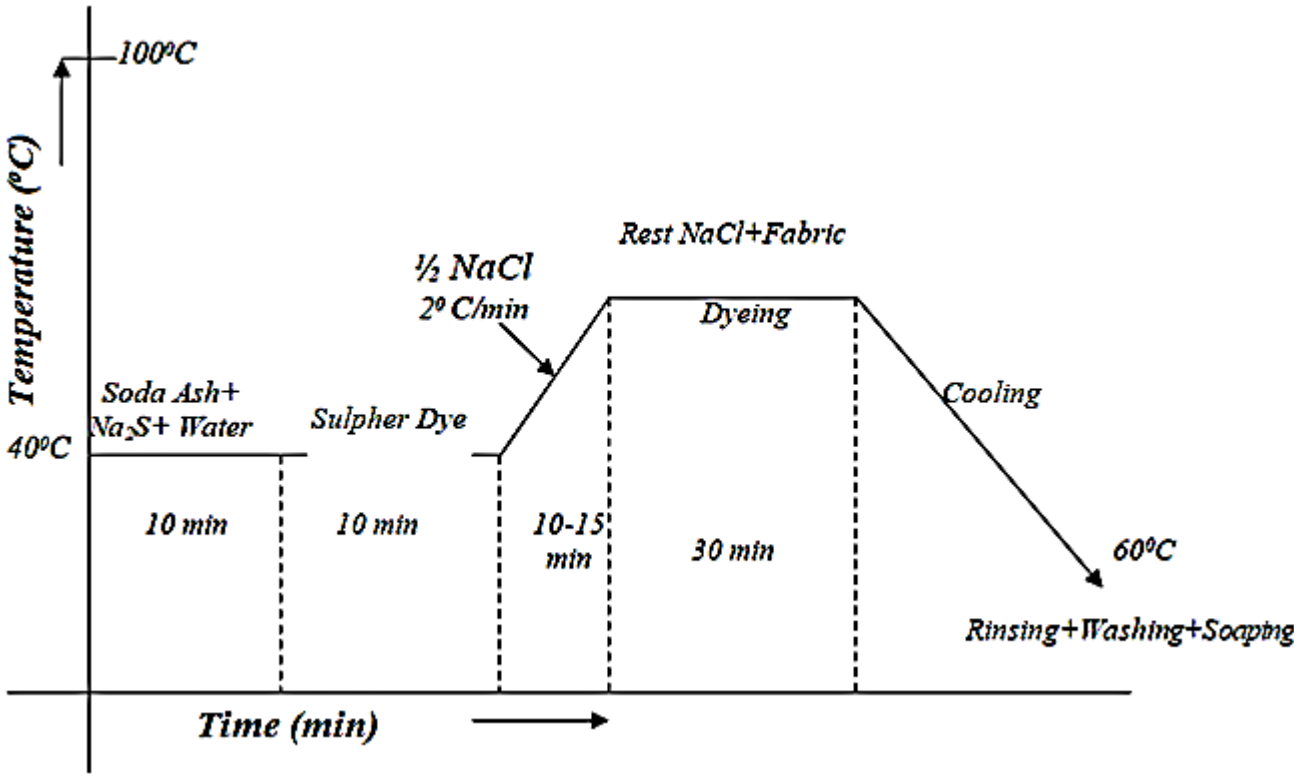

Figure 1. The experimental steps of sulfur dyes.

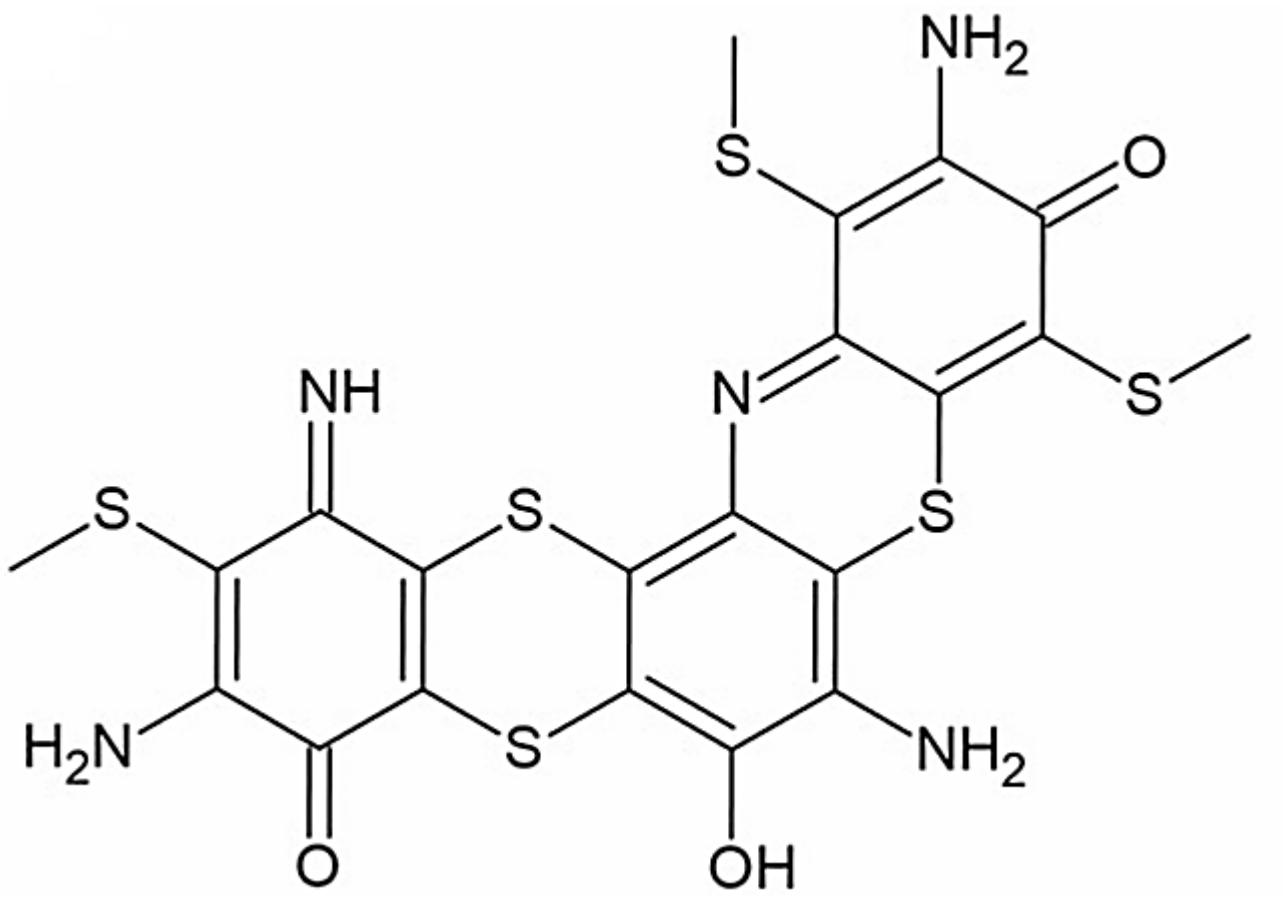

Figure 2. Chemical structure of Sulfur Black 1 (SB 1) ($C_{18}H_8N_4O_5S_2$) dyestuff.

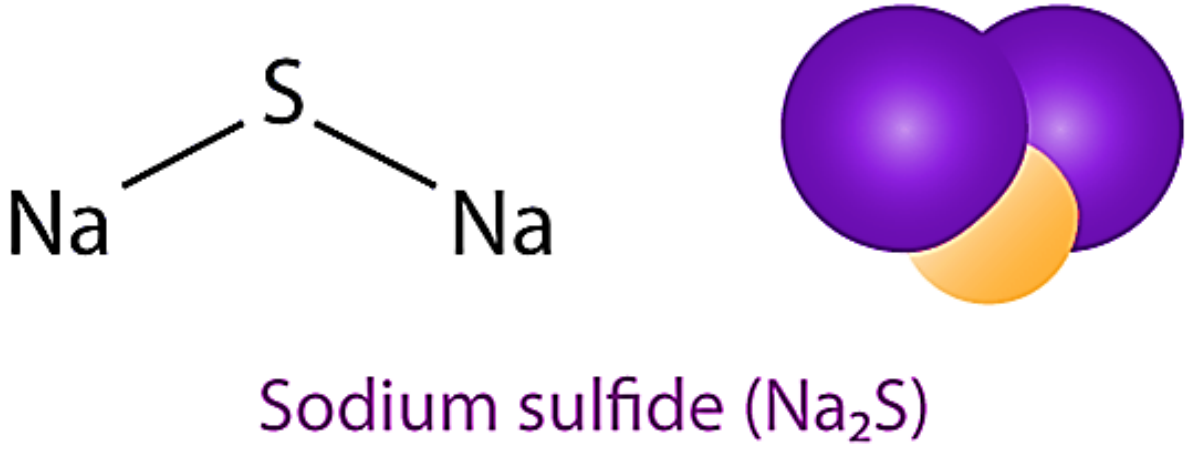

Figure 3. Chemical structure of sodium sulfur (Na_2S).

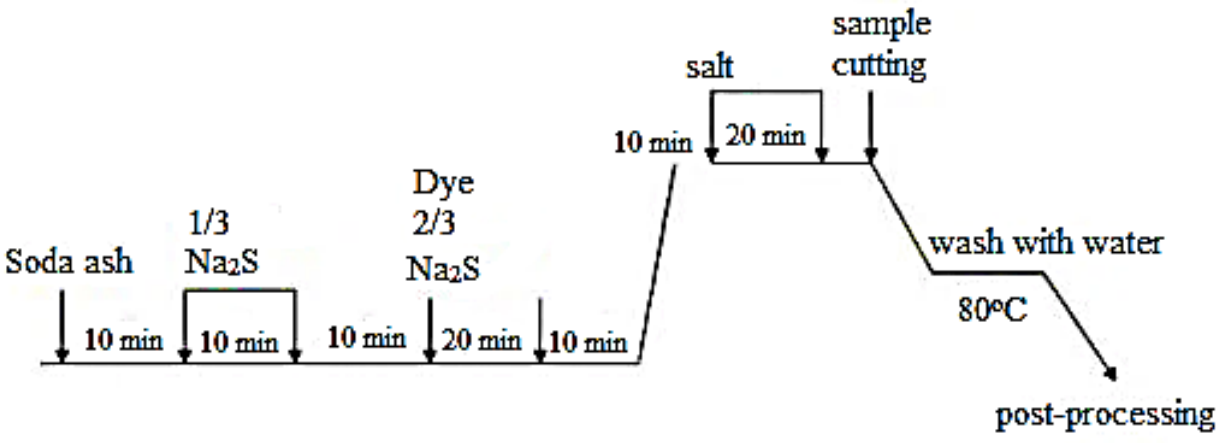

Figure 4. The application of Na_2S chemical at dying process.

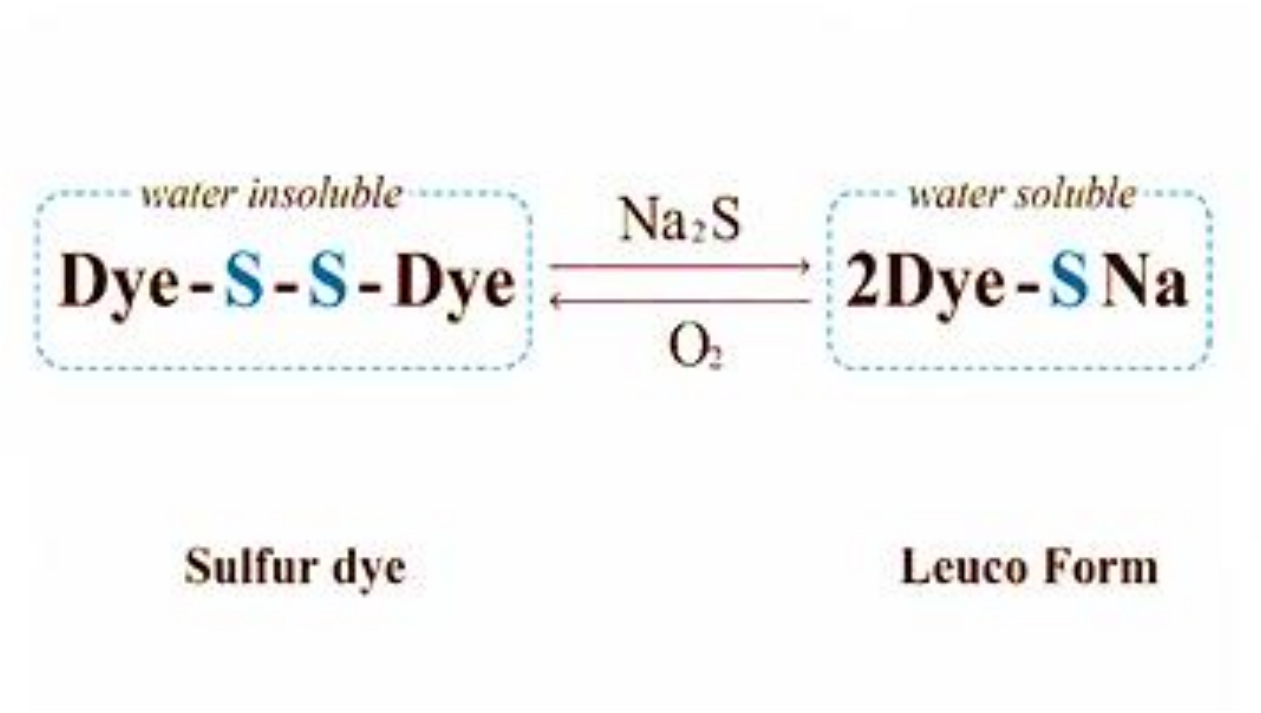

Figure 5. Sulfur dye degradation with Na_2S.

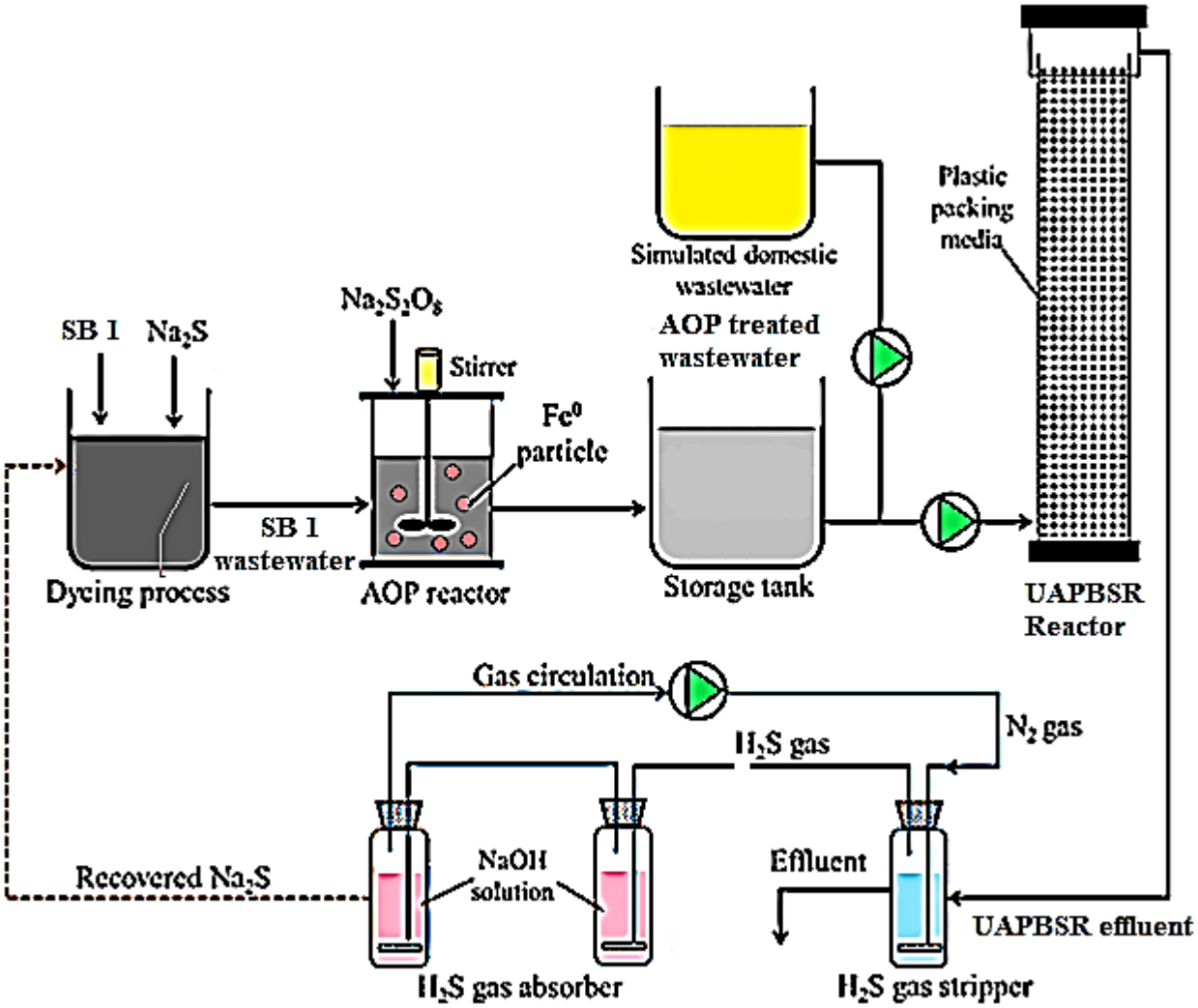

Figure 6. Schematic illustration of the reactor setup for evaluation of Sulfur Black 1 (SB 1) degradation and Na_2S recovery by sulfur-circular process.

Table 1. Experimental conditions of the UAPBSR reactor.

Steps	**Periods (days)**	**Hydraulic Retention Time (HRT) (hours)**	**Volume ratio of AOP-treated wastewater to domestic wastewater**	**Average influent TOC concentration (mg C/l)**	**Average influent SO_4^{-2} concentration (mg S/l)**
Step 1	0 – 150	41	0/1	112	200
Step 2	151 – 300	30	1/3	109	385
Step 3	301 – 450	29	1/2	97	541
Step 4	451 - 600	28	1/4	106	600

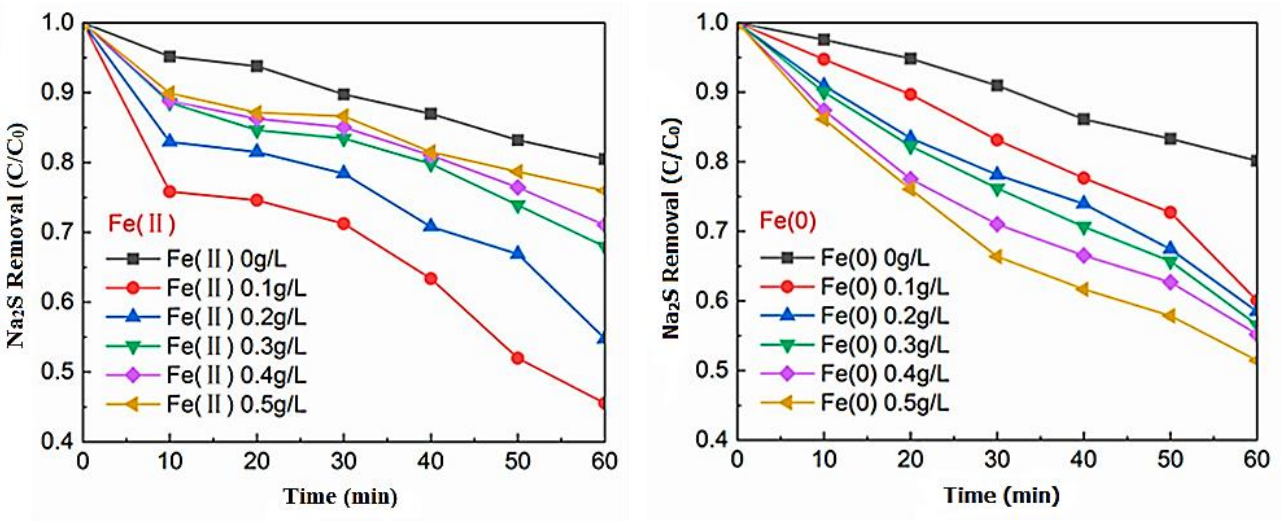

(a) **(b)**

Figure 7. (a) Fe(II) dosage versus Na_2S removal and **(b)** Fe(0) dosage versus Na_2S removal. [Na_2S]=5 mg/l, [PS]=0.2 mM, T=20 ± 1°C, pH= 6.8±0.2, respectively.

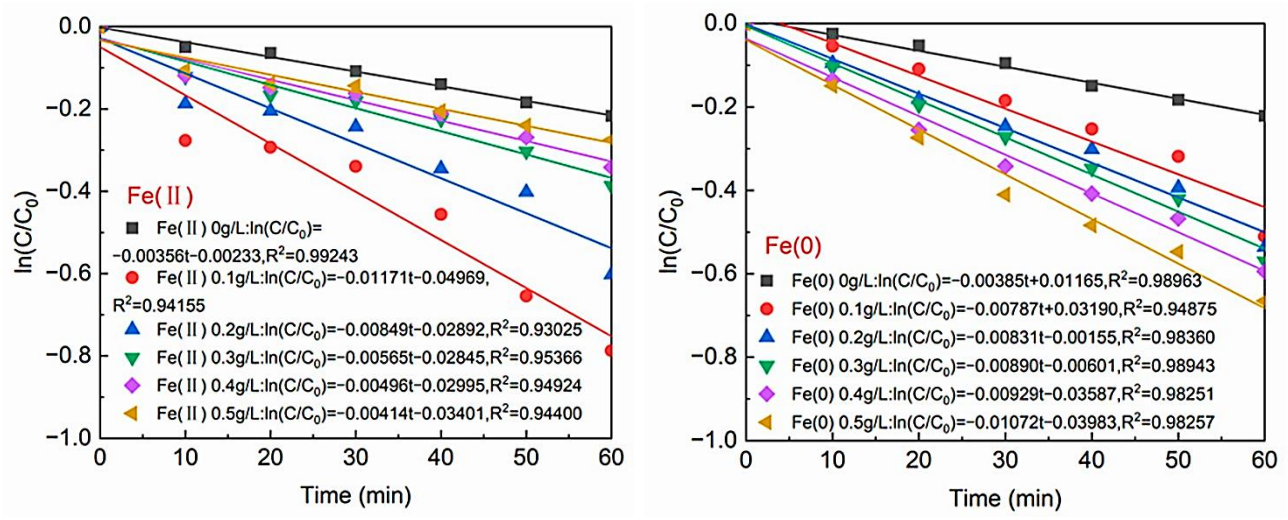

Figure 8. Reaction kinetics of **(a)** Fe(II) and **(b)** Fe(0). [Na_2S]=5 mg/l, [PS]=0.2 mM, T=20±1°C, pH=6.8±0.2, respectively.

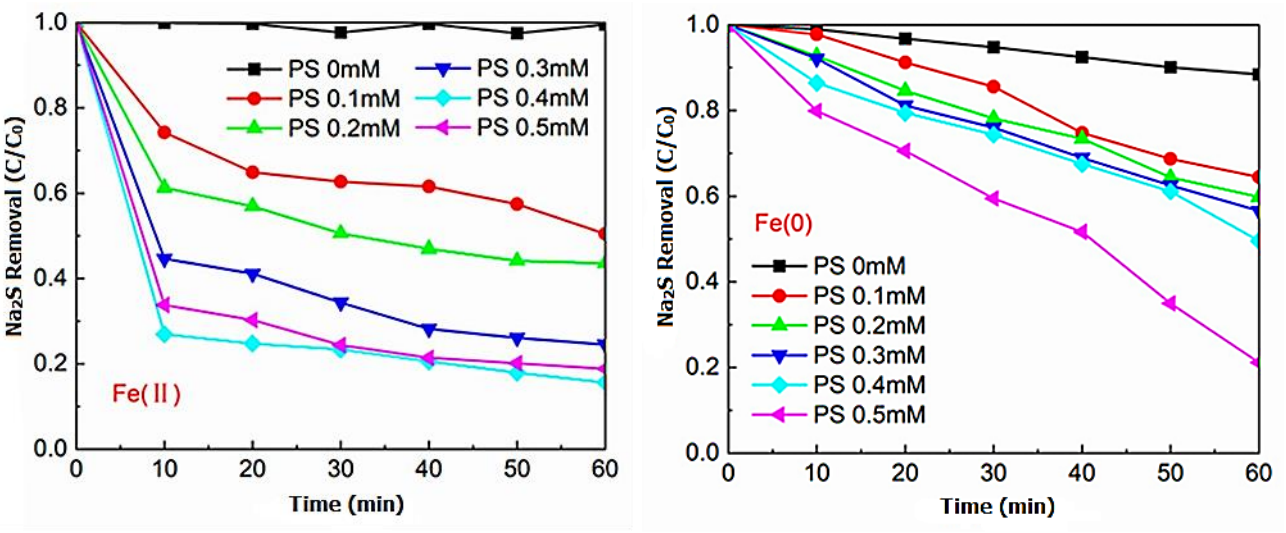

Figure 9. Persulfate (PS) dosage versus Na_2S removal by **(a)** Fe(II) and **(b)** Fe(0). [Na_2S]=5 mg/l, [Fe(II)]=0.1 g/l, [Fe(0)]=0.1 g/l, T=20 ± 1°C, pH = 6.8 ± 0.2, respectively.

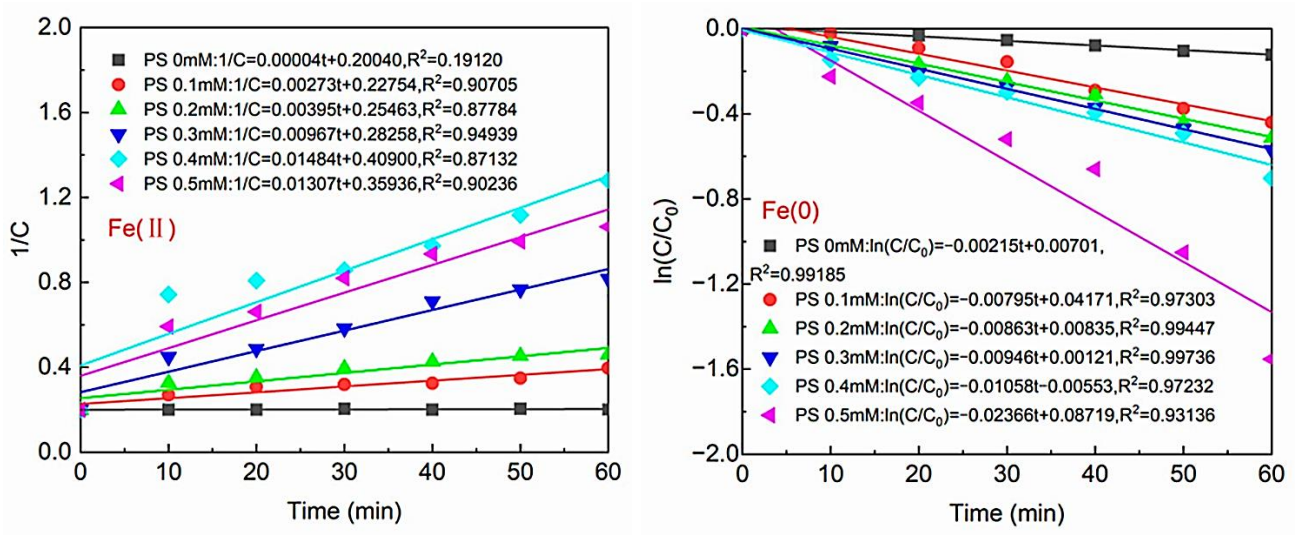

Figure 10. Reaction kinetic of **(a)** Fe(II) and **(b)** Fe(0). [Na_2S]=5 mg/l, [Fe(II)]=0.1 g/l, [Fe(0)]=0.1 g/l, T=20±1°C, pH=6.8±0.2, respectively.

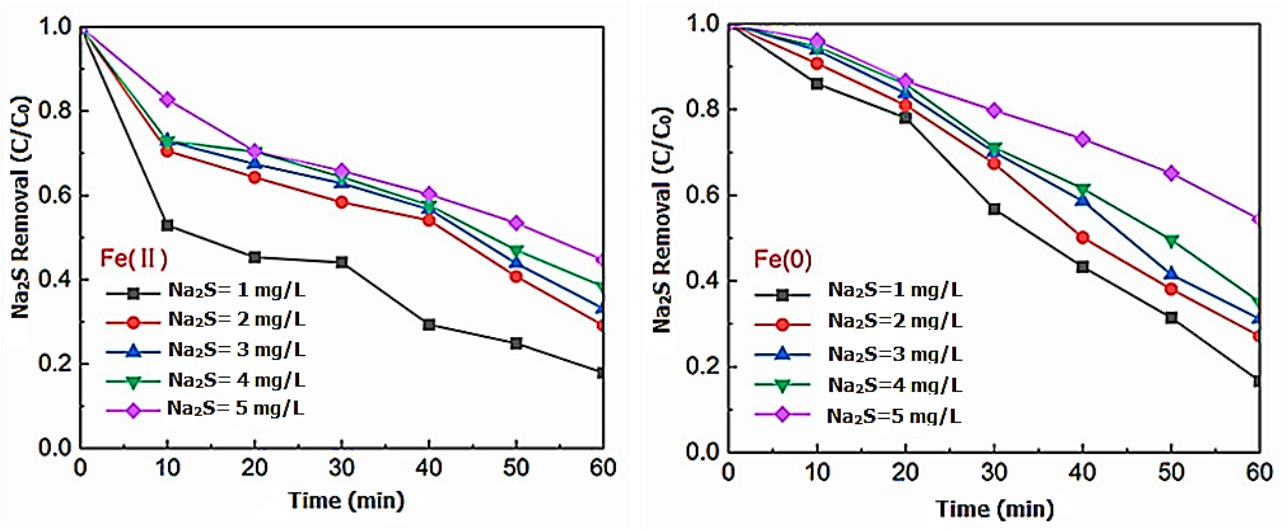

(a) **(b)**

Figure 11. Na_2S concentration versus Na_2S removal by **(a)** Fe(II), and **(b)** Fe(0). [PS]= 0.2 mM, [Fe(II)]=0.1 g/l, [Fe(0)]=0.1 g/l, T=20±1°C, pH=6.8±0.2, respectively.

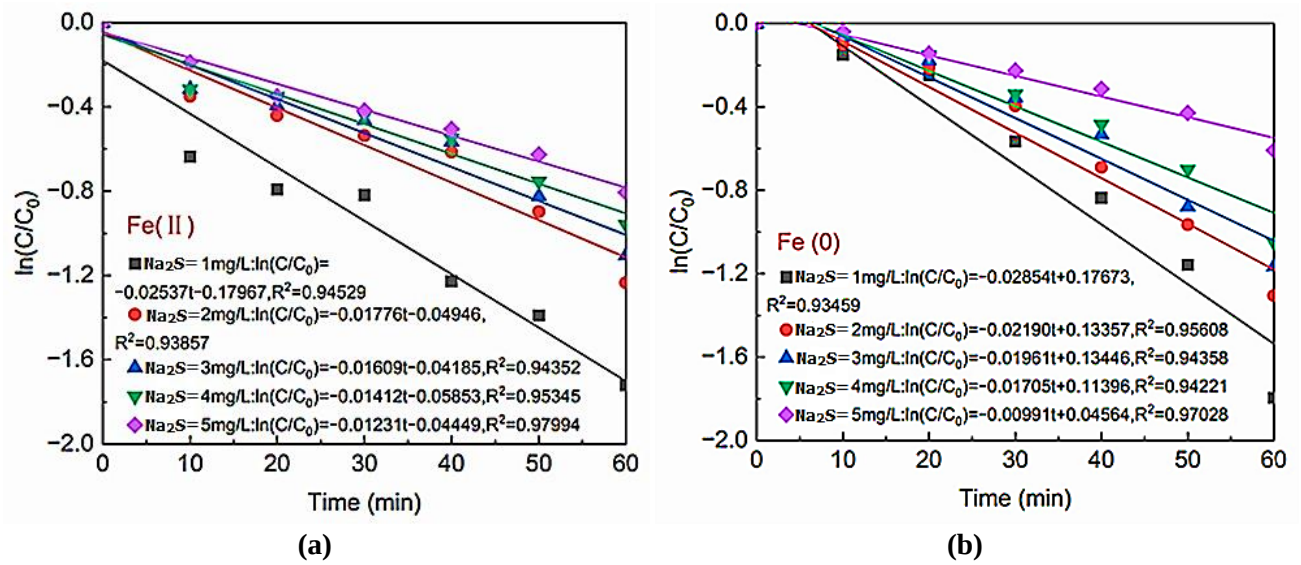

Figure 12. Reaction kinetics of **(a)** Fe(II), and **(b)** Fe(0). [PS]=0.2 mM, [Fe(II)]=0.1 g/l, [Fe(0)]=0.1 g/l, T=20±1°C, pH=6.8±0.2, respectively.

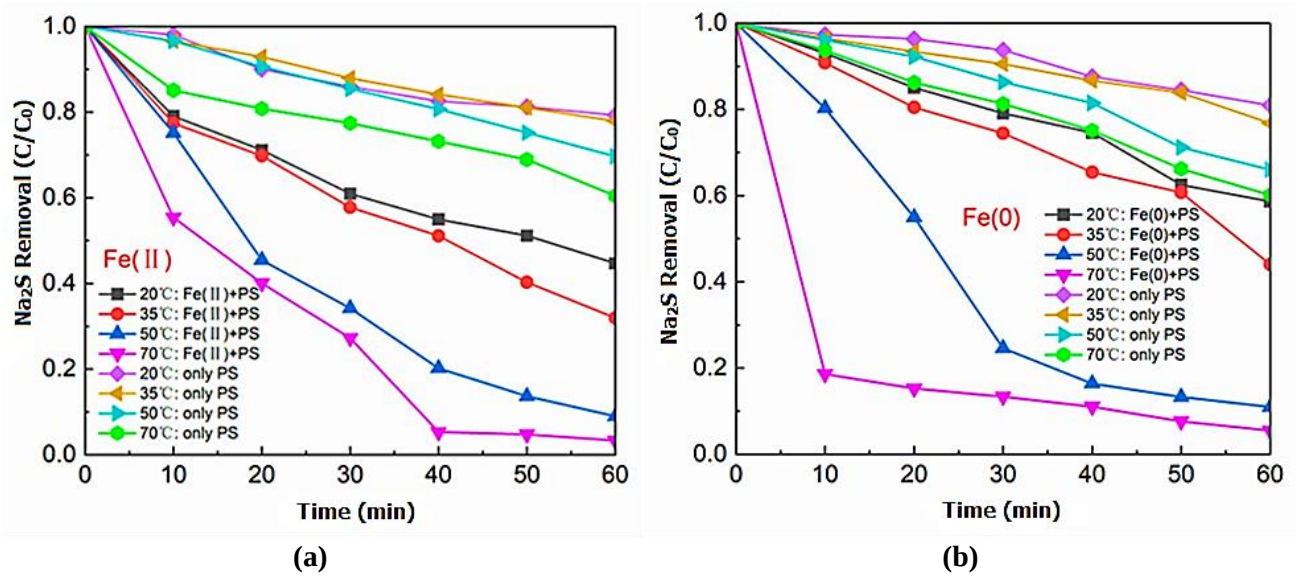

Figure 13. Reaction temperature versus Na_2S removal by **(a)** Fe(II) and **(b)** Fe(0), respectively. [Na_2S]=5 mg/l, [PS]=0.2 mM, [Fe(II)]=0.1 g/l, [Fe(0)]=0.1 g/l, pH=6.8±0.2.

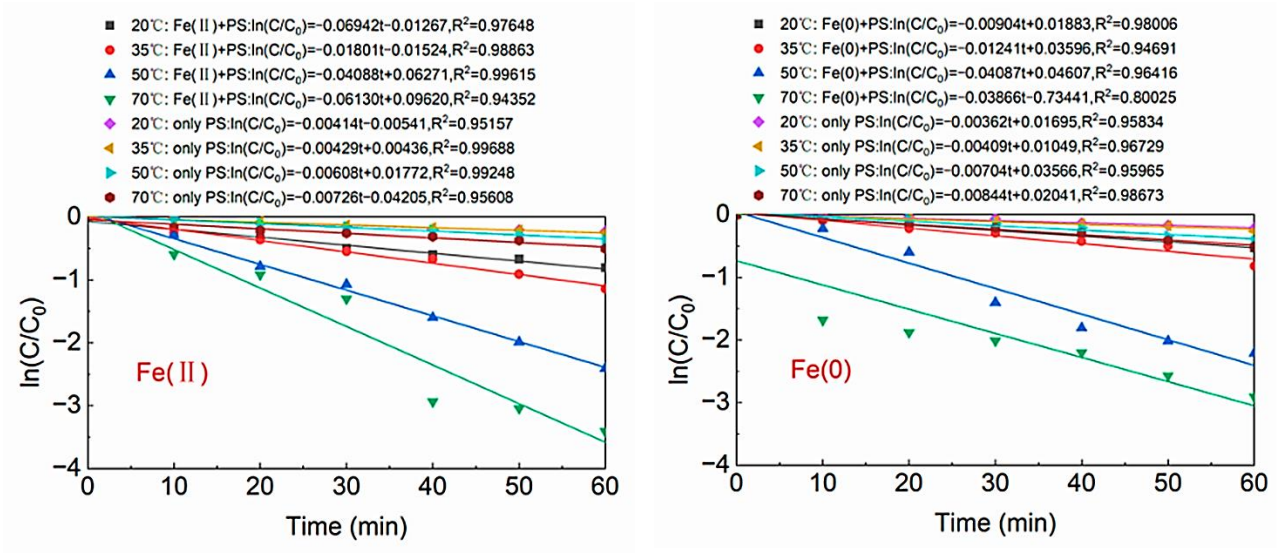

(a) **(b)**

Figure 14. Reaction kinetics of **(a)** Fe(II) and **(b)** Fe(0). [Na2S]=5 mg/l, [PS]=0.2 mM, [Fe(II)]=0.1 g/l, [Fe(0)]=0.1 g/l, pH=6.8±0.2, respectively.

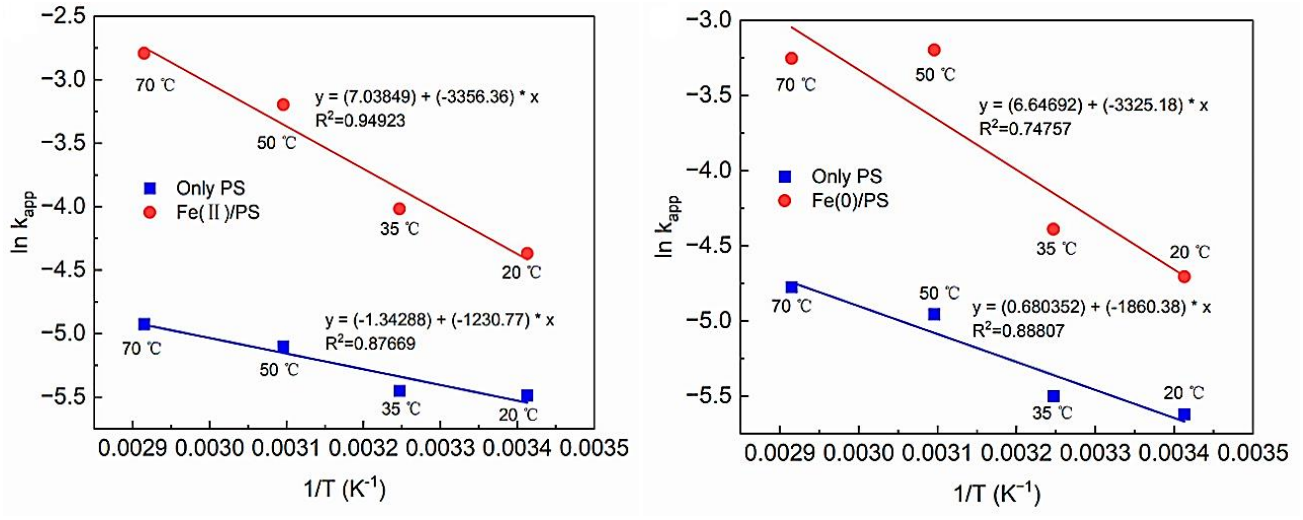

(a) **(b)**

Figure 15. Thermodynamic equation of **(a)** Fe(II); and **(b)** Fe(0). [Na_2S]=5 mg/l, [PS]=0.2 mM, [Fe(II)]=0.1 g/l, [Fe(0)]=0.1 g/l, pH=6.8±0.2, respectively.

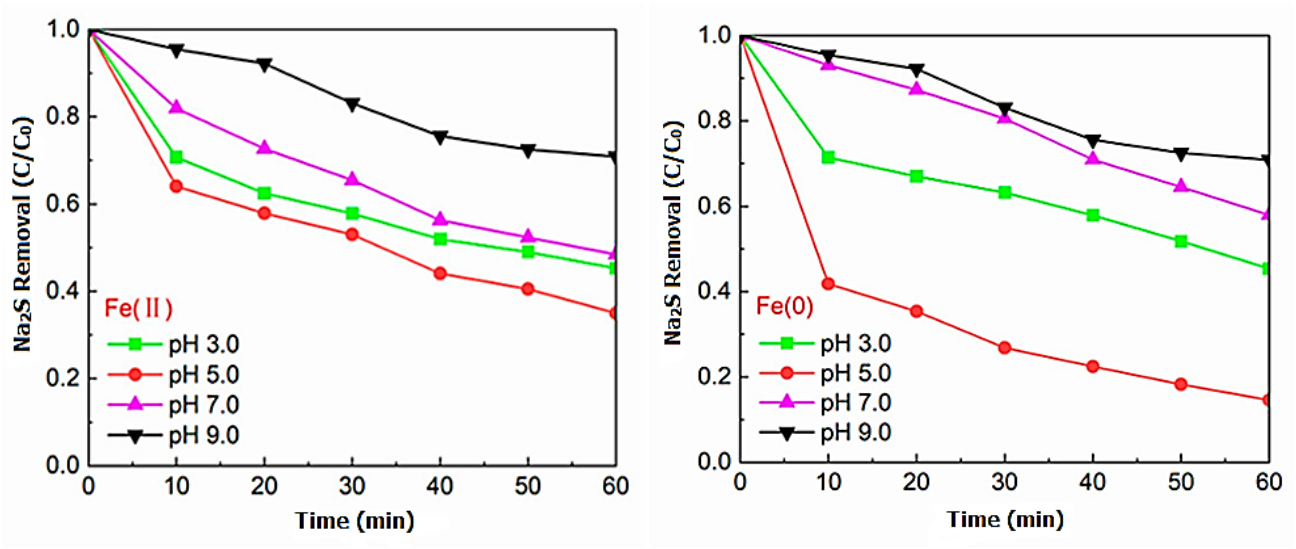

Figure 16. Reaction temperature versus Na_2S removal by **(a)** Fe(II) and **(b)** Fe(0). [Na_2S]=5 mg/l, [PS]=0.2 mM, [Fe(II)]=0.1 g/l, [Fe(0)]=0.1 g/l, T=20±1°C, respectively.

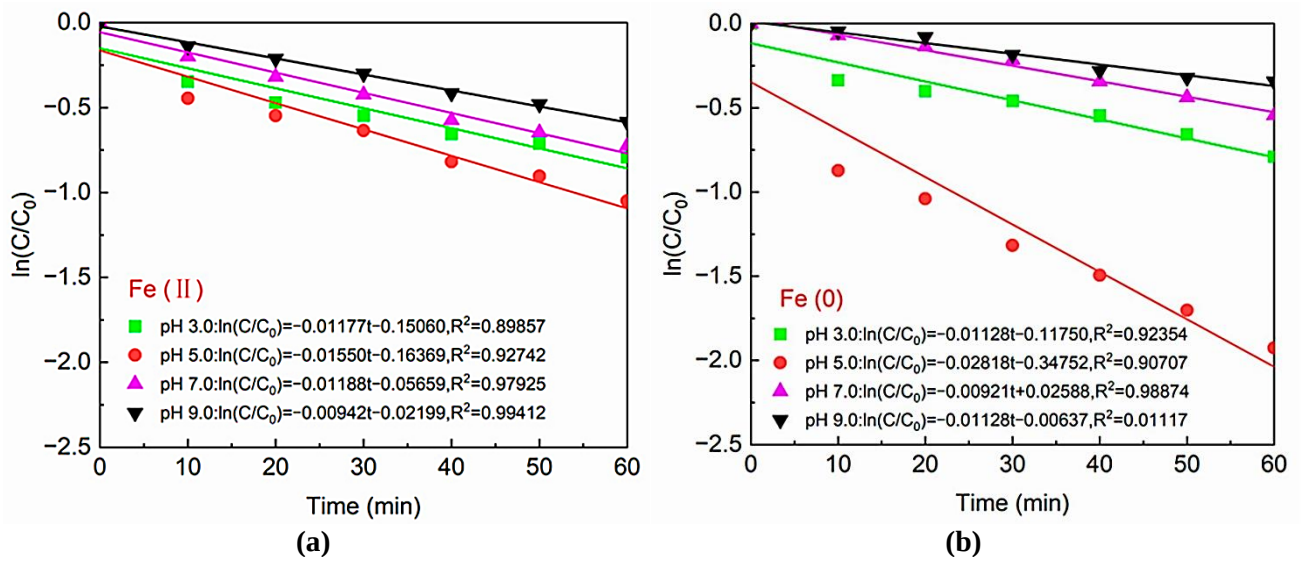

Figure 17. Reaction kinetics of **(a)** Fe(II) and **(b)** Fe(0). [Na_2S]=5 mg/l, [PS]=0.2 mM, [Fe(II)]=0.1 g/l, [Fe(0)]=0.1 g/l, T=20±1°C, respectively.

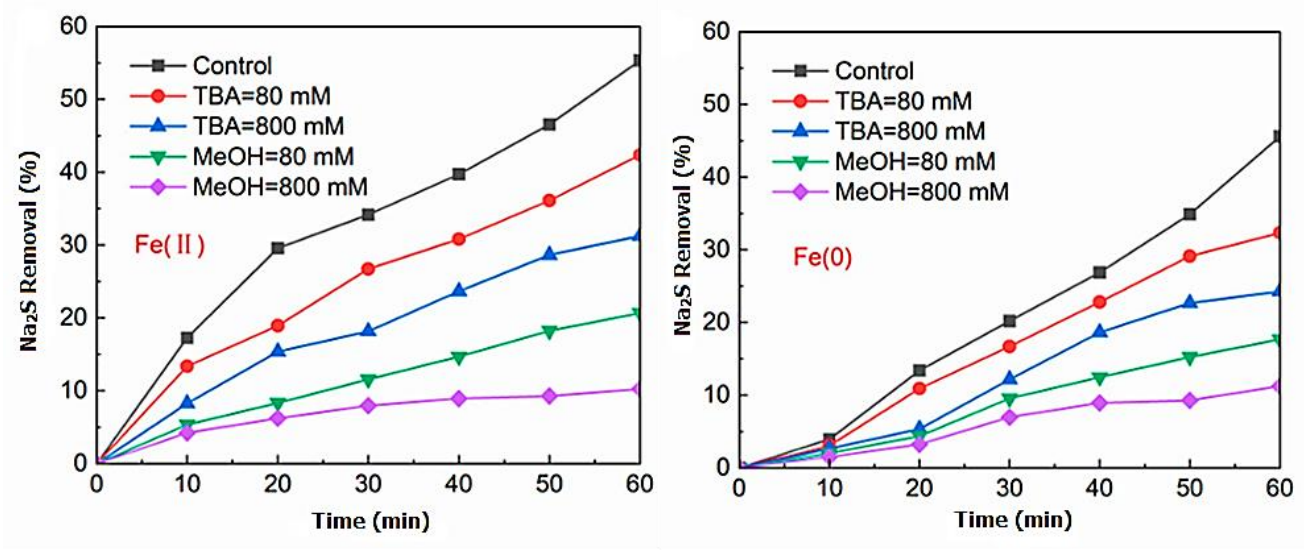

Figure 18. Quenching experiment by **(a)** Fe(II) and **(b)** Fe(0). [Na_2S]=5 mg/l, [PS]=0.2 mM, [Fe(II)]=0.1 g/l, [Fe(0)]=0.1 g/l, T=20±1°C, respectively.

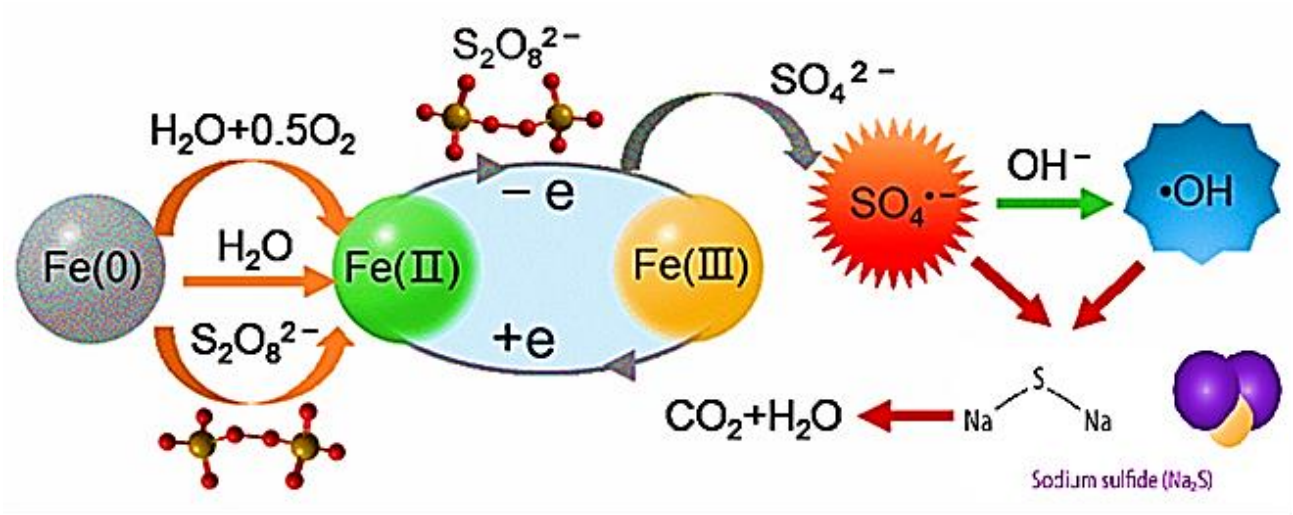

Figure 19. The schematic diagram of the mechanism of the Fe system activating PS to degrade Na_2S.

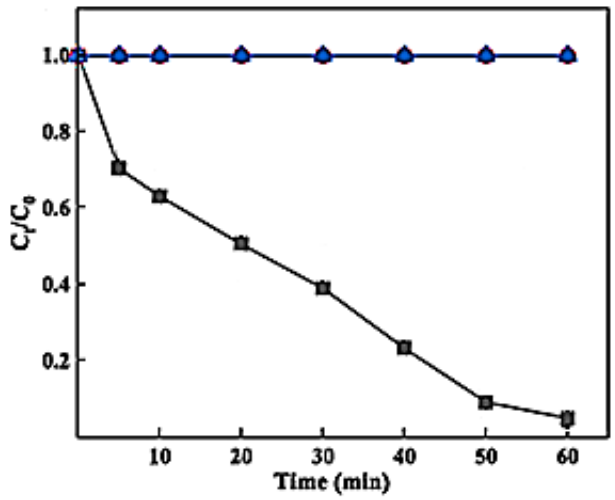

(a)

Black square: Fe^0-SPS, Red circle: Fe^0, Blue triangle: SPS

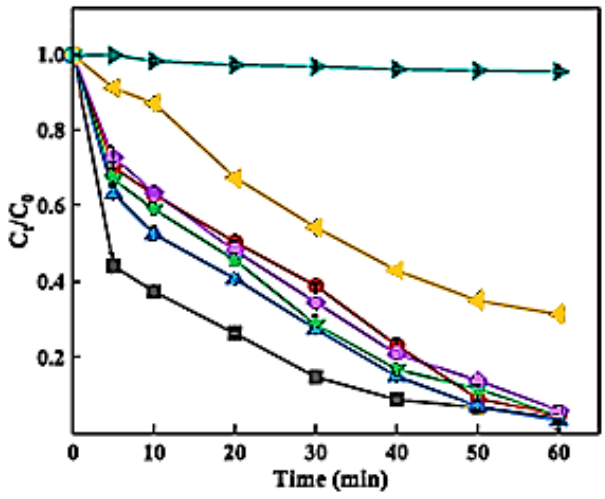

(b)

Black square: pH=5.0, Red circle: pH=6.0, Blue triangle: pH=7.0, Dark green triangle: pH=8.0, Purple rhombus: pH=9.0, Yellow triangle: pH=10.0, Light green triangle: pH=11.0

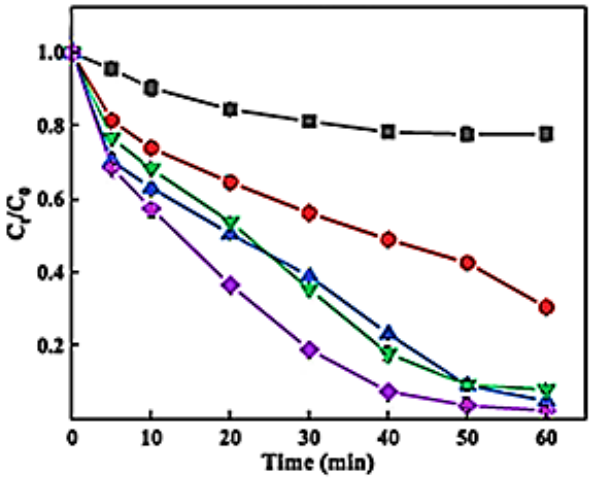

(c)

Black square: SPS/Fe^0=0.25/1, Red circle: SPS/Fe^0=0.5/1, Blue triangle: SPS/Fe^0=0.75/1, Green triangle: SPS/Fe^0=1/1, Purple rhombus: SPS/Fe^0=1.5/1

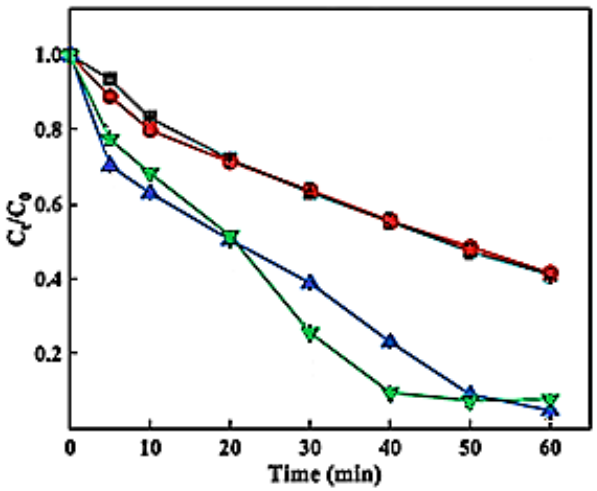

(d)

Black square: SPS/Fe^0=0.75/0.25, Red circle: SPS/Fe^0=0.75/0.5, Blue triangle: SPS/Fe^0=0.75/1, Green triangle: SPS/Fe^0=0.75/1.5

Figure 20. Degradation of Sulfur Black 1 (50 mg/l) by Fe^0-sodium persulfate system under different conditions: **(a)** Degradation of Sulfur Black1 by using only sodium persulfate (SPS, 0.75 g/l), only Fe^0 particles (1.0 g/l) and Fe^0 particles (1.0 g/l) + SPS (0.75 g/l) under initial pH=6.0; **(b)** Effect of initial pH (0.75 g/l SPS and 1.0 g/l Fe^0 particles); **(c)** Effect of SPS dosage at initial pH=6.0 and 1.0 g/l Fe^0 particles; and **(d)** Effect of Fe^0 particles at initial pH=6.0 and 0.75 g/l SPS, respectively.

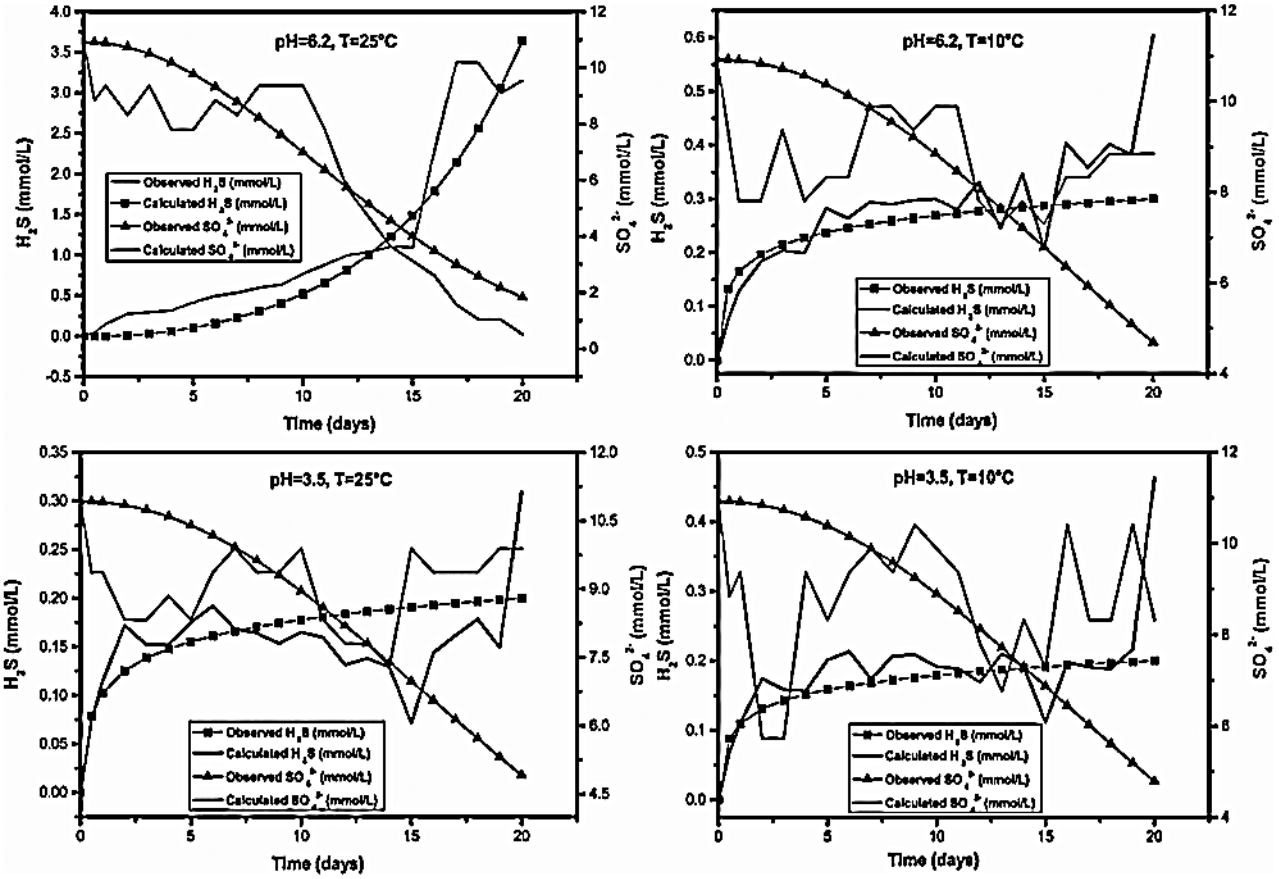

Figure 21. Proposed model with realistic temporal evolution of sulphate (SO42-) and sulphide (H2S) in a closed system.

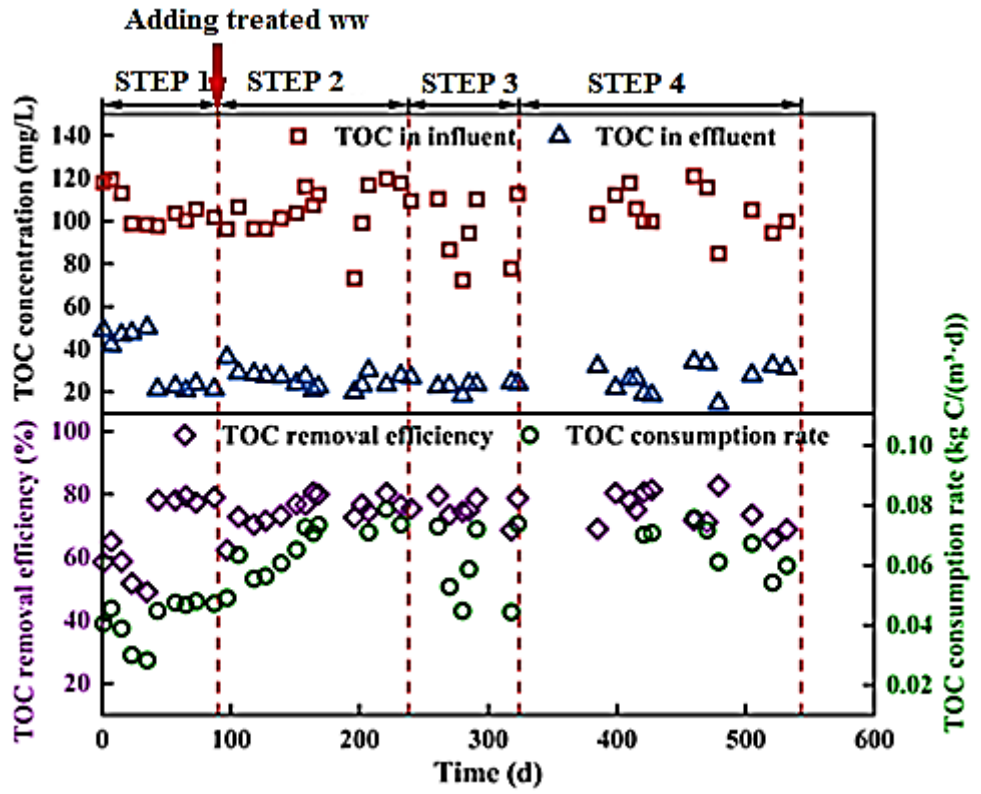

(a)

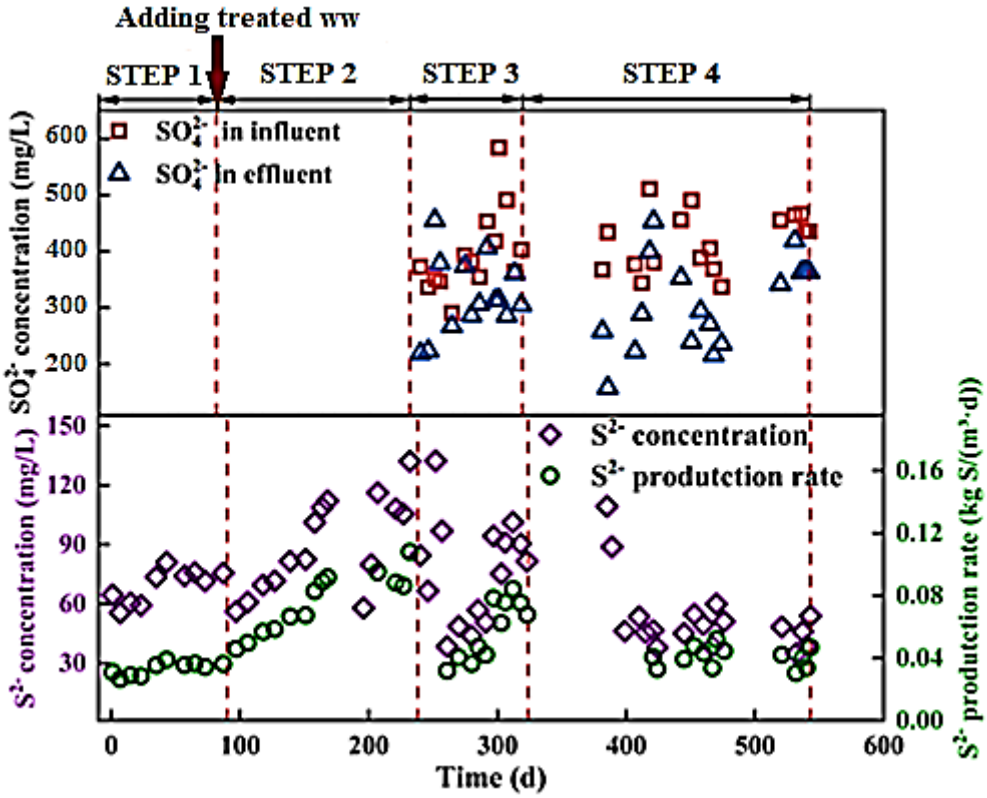

(b)

Figure 22. The performance of the UAPBSR reactor in Steps 1-4: **(a)** TOC removal and **(b)** sulfate consumption and sulfide production, respectively.

Table 2. The efficiencies of stripping and absorption of H_2S from the UAPBSR effluents in various stages

STEPS	**Stripping Efficiencies (%)**	**Absorption Efficiencies (%)**
Step 1	86.70	90.12
Step 2	99.82	99.90
Step 3	99.90	99.90
Step 4	99.90	99.90

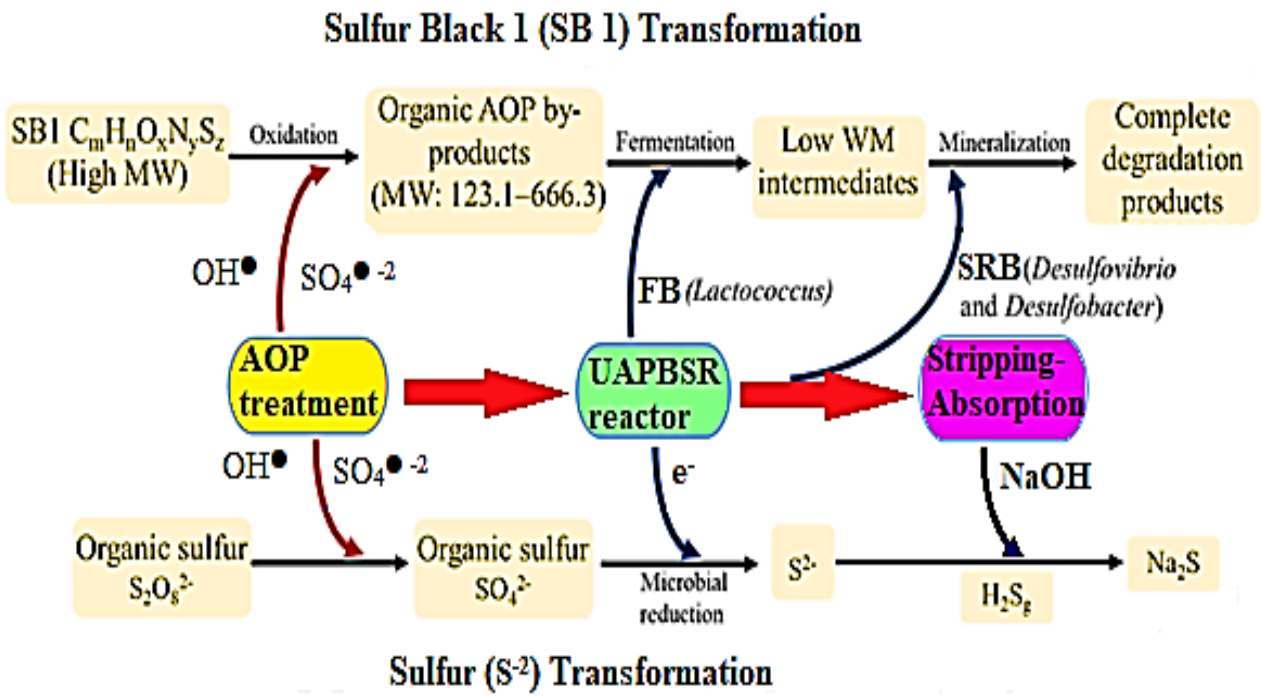

Figure 23. The degradation mechanism of Sulfur Black 1 dyestuff and sulfur (S^{-2}) substance transformation in the sulfur-circular process (FB: fermentative bacteria, SRB: sulphate reduction bacteria, MW: molecular weights).

Table 3. Total mass balance of sulphured substances

INFLUENT	**INSIDE REACTOR**	**Converted amount**	**Removal percentage (%)**	**EFFLUENT**	**Recovery**
Particular Organic sulphide (100 mol)	Soluble organic sulphide (96 mol)		99%		Na_2S (50 mol)
	METHIONIN 40 mol CYSTEIN 40 mol	(20 mol)	CH_3-S-CH_3 (19 mol) (99%)	H_2S (0. mol) HS^- (0.01 mol)	
	H_2S (18 mol) HS^- (17 mol) S^{-2} (12 mol) CS_2 16 mol	CH_3-SH (MM) (18 mol) H_2S (6 mol) HS^- (5 mol) S^{-2} (5 mol)	DMS (14 mol) (99) H^2S (99%) HS^- (99%) S^{-2} (99%)	S^{-2} (0.001 mol) + NaOH H_2S (0.01 mol) HS^- (0.01 mol) S^{-2} (0.01 mol)	
		H_2S (4 mol) HS^- (5 mol) S^{-2} (4 mol)		+ NaOH	

Table 4. Corresponding equations and parameters of the Na_2S kinetic models and intraparticle diffusion (IPD) model for sulfide adsorption on the Na_2S adsorbent.

Model	**Parameters**	**Values**
$Pseudo-first\ order\ Ln[Q_e - Q_t] = \ln[Q_e] - k_t t$	$k_t(min^{-1})$	0.03678
	$Q_{e(cal)}(mg\ g^{-1})$	20.57
	$Q_{e(\exp)}(mg\ g^{-1})$	49.55
		0.9961
$Pseudo-second\ order\ \frac{t}{Q_t} = \frac{1}{k_t Q_e^2} + \frac{t}{Q_e}$	$k_t(mg^{-1}min^{-1})$	0.005194
	$Q_{e(cal)}(mg\ g^{-1})$	50.66
	$Q_{e(\exp)}(mg\ g^{-1})$	49.57
	R^2	0.9996
$Intraparticle\ diffusion\ Q_e = k_t t^{0.5} + C_i$	$k_1(mg\ g^{-1}min^{-0.5})$	6.365
	C_1	14.15
	R_1^2	0.9998
	$k_2(mg\ g^{-1}min^{-0.5})$	5.793
	C_2	13.37
	R_2^2	0.9999
	$k_3(mg\ g^{-1}min^{-0.5})$	0.1581
	C_3	47.41
	R_3^2	0.9982

Table 5. Linear and nonlinear isotherm models and parameters of the Freundlich and Langmuir models for sulfide adsorption on Na_2S.

Model	**Parameters**	**Values**
$Langmuir\ linear\ isotherm\ \frac{1}{Q_e} = \left(\frac{1}{Q_{max} x K_L}\right)\frac{1}{C_e} + \frac{1}{Q_{max}}$	$q_{max}(mg\ g^{-1})$	173.02
	K_L	0.0373
	R^2	0.9988
$Langmuir\ non-linear\ isotherm\ Q_e = \frac{q_{max} K_L C_e}{1+K_L C_e}$	$q_{max}(mg\ g^{-1})$	251.33
	K_L	0.0208
	R^2	0.9941
$Freundlich\ linear\ isotherm\ logq_e = logK_F + \frac{1}{n} logC_e$	1/n	0.7407
	K_F	7.78
	R^2	0.9962
$Freundlich\ linear\ isotherm\ Q_e = K_F C_e^{\frac{1}{n}}$	1/n	0.7069
	K_F	8.62
	R^2	0.9975

Table 6. RMSE and χ^2 values of the linear and nonlinear adsorption isotherm models for sulfide adsorption onto Na_2S.

		Parameters	
Model		**RMSE**	χ^2
Langmuir	Linear	0.0009	0.0004
	Non-linear	2.8999	1.3839
Freundlich	Linear	0.0218	0.0019
	Non-linear	2.1783	0.5736

Table 7. Thermodynamic parameters for the adsorption of sulfide on Na_2S.

Temperature (ºC)	**ΔG (kJ/mol)**	**ΔH (kJ/mol)**	**ΔS (J/mol.K)**
25	-3.2732	5.762	30.4145
35	-3.6663		
45	-3.8776		

Table 8. Synthesis of the different equations used to determine the pH evolution.

Inlet concentrations	**Equations**	**Outlet concentrations**	**Equations**
$[OH^-]_{in} = 10^{pH_{in}-pK_{water}}$	38	$[OH^-]_0 = 10^{pH_0-pK_{water}}$	43
$[H_3O^+]_{in} = 10^{-pH_{in}}$	39	$[H_3O^+]_0 = 10^{-pH_0}$	44
$[H_2S]_{in} = \frac{C_{T,in}}{1+10^{pH_{in}-pK_aH_2S}}$	40	$[H_2S]_0 = \frac{C_{T,0}}{1+10^{pH_0-pK_aH_2S}}$	45
$[CO_3^{-2}]_{in} = \frac{TAC}{1+10^{pK_{a1}-pH_{in}}+10^{pK_{a1}-pK_{a2}-2pH_{in}}}$	41	$[CO_3^{-2}]_0 = \frac{TAC}{1+10^{pK_{a1}-pH_0}+10^{pK_{a1}-pK_{a2}-2pH_0}}$	46
$[H_2CO_3]_{in} = \frac{TAC}{1+10^{pK_{a1}-pH_{in}}+10^{pK_{a2}-pH_{in}}}$	42	$[H_2CO_3]_0 = \frac{TAC}{1+10^{pK_{a1}-pH_0}+10^{pK_{a2}-pH_0}}$	47
Note: pK_{a1} and pK_{a2} are respectively, the acid dissociation constants of H_2CO_3/HCO_3^- and HCO_3^-/CO_3^{-2}			

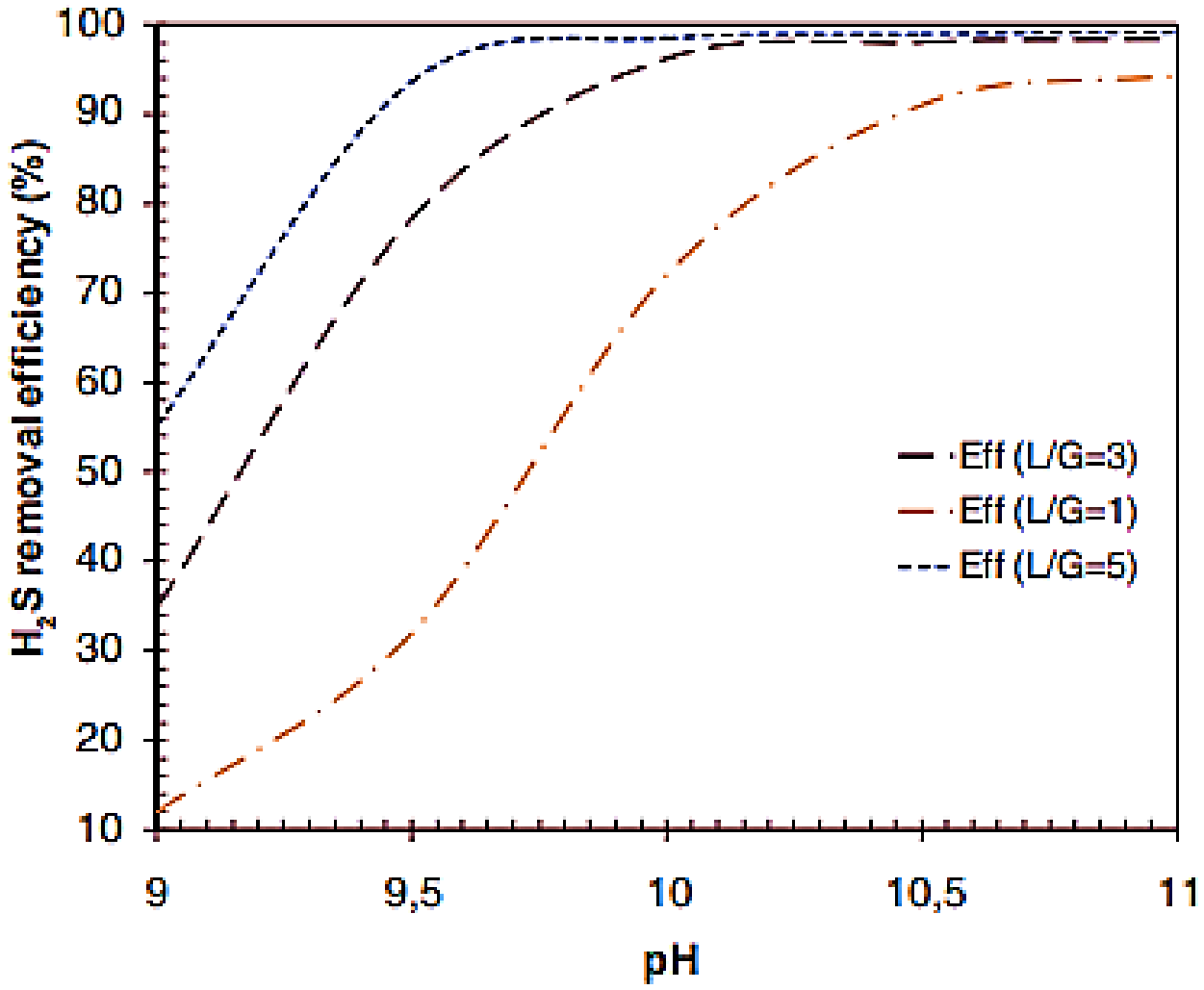

Figure 24. Influence of the pH on the H_2S removal efficiency for different L/G ratios.

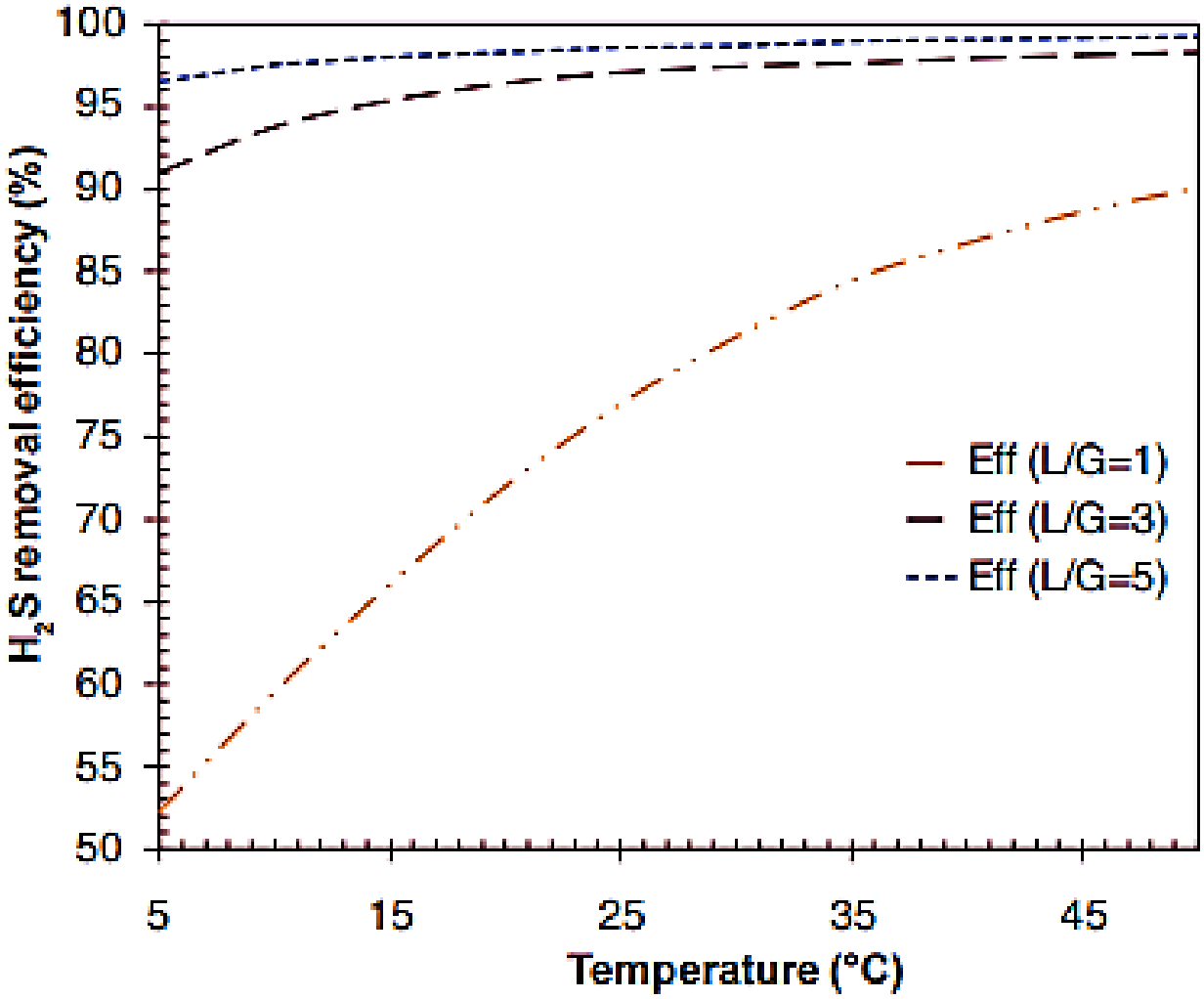

Figure 25. Influence of the temperature on the H2S removal efficiency for different L/G ratio

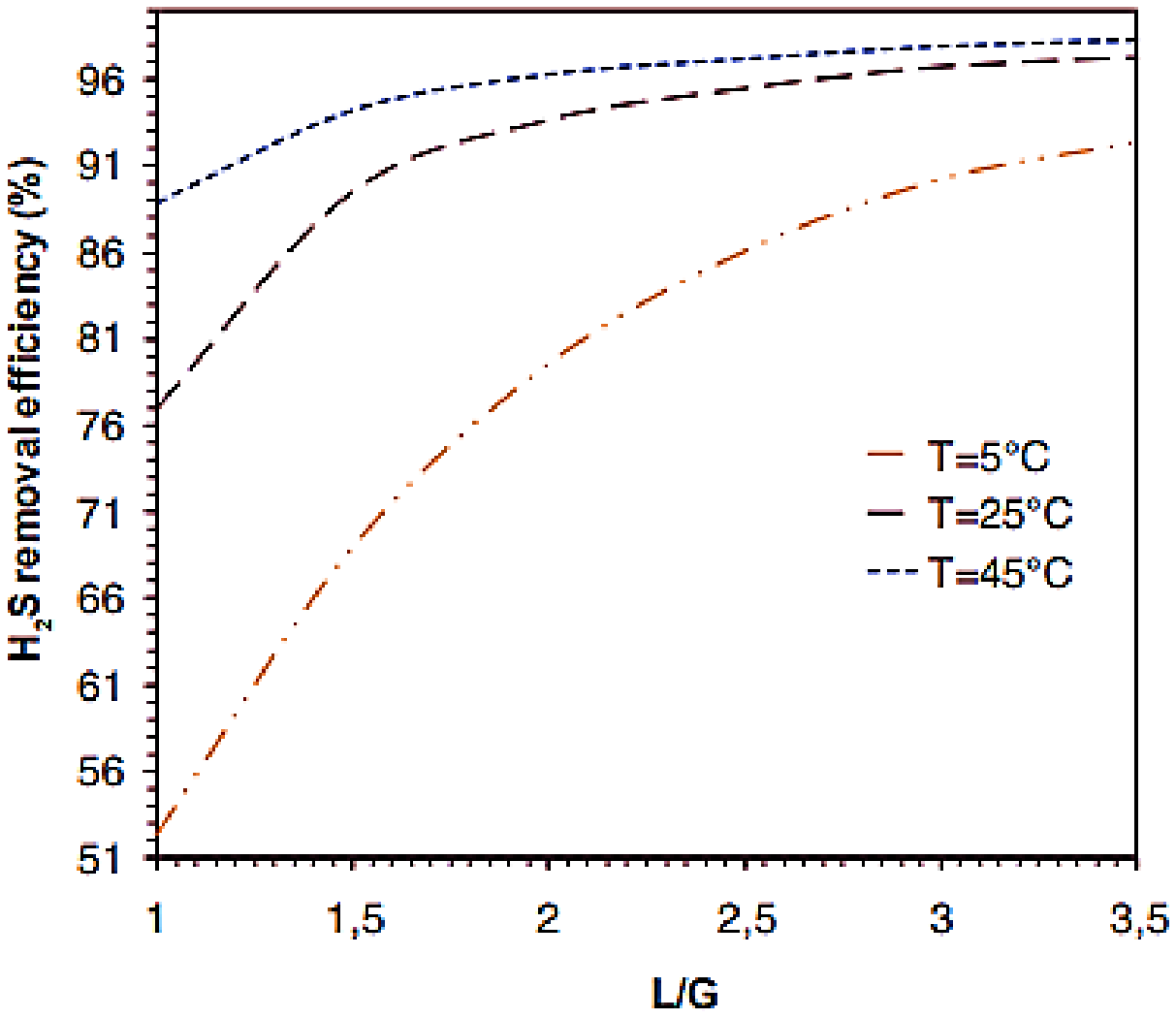

Figure 26. Influence of the L/G ratio on the H_2S removal efficiency for different temperature.

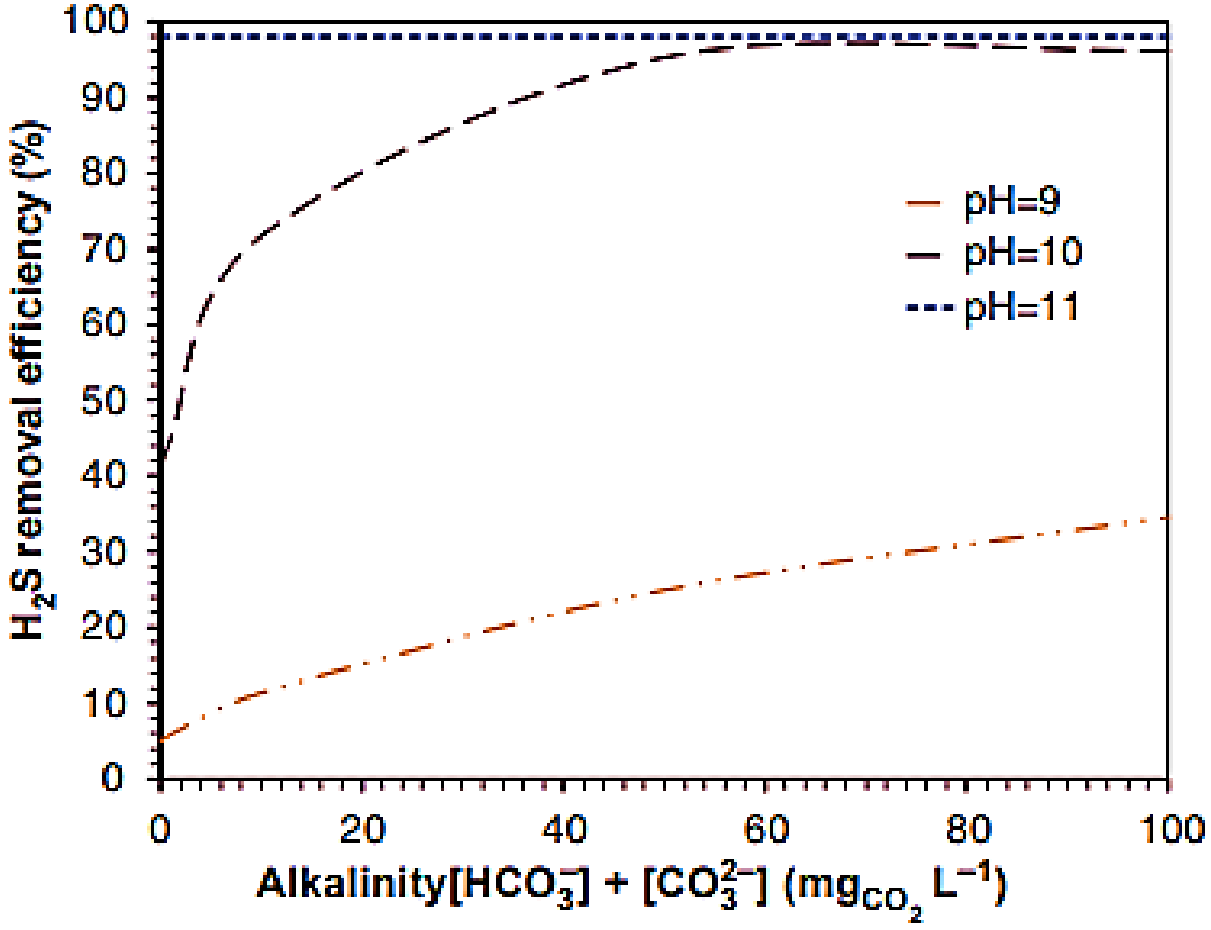

Figure 27. Influence of the alkalinity on the H_2S removal efficiency for different pH.